Università degli Studi di Napoli “Federico II”

Scuola Politecnica e delle Scienze di Base
Area Didattica di Scienze Matematiche Fisiche e Naturali

Dipartimento di Fisica “Ettore Pancini”

Laurea Magistrale in Fisica

Search for a singly produced Vector-Like Quark T in single lepton final states

Relatori:
Dott. Alberto Orso Maria Iorio
Prof. Luca Lista

Correlatore:
Prof. Francesco Tramontano

Candidato:
Lorenzo Vigilante
Matricola N94000264

A.A. 2018/2019

To my family.

Contents

Introduction

The Standard Model (SM) of particle physics is the most consolidated and successful theory for the description of fundamental particles and their interactions. All the predictions of the SM have been confirmed by experimental evidence, and the features of the fundamental interactions it encompasses have been described with accuracy. However, the Standard Model fails to give a full picture of the Universe, since it presents several unsolved issues, such as the large set of parameters not postulated by the theory, the lack of an explanation for the many astronomical and cosmological evidences of dark matter and dark energy, and the failure in providing a quantistic description of gravity. Theoretical hints towards new physics are provided also by the hierarchy problem, that is related to the divergences introduced by the corrections to the Higgs mass from particles it couples with. Some of the most promising new physics theories that have been formulated to solve it predict the existence of new particles called Vector-Like quarks (VLQs). They appear at the TeV scale, and they behave differently under electroweak tinteractions with respect to the SM quarks since they present a chirality symmetry.
The Large Hadron Collider (LHC), whose energy reach span up to the tens of TeV, is the best candidate to find evidence of such particles. The LHC is an hadronic collider providing proton-proton collisions at a design centre-of-mass energy of $\sqrt{s} = 14$ TeV, and a design luminosity of 10^{34} cm^{-2}s^{-1}. The LHC is equipped with four main experiments around the collision points: ALICE, ATLAS, CMS and LHCb.
The aim of this thesis is to search for a singly produced Vector-Like quark T, in channels with a top quark and a Z boson, to verify the presence of new physics. The final state under investigation consists of a top quark that decays leptonically, and a Z boson that decays to two collimated quarks, so that the products of their hadronization cluster in a single jet of particles. In this thesis, data collected by the Compact Muon Solenoid experiment at the LHC during 2017 have been analysed, and simulated samples have been used in order to emulate the VLQ T signal under investigation, as well as the backgrounds from the SM that can mimic its signature in the detector.
The content of this thesis is organised in five Chapters:
Chapter 1 introduces the theoretical framework of the Standard Model and its unsolved issues.

Chapter 2 describes the Large Hadron Collider accelerator and one of the four main experiments: The Compact Muon Solenoid.
Chapter 3 presents the main theories that lead to the introduction of VLQs, with a description of their production mechanism and their decays channels. A summary of the experimental searches of the Vector-Like quarks conducted at the hadronic colliders is provided.
Chapter 4 defines the final state looked for in this analysis and provides a description of the algorithms used to identify and reconstruct physics objects employed.
Chapter 5 introduces the data set and the MC simulation used, the event selection performed and the signal optimization applied. Finally the fit procedure is described and the results are presented.

Chapter 1

The Standard Model of particle physics

The main goal of Particle Physics is to identify fundamental components of matter and to describe interactions that occur among them. The quantum field theory that best describes such interactions is the so called Standard Model (SM). It has provided precise predictions of fundamental interactions that have been confirmed by experiments throughout the years [1–6]. However, SM is not enough to provide a full picture of the known Universe, as it fails to explain several phenomena, like the evidence for neutrino masses, the presence of the dark matter and the dark energy, and does not include the gravitation.

1.1 Standard Model overview

The SM is the quantum field theory that succesfully describe in a coerent way three of the four known interactions between the fundamental particles: the electromagnetic and weak interactions, unified in the GWS theory [10–12], and the strong interaction [13, 14] trought the Quantum Chromodynamics (QCD) [15]. The SM also provides a theoretical framework, the Higgs mechanism [7–9], to give the mass to the particles. Unfortunately, the SM is not able to include the General Relativity of gravitation.

The dynamics equations for the Standard Model are obtained from a gauge principle; a free lagrangian particle L is requested to be invariant under a local (gauge) transformation of the symmetry group:

$$SU(3)_C \otimes SU(2)_L \otimes U(1)_Y$$

Those gauge groups are:

- the group $U(1)_Y$, these transformation can be represented by a unitary scalar complex operator multiplied by its quantum number, acting as the equivalent of

Interaction	Mediators	Spin	Electric charge
Electromagnetic	γ	1	0
Weak	W^+, W^-, Z	1	$1, -1, 0$
Strong	8 gluons (g)	1	0

Table 1.1: Standard Model mediator bosons and fundamental interactions.

the electromagnetic charge, called the weak hypercharge Y. The associated vector field is called B_μ ;

- the n = 2 Special Unitary group $SU(2)_L$, whose three transformations can be represented by the 2×2 Pauli matrices σ_i (i = 1, 2, 3) multiplied by the third component of weak isospin I_3. The three associated vector fields are $W_\mu^{1,2,3}$;
- the n = 3 special unitary group $SU(3)_C$, whose eight operations can be represented by the 3×3 Gell-Mann matrices λ^j (j = 1, ..., 8) multiplied by a charge called the colour $C = (r, g, b)$. The eight associated vector fields are $G_\mu^{1,...,8}$.

Each interaction is associated to a multiplet and to an absolutely conserved quantum number, for example the charge in the case of electromagnetism. The components are called bosons since they have spin qual to one and they obey the Bose-Einstein statisctics. For example the electromagnetic force is carried by spin-1 photons (γ) and acts between electrically charged particles; the weak interaction is ruled by three gauge vector bosons, $W^\pm$ and Z, discovered in 1983 by the UA1 and UA2 experiments [1–3] , and it is responsible for phenomena like nuclear β-decays. The number of the mediator bosons for an interaction is determined by the number of the generetor of the symmetry group associated with it and that makes 12 vector fields associated with three gauge symmetries. As will be shown in section 1.3.1, three of these massless fields acquire mass and become the known physics boson: W^+, W^-, Z. The eight gluons and the photon remain without mass. A list of the phyisical bosons is reported in Table 1.1.

The SM also has 12 fermion fields with half-integer spin which obey to the Fermi-Dirac statistics and are classified as lepton or quark fields. Among the lepton fields, fermions are listed in three generations, or families, as can be seen in Table 1.2. Each family is a doublet of particles associated to an isospin quantum number and each particle carries electron-weak and strong charges. In particular the colour for the strong interactions plays the same role of the charge for the electromagnetic interactions. Quarks are grouped in three families and are listed in Table 1.3. According to Dirac equation all these fermions have an associated anti-particle that has the same mass but opposite quantum numbers.

Fermions have also a property called chirality, and they can either be left-chiral,

Particles			Spin	Charge
$\begin{pmatrix}\nu_e\\ e\end{pmatrix}$	$\begin{pmatrix}\nu_\mu\\ \mu\end{pmatrix}$	$\begin{pmatrix}\nu_\tau\\ \tau\end{pmatrix}$	1/2	$\begin{matrix}0\\ -1\end{matrix}$

Table 1.2: Standard Model leptons.

Particles			Spin	Charge
$\begin{pmatrix}\mathrm{u}\\ \mathrm{d}\end{pmatrix}$	$\begin{pmatrix}\mathrm{c}\\ \mathrm{s}\end{pmatrix}$	$\begin{pmatrix}\mathrm{t}\\ \mathrm{b}\end{pmatrix}$	1/2	$\begin{matrix}2/3\\ -1/3\end{matrix}$

Table 1.3: Standard Model quarks.

or right-chiral. It is experimentally verified that left-handed fermion fields transform differently under the $SU(2)_L$ gauge symmetry than the right-handed fermion fields, which results in an asymmetry in the properties of fermions. Specifically, there are left-chiral and right-chiral charged leptons, left-chiral neutrinos, but no right-chiral neutrinos. This does not yet have an explanation from prime principles.

The last field in the Standard Model is a complex scalar doublet field (ϕ), named the Higgs field after one of the theorists who predicted its existence in 1964 [8]. In Figure 1.1 the particles predicted by the SM are shown.

1.2 Quantum electrodynamics

The Quantum Electrodynamics (QED) is the relativistic quantum field theory that describes the dynamics and interactions between fermions when they are in an electromagnetic field. In this case the symmetry group involved is the abelian $U(1)_q$ group, where the subscript indicates the charge as conserved quantum number, that assumes the meaning of the charge of the particles.

The lagrangian density for QED can be obtained starting from the free lagrangian density of Dirac field ψ with mass m:

$$\mathcal{L}_D = i\bar{\psi}\gamma^\mu\partial_\mu\psi - m\bar{\psi}\psi, \tag{1.1}$$

where $\bar{\psi}\gamma^\mu\partial_\mu\psi$ is the kinetic term, $m\bar{\psi}\psi$ is the mass term, γ^μ are the Dirac matrices and ψ and $\bar{\psi}$ are the 4-components spinor and its adjoint.

The term related to the boson kinetic energy, which is invariant for local gauge transformation. is added to the equation (1.1) in order to include the propagation of free photons:

$$\mathcal{L}_\gamma = -\frac{1}{4}F^{\mu\nu}F_{\mu\nu}, \tag{1.2}$$

$F^{\mu\nu}$ is the field strength tensor which can be written in terms of 4-vector electromagnetic

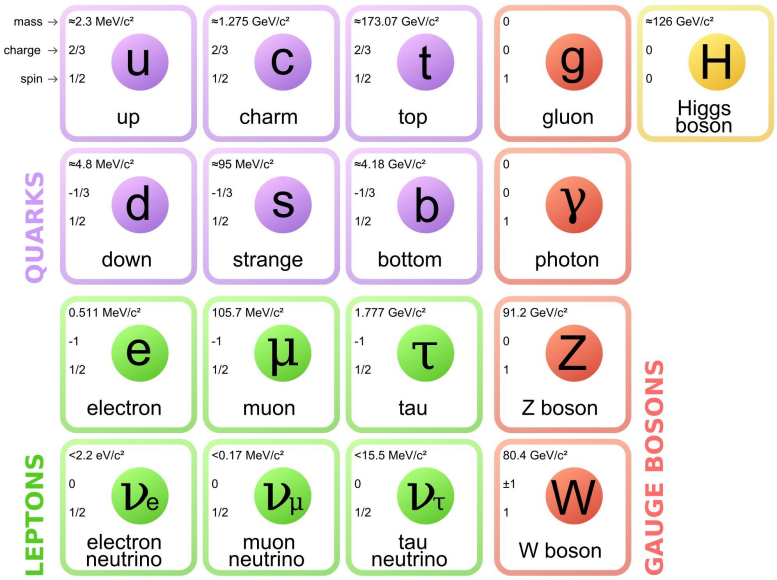

Figure 1.1: Standard Model particles: in violet the quarks, in green the leptons, in red the gauge bosons, and in yellow the Higgs boson.

field A^μ in the following way:

$$F^{\mu\nu} = -F^{\nu\mu} = \partial^\mu A^\nu - \partial^\nu A^\mu. \tag{1.3}$$

By adding 1.1 and 1.2 we obtain a new lagrangian:

$$\mathcal{L}_{QED} = \mathcal{L}_D + \mathcal{L}_\gamma = i\bar{\psi}\gamma^\mu\partial_\mu\psi - m\bar{\psi}\psi - \frac{1}{4}F^{\mu\nu}F_{\mu\nu}. \tag{1.4}$$

As said before, equation (1.4) must follow the gauge principle, which force every pyhisical Lagrangian to be invariant under local gauge trasformations. The Equation (1.4) is globally invariant under a $U(1)_q$ transformation:

$$\psi \to \psi' = e^{i\theta}\psi \tag{1.5}$$

with θ arbitrary constant. Instead a local gauge transformation $U(1)_q$ could be written as:

$$\begin{aligned} \psi &\to \psi' = e^{i\theta(x)}\psi \\ \bar{\psi} &\to \bar{\psi}' = e^{-i\theta(x)}\bar{\psi} \end{aligned} \tag{1.6}$$

where $\theta(x)$ is an arbitrary function depending on the spacetime coordinates. Since the fermionic kinetic term is not invariant under local gauge transformation, the (1.4) is not

invariant too:

$$\partial_\mu \psi \to \partial_\mu \psi' = e^{iq\theta(x)} \partial_\mu \psi(x) + iq e^{iq\theta(x)} \psi(x) \partial_\mu \theta(x) \tag{1.7}$$

To force this invariance is necessary to introduce the so called *covariant derivative* D, a particular derivative that undergoes the same phase transformation of the field:

$$\mathcal{D}_\mu \psi \to e^{iq\theta(x)} \mathcal{D}_\mu \psi$$
$$\mathcal{D}_\mu \equiv \partial_\mu + iqA_\mu(x)$$

where A_μ is the electromagnetic vectorial field. Under a local gauge trasformation it becomes like:

$$A_\mu(x) \to A_\mu(x) - \partial_\mu \theta(x) \tag{1.8}$$

obtained using the minimal substitution. The fermionic kinetic term, and so the lagrangian, now are invariant under local gauge transformation and can be written as:

$$\mathcal{L}_D = i\bar{\psi}\gamma^\mu \mathcal{D}_\mu \psi - m\bar{\psi}\psi,$$

and making explicit covariant derivative:

$$\mathcal{L}_D = i\bar{\psi}\gamma^\mu \partial_\mu \psi - m\bar{\psi}\psi - q\bar{\psi}\gamma^\mu \psi A_\mu = \mathcal{L}_0 - J^\mu A_\mu \tag{1.9}$$

where the latter term contains interaction between the Dirac particle and the electromagnetic field. The quantity J^μ is interpreted as the charge current, i.e. the probability current of the particle multiplied by its charge.

So the local invariant QED lagrangian for a Dirac particle in a electromagnetic field can be obtained by adding 1.9 and 1.4:

$$\mathcal{L}_{QED} = \mathcal{L}_D + \mathcal{L}_\gamma = i\bar{\psi}\gamma^\mu \partial_\mu \psi - m\bar{\psi}\psi - q\bar{\psi}\gamma^\mu \psi - \frac{1}{4} F^{\mu\nu} F_{\mu\nu}. \tag{1.10}$$

From the $\mathcal{L}_{QED}$ lagrangian is possible to extract the Feynamn rules which allow a diagramatic representation of the process amplitudes. In Figure 1.2 some of the fundamental transitions associated to the lagrangian in (1.10) can be seen.

1.3 The Electroweak theory

In 1933 Italian physicist Enrico Fermi (1901-1954) in his article "Tentativo di una teoria dell'emissione dei raggi beta" [17], provides the first quantum field theory able to describe the nucler β decay. He proposed a phenomenological description of weak interactions determined by the current-current lagrangian, known as Fermi-like interaction:

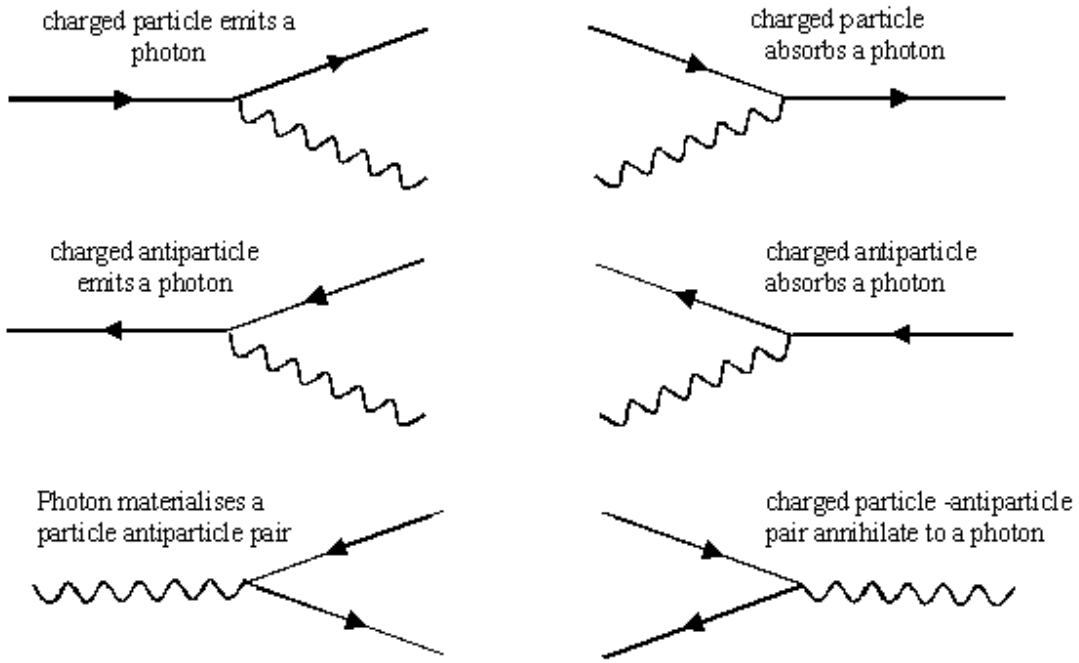

Figure 1.2: Basics vertices in Quantum Electrodynamics.

$$\mathcal{L}_F = \frac{G}{\sqrt{2}} J^{\dagger\mu}(x) J_\mu(x) \tag{1.11}$$

where G is the Fermi constant

$$G = 1.16638 \times 10^{-5}\ \text{GeV}^{-2}$$

and J^μ is the weak current composed by the sum of a weak leptonic current, $l^\mu(x)$ and a weak hadronic current $h^\mu(x)$.

With his teory, Fermi manages to describe successfully the short-range interaction approximation. However, the dimensionality of the operator $J^{\dagger\mu}(x)J_\mu(x)$, leads to divergences, in particular the violation of the unitarity limit of the Fermi-like cross-section. In order to solve those divergences, during 60's and 70's [10–12], S. Glashow, A. Salam and S. Weinberg proposed the Electroweak theory (also known as the GWS model) which is a natural development of Fermi's theory, where has been introduced an adimensional coupling constant and three intermediate vector bosons. For their work, Glashow, Salam and Weinber won the Nobel prize in Physics in 1979.

1.3.1 GSW Model

The group $SU(2)_L$ is the symmetry group for the GWS Model quantum field theory. Subscript L means that only the left-handed chiral components of the fields can take part in weak interactions. Since the generators of $SU(2)_L$ are the Pauli 2×2 matrices σ_i (i = 1, 2, 3), it is convinient to adopt the formalism of the angular momentum. In this way particles, eigenstates of the weak interaction, are arranged in six doublets of weak isospin. By naming I the weak isospin and I_3 its observed component, such doublets for leptons are:

$$I = 1/2 \qquad \begin{matrix} I_3 = +1/2 \\ I_3 = -1/2 \end{matrix} \qquad \begin{pmatrix} \nu_e \\ e \end{pmatrix}_L \begin{pmatrix} \nu_\mu \\ \mu \end{pmatrix}_L \begin{pmatrix} \nu_\tau \\ \tau \end{pmatrix}_L ,$$

and for quarks are:

$$I = 1/2 \qquad \begin{matrix} I_3 = +1/2 \\ I_3 = -1/2 \end{matrix} \qquad \begin{pmatrix} \mathrm{u} \\ \mathrm{d}' \end{pmatrix}_L \begin{pmatrix} \mathrm{c} \\ \mathrm{s}' \end{pmatrix}_L \begin{pmatrix} \mathrm{t} \\ \mathrm{b}' \end{pmatrix}_L .$$

where d′, s′ and b′ are weak interaction eigenstates that are obtained as linear combination between the mass eigenstates. This mix of different flavours is given by a complex unitary matrix V, named Cabibbo-Kobayashi-Maskawa (CKM [1]) matrix :

$$\begin{pmatrix} \mathrm{d}' \\ \mathrm{s}' \\ \mathrm{b}' \end{pmatrix} = V \begin{pmatrix} \mathrm{d} \\ \mathrm{s} \\ \mathrm{b} \end{pmatrix},$$

where:

$$V = \begin{pmatrix} \mathrm{V_{ud}} & \mathrm{V_{us}} & \mathrm{V_{ub}} \\ \mathrm{V_{cd}} & \mathrm{V_{cs}} & \mathrm{V_{cb}} \\ \mathrm{V_{td}} & \mathrm{V_{ts}} & \mathrm{V_{tb}} \end{pmatrix}.$$

Measurments of CKM matrix elements [16] have highlighted that the matrix is almost diagonal ($V_{ii} \sim 1; i = 1, 2, 3$). This means that quarks are inclined to be associated with quarks of the same family during interactions: a simple example is the top quark that decays in Wb almost 100% of the times, according the measurment of the ratio

$$R = \frac{BR(t \to Wb)}{BR(t \to Wq)} = \frac{|V_{tb}|^2}{|V_{tb}|^2 + |V_{ts}|^2 + |V_{td}|^2} = 1.014 \pm 0.003(stat) \pm 0.032(syst)$$

provided by the CMS collaboration [18] in 2014.

As for the QED development also in the GSW model a local gauge transformation

[1] Analogously a mixing matrix can be introduced also for the neutrino sector, the PMNS matrix from Pontecorvo, Maki, Nakagawa e Sakata.

invariance is required. The action of the $SU(2)_L$ on weak isospin doublets leads to:

$$\begin{pmatrix} \nu_\ell \\ \ell^- \end{pmatrix}'_L = e^{-i\vec{\alpha}(x)\cdot\vec{\tau}} \begin{pmatrix} \nu_\ell \\ \ell^- \end{pmatrix}_L , \tag{1.12}$$

where $\vec{\tau}$ are the Pauli matrices divided by 2 and $\vec{\alpha}(x)$ is a vector of real parameters of the transformation that depends upon spacetime coordinates.
Only the left-handed components can take part to weak charged-current processes, while the right-handed of charged fermions can take part to neutral current weak process. Right-handed components are singlet of $SU(2)_L$:

$$I = 0 \qquad e^-_R, \mu^-_R, \tau^-_R, d_R, u_R, s_R, c_R, b_R, t_R.$$

The request of invariance under $SU(2)_L$ group leads to the introduction of an isospin triplet of Yang-Mills fields: $W^\mu_{(i)}$ with $i = (1, 2, 3)$. To unify weak and electromagnetic interactions a $U(1)_Y$ simmetry group and his related boson, the singlet B^μ, are introduced. The associeted quantum number is called the weak hypercharge Y and its defined as:

$$Q = I_3 + \frac{Y}{2} \tag{1.13}$$

which represents the electric charge Q (in units of e) of the I_3 member of a weak isomultiplet, assigned a weak hypercharge Y. This leads to the introduction of a new simmetry group: $SU(2)_L \times U(1)_Y$. The definition (1.13) was proposed by Glashow and is an extension of the Gell–Mann-Nishijima relation for charges valid also for these weak quantum numbers. So the symmetry group of transformation is $SU(2)_L \otimes U(1)_Y$ and leads to 4 gauge fields, 3 as said before coming from the $SU(2)_L$ and 1 coming from the group $U(1)_Y$.

The Electroweak lagrangian could be obtained in a similar way as done for the Electromagnetic one (see Quantum elctrodynamics). According to gauge principle, a covariant derivative term is introduced in the lagrangian in order to make it invariant under $SU(2)_L \otimes U(1)_Y$ local gauge trasformation:

$$D_\mu = \partial_\mu + ig\frac{\vec{\tau}}{2}W_\mu + ig'\frac{Y}{2}B_\mu, \tag{1.14}$$

where g and g' are the equivanlent of the electromagnetic coupling costant e.

Starting from a free fermionic lagrangian, neglecting mass terms and introducing the (1.14), the electroweak lagrangian for fermions can be written as:

$$\mathcal{L}_{fermions} = \sum_f \bar{\psi}\gamma^\mu D_\mu \psi. \tag{1.15}$$

In order to obtain a complete electroweak lagrangian is mandatory to add a term for the dynamics of the gauge boson fields:

$$\mathcal{L}_{gauge} = -\frac{1}{4} W_i^{\mu\nu} W^i_{\mu\nu} - \frac{1}{4} B^{\mu\nu} B_{\mu\nu} \tag{1.16}$$

with $W_i^{\mu\nu}$ and $B^{\mu\nu}$ the tensor fields:

$$\begin{aligned} W_i^{\mu\nu} &= \partial^\mu W_i^\nu - \partial^\nu W_i^\mu \\ B_i^{\mu\nu} &= \partial^\mu B^\nu - \partial^\nu B^\mu \end{aligned} \tag{1.17}$$

The following lagrangian is the results of the sum:

$$\begin{aligned} \mathcal{L}_{EW} = &- i\psi_L \gamma^\mu \left(\partial_\mu + ig \frac{\vec{\tau}}{2} \cdot W_\mu + ig' Y B_\mu \right) \psi_L + \\ &- i\psi_R \gamma^\mu \left(\partial_\mu + ig' Y B_\mu \right) \psi_R + \\ &- \frac{1}{4} W_i^{\mu\nu} W^i_{\mu\nu} - \frac{1}{4} B^{\mu\nu} B_{\mu\nu} + \\ &+ \frac{1}{2} g \, \epsilon_{ijk} W_i^{\mu\nu} W_{j\mu} W_{k\nu} + \frac{1}{4} g^2 \, \epsilon_{ijk} \epsilon_{imn} W_{j\mu} W_{k\nu} W_m^\mu W_n^\nu, \end{aligned} \tag{1.18}$$

where ψ_L and ψ_R are the left and right-handed chiral components of the particles, and the term in the last line describes the three and four-point self interactions of the vector bosons that arise because of the non-Abelian nature of the $SU(2)_L$ group. Physical charged vector fields for the $W^\pm, Z$ bosons and photon can be obtained by combining the four gauge fields:

$$W_\mu^\pm = \frac{1}{\sqrt{2}} \left(W_\mu^1 \mp i W_\mu^2 \right) \tag{1.19}$$

while for the neutral bosons in the following way:

$$\begin{pmatrix} Z^\mu \\ A^\mu \end{pmatrix} = \begin{pmatrix} \cos\theta_W & -\sin\theta_W \\ \sin\theta_W & \cos\theta_W \end{pmatrix} \begin{pmatrix} W^\mu \\ B^\mu \end{pmatrix} \tag{1.20}$$

with

$$\cos\theta_W = \frac{g}{\sqrt{g^2 + g'^2}}, \quad \text{and} \quad \sin\theta_W = \frac{g'}{\sqrt{g^2 + g'^2}} \tag{1.21}$$

The parameter θ_W is called Weinberg angle and it has to be determined experimentally. The electromagnetic charge therefore is:

$$q = g' \cos\theta_W = g \sin\theta_W \tag{1.22}$$

Two of these are combined together in order to give two vector bosons $W^\pm$, that are electrically charged and can induce transitions between the members of the weak isospin

doublets. The third gauge boson of the triplet should be electrically neutral.

1.3.2 Spontaneous symmetry breaking and Higgs mechanism

As shown in subsection 1.3.1, the gauge principle manages to succesfully describe the interactions between particle. However all the gauge fields found so far are strictly massless, since introducing a mass term like

$$(1/2)m^2 B_\mu B^\mu$$

in Equation (1.18) would break gauge symmetry. The simplest and most elegant way to provide mass to the intermidiate bosons is the spontaneous symmetry breaking (SSB) and the Higgs mechanism. This mechanism hinges on the existence of a new boson field, the Higgs particle,which is a isospin doublet of complex scalar fields that can be written as:

$$\begin{pmatrix} \phi^+ \\ \phi^0 \end{pmatrix} = \begin{pmatrix} \phi_1 + i\phi_2 \\ \phi_3 + i\phi_4 \end{pmatrix} \tag{1.23}$$

in the form of $SU(2)_L \otimes U(1)_Y$ multiplet to ensure that the lagrangian remains invariant. Complex scalar field ϕ^+ destroys positive charged particles and creates negative particles while ϕ^0 destroys neutral particles and creates neutral antiparticles. The lagrangian for ϕ field is:

$$\begin{aligned} \mathcal{L}_H &= (D^\mu \phi)^\dagger D_\mu \phi - V(\phi) = \\ &= (D^\mu \phi)^\dagger D_\mu \phi - \frac{1}{2}\mu^2 \phi^\dagger \phi - \frac{1}{4}\lambda (\phi^\dagger \phi)^2, \end{aligned} \tag{1.24}$$

where $V(\phi)$ is the potential responsible of the symmetry breaking, and the λ parameter is assumed to be positive. The ground (vacuum) state, ϕ_0, chosen is the one that minimize the potential V. For $\mu^2 > 0$ it assumes a unique minimum at $\phi_0 = 0$ and the ground state is symmetric under $SU(2)_I$. Instead, for $\mu^2 < 0$, the shape of the potential is modified as can be seen in the Figure 1.3, and V assumes a non-trivial minimum:

$$\phi_0^2 = -\frac{\mu^2}{2\lambda} \equiv \frac{v^2}{2}.$$

The vacuum expectation value, defined as the absolute value of the field at the minimum of the potential, is non-zero and corresponds to the radius of a circumference in the complex plane $Re(\phi) - Im(\phi)$. Without any loss of generality a reference minimum can be chosen among all possible ground states:

$$\phi = \frac{1}{\sqrt{2}} \begin{pmatrix} 0 \\ v \end{pmatrix}$$

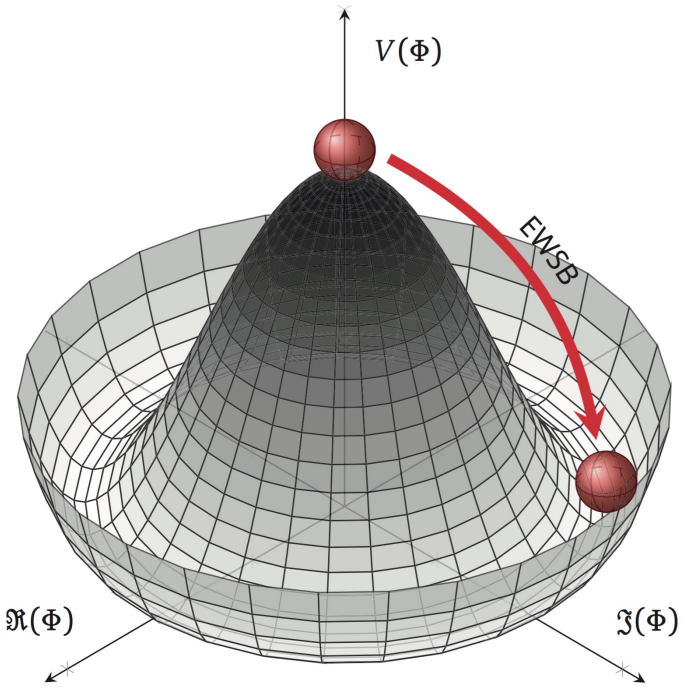

Figure 1.3: Shape of the Higgs potential $V(\phi) = \mu^2\phi^2 + \lambda\phi^4$ for $\lambda > 0$ and $\mu^2 < 0$.

Adding the potential in Equation (1.24) to the lagrangian of gauge field sector, when the covariant derivative acts, one has:

$$\mathcal{L}_H = (D^\mu\phi)^\dagger D_\mu\phi - \frac{1}{2}\mu^2\phi^\dagger\phi - \frac{\lambda}{4}(\phi^\dagger\phi)^2 - \frac{1}{4}F^{\mu\nu}F_{\mu\nu} - \frac{1}{4}B^{\mu\nu}B_{\mu\nu}, \tag{1.25}$$

with:

$$D^\mu\phi = \left(\partial^\mu + ig\frac{\vec{\tau}}{2}W^\mu + ig'YB^\mu\right)\phi \tag{1.26}$$

$$F^{\mu\nu} = \partial^\mu W^\nu - \partial^\nu W^\mu - gW^\mu \times W^\nu \tag{1.27}$$

$$B^{\mu\nu} = \partial^\mu B^\nu - \partial^\nu B^\mu. \tag{1.28}$$

Trought the parametrization of fluctuations of the ϕ field around the vacuum, the Higgs field assumes the value:

$$\phi = \begin{pmatrix} 0 \\ \frac{1}{\sqrt{2}}\left(v + H(x)\right), \end{pmatrix} \tag{1.29}$$

with:

$$v = \sqrt{-\frac{\mu^2}{\lambda}}. \tag{1.30}$$

The substitution of the Equation 1.29 in the 1.25, taking into account the Eq. 1.20,

leads to:

$$\begin{aligned}\mathcal{L}_{G\Phi} = &\frac{1}{2}\partial_\mu H \partial^\mu H - \mu^2 H^2 + \\ &- \frac{1}{4}(\partial_\mu W^1_\nu - \partial_\nu W^1_\mu)(\partial^\mu W^{1\nu} - \partial^\nu W^{1\mu}) + \frac{1}{8}g^2 v^2 W^1_\nu W^{1\nu} \\ &- \frac{1}{4}(\partial_\mu W^2_\nu - \partial_\nu W^2_\mu)(\partial^\mu W^{2\nu} - \partial^\nu W^{2\mu}) + \frac{1}{8}g^2 v^2 W^2_\nu W^{2\nu} \\ &- \frac{1}{4}(\partial_\mu Z_\nu - \partial_\nu Z_\mu)(\partial^\mu Z^\nu - \partial^\nu Z^\mu) + \frac{1}{8}(g^2 + g'^2)v^2 Z_\nu Z^\nu \\ &- \frac{1}{4}F^{\mu\nu}F_{\mu\nu}.\end{aligned} \tag{1.31}$$

The first line of (1.31) is the lagrangian of the Higgs scalar field, with mass $\sqrt{2}\mu$. The next two lines show that the components W^μ_1 and W^μ_2 of the triplet $\mathbf{W}^\mu$ acquire mass:

$$M_1 = M_2 = \frac{1}{2}gv \equiv M_W. \tag{1.32}$$

while the fourth line shows that the field Z^μ acquires a mass:

$$M_Z \equiv \frac{1}{2}v\sqrt{g^2 + g'^2} = \frac{M_W}{\cos\theta_W}. \tag{1.33}$$

In the end the last line shows that the photon field A^μ has a zero mass.

1.3.3 Masses of leptons

The spontaneous breaking of the $SU(2)_L \otimes U(1)_Y$ gauge symmetry could also generate the masses of fermions. Since the fermionic mass term $-m\bar{\psi}\psi$ is not invariant under the $SU(2)_L \otimes U(1)_Y$ group because of the different transformation of the right and left-handed chiral components of the fields, the procedure is different from the one used in the bosons case. However, in a theory where the symmetry is spontaneously broken it is not necessary introduce in the lagrangian mass terms in an explicit way, but it can be done by coupling them to the scalar field that acquires a vacuum expectation value. This can be achieved by introducing a Yukawa coupling between the fermion field and the Higgs field, and can be written as:

$$\mathcal{L}_Y = g_f(\bar{\psi}_L \phi \psi_R - \bar{\psi}_R \phi^\dagger \psi_L), \tag{1.34}$$

where g_f is the Yukawa coupling constant. By substituting 1.29 in 1.34 one obtains:

$$\begin{aligned}\mathcal{L}_Y =& \frac{g_f}{\sqrt{2}}\left[(\nu_\ell,\ \ell)\begin{pmatrix}0\\ v+H\end{pmatrix}\ell_R + \ell_R(0,\ v+H)\begin{pmatrix}\nu_\ell\\ \ell\end{pmatrix}\right] = \\ =& \frac{g_f}{\sqrt{2}}(v+H)(\ell_L\ell_R + \ell_R\ell_L)\end{aligned} \tag{1.35}$$

The first term of the second line is a mass term "a la Dirac" and allows to identify the constant coefficient of $(\ell_L\ell_R + \ell_R\ell_L)$ as the mass term for leptons:

$$m_f = \frac{v}{\sqrt{2}} g_f. \tag{1.36}$$

This is the least satisfactory part of the model because even if this kind of Yukawa coupling solves the problem of leptons' masses, it does not arise from a gauge principle, it is purely phenomenological and needs a specific coupling constant for each fermion-Higgs interaction. Moreover the couplings turn out to be very different from each other, given the wide range of fermion masses experimentally observed.

1.3.4 Masses of quarks

The mechanism illustrated in 1.3.3 could also be used to give mass to quarks:

$$\begin{aligned}\mathcal{L}_Y =& \frac{1}{\sqrt{2}}\left[g^d_{i,j}(u_{i,L},\ d_{i,L}) \begin{pmatrix} 0 \\ v+H \end{pmatrix} d_{j,R} + g^u_{i,j}(u_{i,L},\ d_{i,L}) \begin{pmatrix} -(v+H)^* \\ 0 \end{pmatrix} u_{j,R} + h.c.\right] = \\ =& \frac{1}{\sqrt{2}}(v+H)[g^u_{ij}(u_{i,L}u_{j,R} + u_{j,R}u_{i,L}) + g^d_{ij}(d_{i,L}d_{j,R} + d_{j,R}d_{i,L}) + h.c.]\end{aligned} \tag{1.37}$$

with u_i = (u, c, t) and d_i = (d, s, b). The matrix of mass terms is not diagonal in the weak interaction basis, so the mass eigenstates are not equal to the weak ones:

$$m^u_{ij} = -\frac{v}{\sqrt{2}} g^u_{ij} \quad m^d_{ij} = -\frac{v}{\sqrt{2}} g^d_{ij}. \tag{1.38}$$

It can be made diagonal with four different transformations on the family triplets $u_{i,L}$, $u_{i,R}$, $d_{i,L}$, and $d_{i,R}$ through:

$$u_{\alpha,L} = (\mathcal{U}^u_L)_{\alpha i} u_{i,L} \quad u_{\alpha,R} = (\mathcal{U}^u_R)_{\alpha i} u_{i,R} \tag{1.39}$$

$$d_{\alpha,L} = (\mathcal{U}^d_L)_{\alpha i} d_{i,L} \quad d_{\alpha,R} = (\mathcal{U}^d_R)_{\alpha i} d_{i,R} \tag{1.40}$$

where α is the index in the mass diagonal basis and i is the index in the non-diagonal weak interaction basis.

$$\mathcal{L}_Y = \frac{1}{\sqrt{2}}(v+H)\left[m^u \mathrm{u}\bar{\mathrm{u}} + m^d \mathrm{d}\bar{\mathrm{d}} + m^s \mathrm{s}\bar{\mathrm{s}} + m^c \mathrm{c}\bar{\mathrm{c}} + m^t \mathrm{t}\bar{\mathrm{t}} + m^b \mathrm{b}\bar{\mathrm{b}}\right] \tag{1.41}$$

The same transformations must be applied to the interacting term, invariant under the $SU(2)_L \otimes U(1)_Y$ symmetry, that still contains the eigenkets of the weak interaction. When this operation is worked out the term of the coupling with the Z boson, i.e. neutral current coupling term, is diagonal also in the mass basis because the transformations of Eq. (1.39) and 1.40 are unitary. Instead the term of the coupling with the W boson, i.e.

charged current coupling term, is:

$$\begin{aligned}\mathcal{L}_{CC} &= -\frac{g}{\sqrt{2}}(\bar{u}_{i,L},\ \bar{d}_{i,L})\gamma^{\mu}\tau_{+}W_{\mu}^{+}\begin{pmatrix}u_{Li}\\ d_{Li}\end{pmatrix} + h.c. \\ &= -\frac{g}{\sqrt{2}}\bar{u}_{iL}\gamma^{\mu}d_{Li}W_{\mu}^{+} + h.c. \\ &= -\frac{g}{\sqrt{2}}\bar{u}_{\alpha_L}\left[(\mathcal{U}_L^{u})_{\alpha i}(\mathcal{U}_L^{d})^{\dagger}_{\beta i}\right]\gamma^{\mu}d_{L\beta}W_{\mu}^{+} + h.c.,\end{aligned} \tag{1.42}$$

where:

$$V_{\alpha\beta} = \left[\mathcal{U}_L^{u}\mathcal{U}_L^{d\dagger}\right]_{\alpha\beta} \tag{1.43}$$

is the CKM matrix. The charged current lagrangian can be ultimately written as:

$$\mathcal{L}_{CC} = -\frac{g}{\sqrt{2}}\bar{u}_{L\alpha}\gamma^{\mu}V_{\alpha\beta}d_{L\beta}W_{\mu}^{+} - \frac{g}{\sqrt{2}}\bar{d}_{L\alpha}\gamma^{\mu}V_{\alpha\beta}^{\dagger}d_{L\beta}W_{\mu}^{-} \tag{1.44}$$

1.4 Quantum Chromodynamics

Quantum Chromodynamics [19] (QCD) is the gauge theory of strong interactions. The symmetry group is $SU(3)_C$, where the subscript C stands for the charge associated with this symmetry, named colour. In the strong interactions, the colour is identified with the strong charge, so as the source of the cromodynamic field. QCD is similar to QED, while the most relevant difference among $U(1)_Y$ and $SU(3)_C$ is that $U(1)_Y$ is an abelian group, while $SU(3)_C$ is not. Therefore, the generators of the symmetry group $SU(3)_C$ do not commute between themselves and this leads to the introduction, in the The QCD lagrangian, of interaction terms among the gauge fields. This means that the particles of the gauge fields, called gluons, bring the charge of the group while photons do not have electrical charge and therefore self-interaction terms do not exist in the QED. The QCD is invariant under local gauge transformations of $SU(3)_C$ group, i.e.:

$$\psi \to \psi' = e^{ig_s\vec{\theta}(x)\cdot\vec{T}}\psi, \tag{1.45}$$

where g_s is the strong coupling constant, $\vec{\theta}(x)$ are eight functions of the space-time coordinates. The $\vec{T} = T^{\alpha}$ ($\alpha = (1, ..., 8)$)terms are the generators of the $SU(3)_C$ group that come from the Gell-Mann matrices:

$$T^{\alpha} = \frac{1}{2}\lambda^{\alpha} \tag{1.46}$$

and follow the commutation rules:

$$[T_{\alpha}, T_{\beta}] = if_{\alpha\beta\gamma}T_{\gamma}, \tag{1.47}$$

where $f_{\alpha\beta\gamma}$ are the structure constants of the group $SU(3)_C$ and the indices run from 1 to 8. Since the generators of $SU(3)_C$ are represented by 3×3 matrices, a new degree of freedom is needed, the colour. In this way the field ψ has three possible states labelled as red, green, and blue. The lagrangian of free quarks, assuming massless quarks, is:

$$\mathcal{L} = \sum_{f=1}^{6} \bar{\psi}^f i\gamma^\mu \partial_\mu \psi^f \tag{1.48}$$

The request of local gauge introduces 8 fields of gauge,the gluons. In order to impose the invariance of the 1.48 under $SU(3)_C$, one has to introduce the covariant derivative, $\mathcal{D}_\mu$, given by:

$$D_\mu = \partial_\mu + ig_s T_\alpha G_\mu^\alpha. \tag{1.49}$$

The G_μ^α terms are the 8 massless gauge fields, or gluon fields, that transform as:

$$G_\mu^\alpha \rightarrow G_\mu'^\alpha = G_\mu^\alpha + ig_s f^{\alpha\beta\gamma}\theta_\beta(x) G_{\gamma,\mu} \tag{1.50}$$

To complete the Lagrangian density for the QCD it is necessary to add the contribution of the kinetic energy for each gluon:

$$\mathcal{L}_{QCD} = \bar{\psi}\gamma^\mu \partial_\mu \psi - m\bar{\psi}\psi - ig_s \bar{\psi}\gamma^\mu \lambda_\alpha \psi G_\mu^\alpha - \frac{1}{4} G_\alpha^{\mu\nu} G_{\mu\nu}^\alpha \tag{1.51}$$

where $G_\alpha^{\mu\nu}$ is the tensor field that is defined as

$$G_\alpha^{\mu\nu} = \partial^\mu G_\alpha^\nu - \partial^\nu G_\alpha^\mu - g_s f_{\alpha\beta\gamma} G^{\beta,\mu} G^{\gamma,\nu} \tag{1.52}$$

It is possible to associate each lagrangian interaction term with a Feynman diagram; Figure 1.4 shows all the fundamental transitions associated to the lagrangian in (1.51). The feature that strong interactions are weaker at short distances rather than longer distances is called the *asymptotic freedom*, and significantly differentiate the QCD from QED. The asymptotic freedom implies that a perturbative approach can not be applied at great distances, leading to the failure of the QCD to describe another important feature, the *colour confinement*, in an analytic way. It is based on the experimental evidence that no coloured hardons are observed in nature constraing the hadrons to be colour singlets, since they are interpreted as bound states of quarks in the QCD parton model. This imposes restrictions on the types of bound quark state configurations that can exist. All this can be summarized by saying that the quark colour degree of freedom must be confined. The running coupling constant of the strong force has the following expression:

$$\alpha_s\left(|q^2|\right) = \frac{\alpha_s(\mu^2)}{\left[1 + \alpha_s(\mu^2)\frac{33-2N_f}{12\pi} \ln \frac{q^2}{\mu^2}\right]}, \tag{1.53}$$

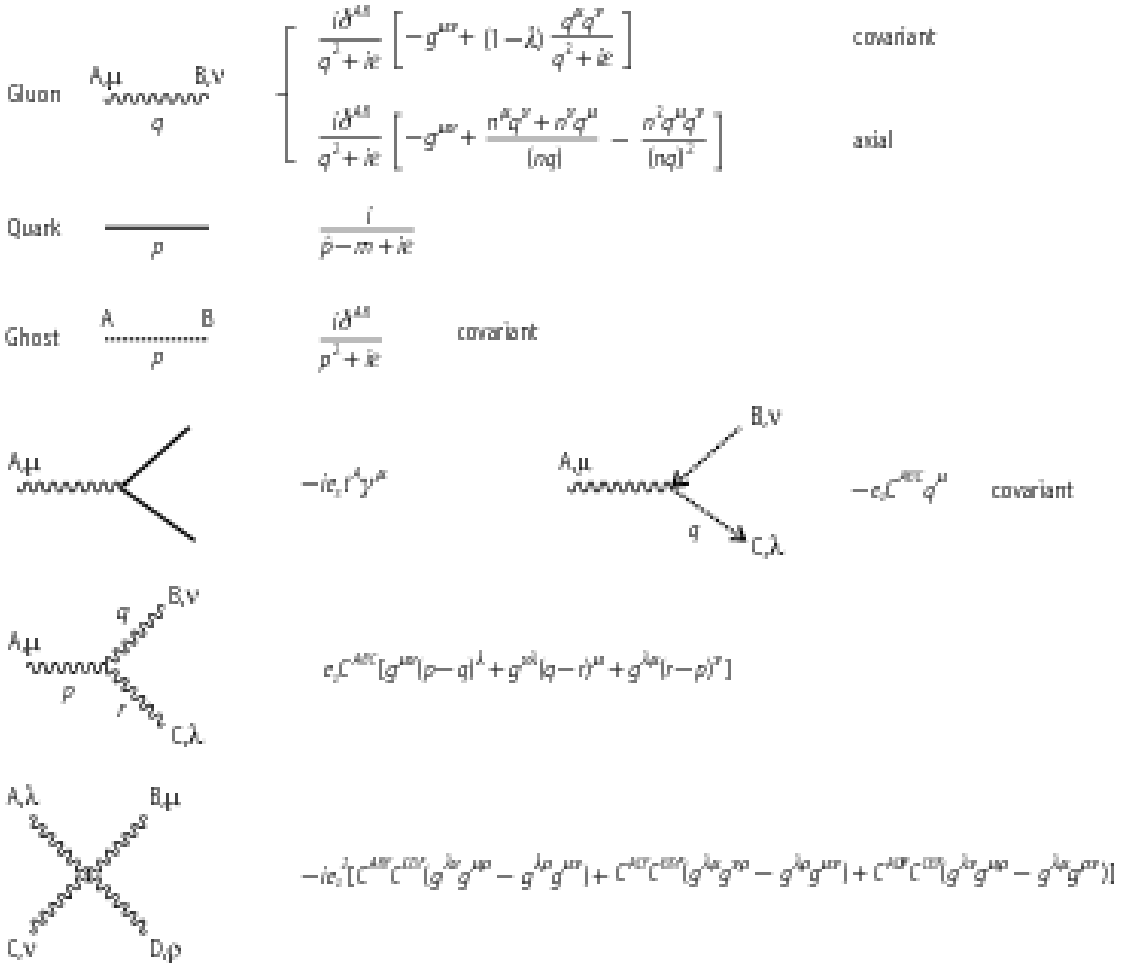

Figure 1.4: Basics vertices and Feynmann rules in Quantum Cromodynamics, QCD.

with:

- q^2, transferred 4-momentum;
- μ, the reference scale for the strength of the coupling;
- N_f, number of fermions capable of strong interactions at the scale considered.

The Equation 1.53 that $\alpha_s(q^2)$ decreases as q^2 increases. For $|q| \sim 200$ MeV the value of α_s is large enough that any perturbative approach cannot be applied. In this region the calculations are carried on with the QCD-lattice approach. For increasing values of q^2, $\alpha_s(q^2)$ decreases and one moves towards a regime in which perturbative approach is a good approximation.

1.5 Unsolved issues in the Standard Model

In the last 50 years the Standard Model has been tested by several experiments in different ways: every predicted particle has been found, features of the electromagnetic and strong interactions have been described with great accuracy, and in many cases, as for instance for the case of the electron gyromagnetic ratio [24], predictions of the SM were verified with a precision up to 12 orders of magnitude. However, the SM is not a fully satisfactory theory of the known universe; there are several phenomena and observations in nature that the SM fails to describe at all. Some of the most important issues that are not closed within the SM are:

- **Large set of parameters:** the SM postules several parameters that can not be evaluated by the theory itself:
  - 3 coupling constants: g, g' and g_s;
  - fermion masses;
  - mass and VEV of the Higgs boson;
  - CKM matrix elements;
  - PMNS matrix elements.

  The values of this quantities must therefore be obtained via measurements.

- **Electroweak unification:** the GWS model can not be considered a real unification theory because the symmetry group is the product of two different groups each one with its own constant, g and g' not linked by the theory. The ratio:

$$\frac{g'}{g} = \tan\theta_W$$

  has to be determined experimentally.

- **Fermion masses:** the SM does not predict or explain any values of fermion masses. In the Figure 1.5 are shown the differences of magnitudes between fermions, that reach till 5 order of magnitudes between the top quark and the electron. These difference and their causes are still under investigation.

- **Hierarchy problem:** also known as **naturalness,** is related to the radiative corrections to the Higgs mass from bosoninc and fermionic loops, as can be seen in the Figure 1.6. The self-interaction terms came from theory as:

$$m_H^2 \approx M_{H,0}^2 + \frac{\lambda}{4\pi^2}\Lambda^2. \tag{1.54}$$

$M_{H,0}$ is the bare mass of the Higgs, λ is the strength of the coupling and Λ^2 is the energy scale under investigation. The one-loop corrections to Higgs mass provided by a hypotetic fermionic particle f can be evaluated as:

$$\left(\delta m_H^2\right)_f \approx -\frac{\lambda_f^2}{16\pi^2}\left[2\Lambda^2 - 6m_f^2 ln\frac{\Lambda}{m_f} + \dots\right], \tag{1.55}$$

while the ones provided by a scalar particle s are:

$$\left(\delta m_H^2\right)_S \approx -\frac{g_S}{16\pi^2}\left[2\Lambda^2 - 2m_S^2 ln\frac{\Lambda}{m_s} + \dots\right], \tag{1.56}$$

where λ_f and g_S are the coupling constants of fermion and scalar particles to the Higgs and m_f and m_S are the related mass terms. The concept of naturalness is related to the magnitude of this corrections [23]. If the correction is smaller or of the same order of the measured value, the result is said to be natural. If, on the contrary, the measured value is much smaller than the quantum correction the result is unnatural because the bare value and the quantum correction appear to have an unexpected cancelation to give a result that is much smaller than either component.

Since the corrections depends on Λ, their behaviour is very different at high energy scales rather than low ones. Indeed, at the $\Lambda \sim 1$ TeV scale, the corrections are of the same order of magnitude of m_H^2, while at the Planck scale, the corrections are $\sim 10^{30}\ m_H^2$, many orders of magnitude larger than the Higgs mass at tree level. These divergences can be reduced or deleted by applying a fine tuning between fermions and scalars. This balance should also keep into account the tight constraints on the Higgs mass as shown in Figure 1.7.

- **Flavour Changing Neutral Currents (FCNC):** another observation not predicted by the SM is the presence of just three families of quarks and leptons that can be identified by the flavour quantum number. The suppression of flavour changing neutral currents at tree level, as expected from the Glashow, Iliopoulos and Maiani mechanism, GIM, is also entered by hand in the full theory.

- **Neutrino sector:** the experimental observations of flavour oscillations of neutrinos can only be explained by the assumption that neutrinos acquire mass trought the mixing of the EW eigenstates, in sharp contranst with the SM prediction of massless neutrinos. The seesaw mechanism, indeed, incorporates neutrino masses into the SM by introducing heavy Majorana neutrinos, whose masses are inversely coupled to the light SM neutrino masses, hence motivating their small values of O(1 eV). Despite extensive searches, unfortunately the experimental proof is still pending.

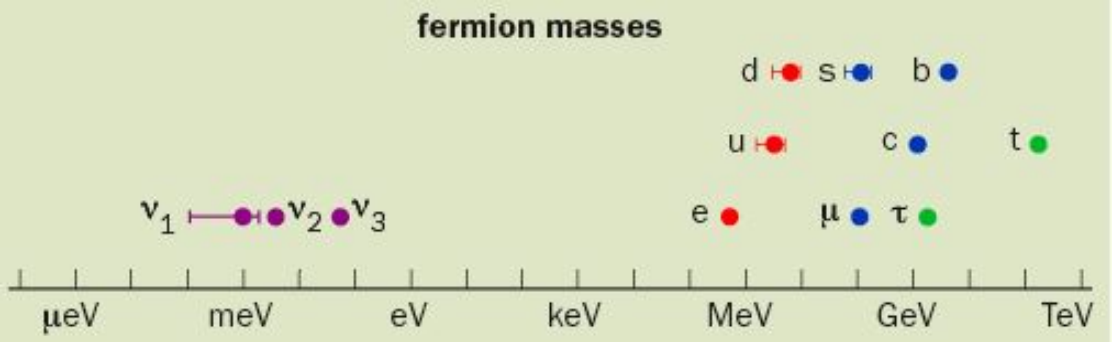

Figure 1.5: Pictorical view of the fermion masses differences.

- **Dark matter and dark energy:** the cosmological observation of the galaxy rotation profiles astronomical is one of the evidences show that the Universe is made up of only for the 5% of ordinary matter, while the rest does not correspond to the matter known. This matter is called *dark matter* and it weakly interact with SM particles. However it should only represent the 24% of the universe while the remaining 71% is ascribed to a constant vacuum energy called dark energy. The existence of the dark energy would account for the accelerating expansion of the Universe.

- **Gravity:** the failure of the Standard Model to introduce a quantistic description for gravity one of the most revelant open issues. The effects of gravity interactions are fully understood over large distances, while, at very short distances, there is not a satisfactory explanation. This is because the coupling strength of gravity is very weak if compared to other interactions, with a coupling constant that is 10^{34} times smaller than the electromagnetic coupling α. The gravitational effects are observable in particle collisions with a centre of mass energy close to the Planck scale (10^{19} GeV), significantly higer than the energetic reached by modern particle colliders. Several theoretical models that could describe the Standard Model and gravity, sometimes referred to as theories of everything, or ultraviolet (UV) completion models, manifest new phenomena only above a large energy scale called Λ_{UV}, roughly in the vicinity of the Planck scale.

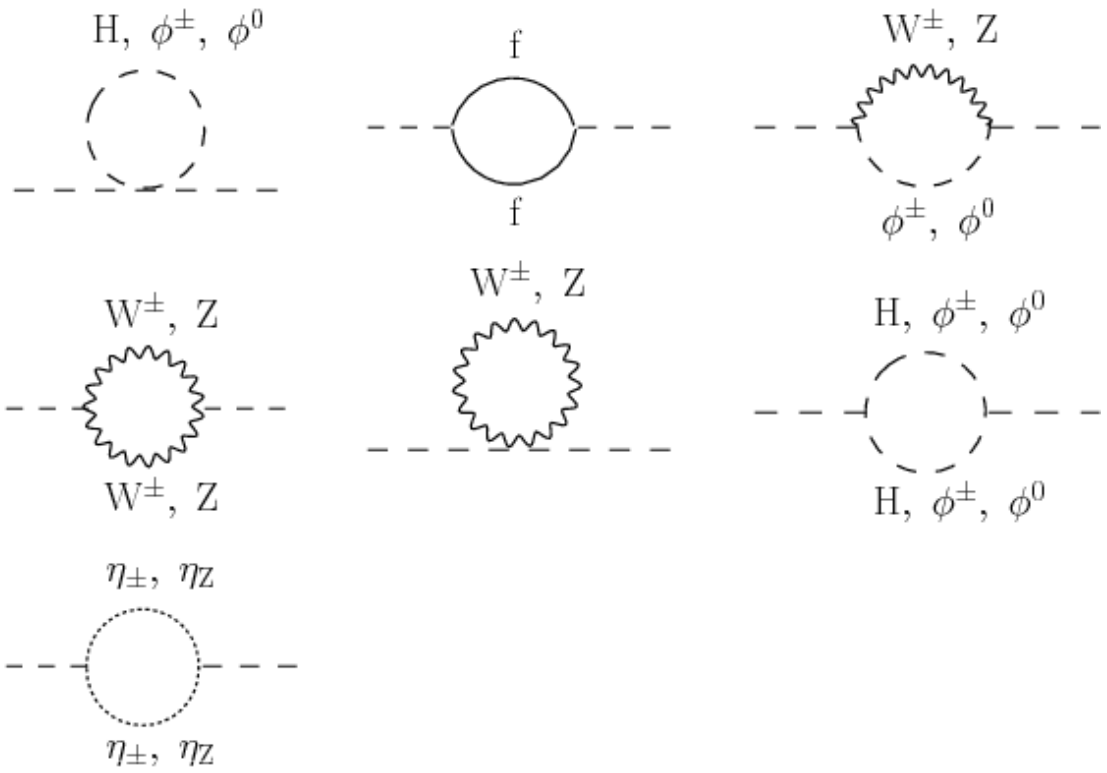

Figure 1.6: One-loop self-energy corrections to the Higgs mass.

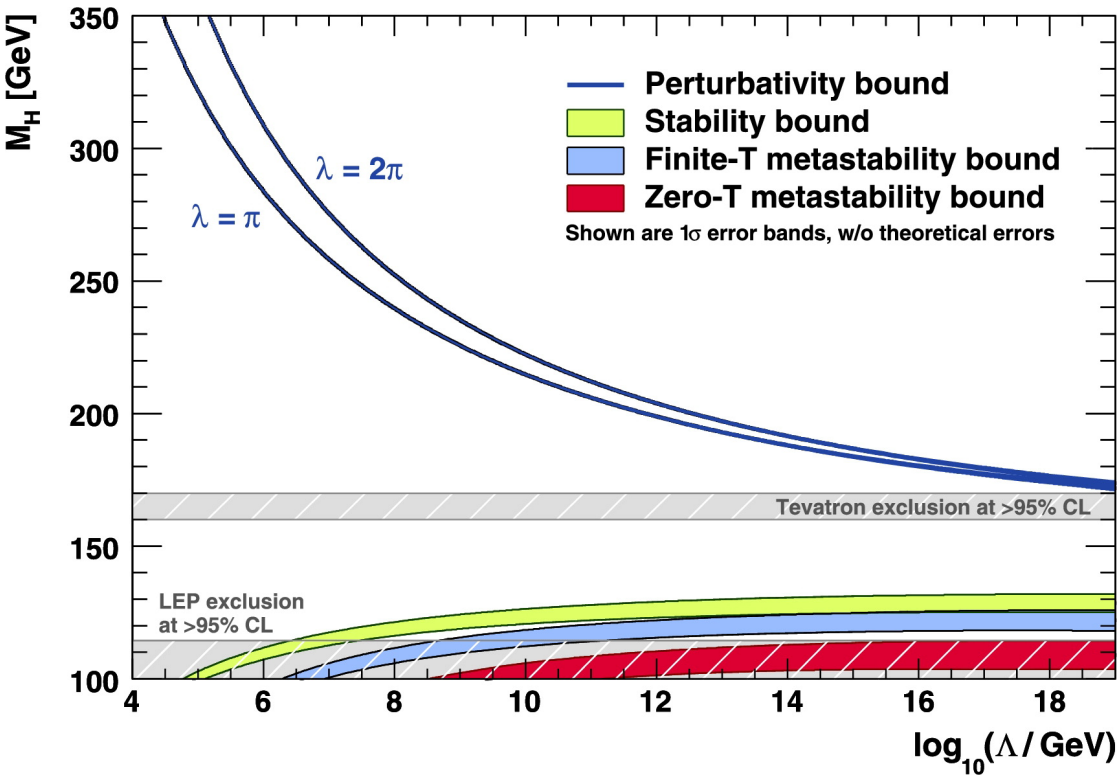

Figure 1.7: The scale Λ at which the two-loop renormalisation-group equations(RGEs) drive the quartic SM Higgs coupling non-perturbative, and the scale Λ at which the RGEs create an instability in the electroweak vacuum ($\lambda < 0$). The width of the bands indicates the errors induced by the uncertainties in and (added quadratically). The perturbativity upper bound (sometimes referred to as "triviality" bound) is given for $\lambda = \pi$ (the blue lower bold line) and $\lambda = 2\pi$ (the blue upper bold line). Their difference indicates the size of the theoretical uncertainty in this bound. The absolute vacuum stability bound is displayed by the light shaded in green band, while the less restrictive finite-temperature and zero-temperature metastability bounds are medium, in blue, and dark shaded, the red one, respectively. The grey hatched areas indicate the LEP [25] and Tevatron [26] exclusion domains.

Chapter 2

The CMS experiment at LHC

2.1 Physics motivation

The main achivment of Standard Model is the description of the interactions between fundamental particles, as we have seen in Chapter 1. The theoretical models and the predictions made by the SM have been tested several times, during the years, by experimental particle physics. One of the most fruitrul avenues to conduct these tests has been through particle accelerators; they are machines able to accelerate elementary particles, like electrons, or composite partices, like protons, to collimate them into beams and to collide them agains fixed target or other beams. In order to study new and increasingly rare processes, the history of the accelerators is characterized by a continuous increase of beam's energy as shown in the Livingston diagram, Figure 2.1. The Large Hadron Collider (LHC) is the most powerful particle accelerator ever built as it is able to collide two proton beams at the design energy in the centre of mass equal to $\sqrt{s} = 13$ TeV, as can be seen from the diagram. Rather than provide more precise measurement of SM charateristics and rather than prove the existence of the Higgs boson, the beam energy and the design luminosity of the LHC have been chosen in order to find some hints of new physic models, like supersymmetry, dark matter or extra dimensions.

2.2 The Large Hadron Collider

The Large Hadron Collider (LHC) at CERN (European Centre for Nuclear Research) near Geneva, consists of two 27 km cirumference rings of superconducting magnets and accelerating structures located in the former LEP[23] collider cave. The tunnel is located between 45 m and 170 m below the ground level and it spans the Swiss-French border. The machine is designed to provide proton-proton collisions with a center-of-mass energy of 14 TeV, with an instantaneous luminosity of 10^{34} cm^{-2}s^{-1}; these features makes LHC the highest energy collider ever built. It is also able to provide lead ion collisions at a

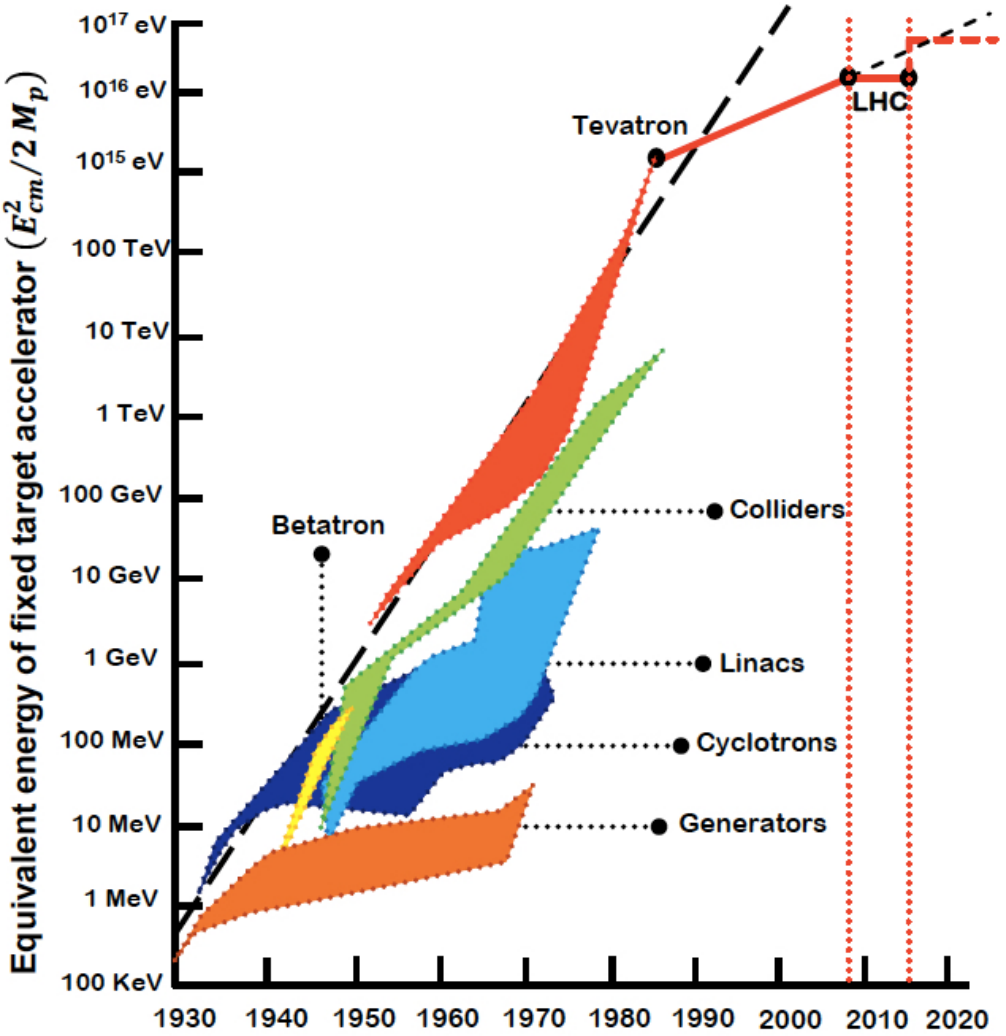

Figure 2.1: The Livingston chart depicting progress in collision energy through 2020. The LHC is the largest collision energy to date, but also represents the first break in the log-linear trend.

center-of-mass energy of 2.76 TeV per nucleon and a peak luminosity of 10^{27} cm^{-2}s^{-1}.

2.2.1 The accelerator complex

During his history, the CERN has built several particle acceleretor in order to bring the energy collisions more and more higher. When a newest machine starts to work, the one previously built act as particle injectors to the more powerful one. This mechanism allows to use structures and technologies specific for the working energetic range of every acceleretor, without a waste of materials and space at least. The acceleration of protons beams from 0 to 13 TeV is accoplished thanks to an apparatus composed of several

pre-existent machines and by the LHC itself. The protons source is a simple tank of hydrogen gas, in which elctrons are stripped from hydrogen atoms by electric fields to yield protons. Figure 2.2 show the acceleretor complex and his first element, LINAC2, a linear accelerator which accelerates the protons to the energy of 50 MeV. The LINAC2 is followed by the Proton Synchrotron Booster (PSB), a machine made up of four superimposed synchrotron rings, that push the beam to 1.4 GeV. The beam is than injected in the Proton Synchrotron (PS),the first syncrothron of CERN organization, that accelerates the protons to 25 GeV. It is a 628 meters ring with 277 conventional (room-temperature) electromagnets, including 100 dipoles to bend the beams round the ring. The last machine before LHC is the Super Proton Synchrotron (SPS), a circular accelerator with a diameter of 2 kilometres. It was originally designed to deliver an energy of 300 GeV and was gradually upgraded to reach 450 GeV,with 1317 conventional electromagnets, including 744 dipoles. The SPS injects the protons into the LHC as bunches of 1.15×10^{11}. LHC uses radio frequency (RF) cavities to accelerate beams by 485 KeV at each turn. The beams have 2808 circulating proton bunches each, and are arranged in 3 or 4 trains of 72 bunches. The trains are spaced by 25 ns each, which means that there are 8 empty bunches between two trains. At every bunch crossing occour the collisions between the beams so the resulting maximum collisions rate is 40 MHz. The accelerator complex is also composed of superconducting magnets, in particular 1232 dipoles which allows to keep the beams in the circular ring and 392 quadrupoles which are employed to focus the beams and sextupole, octupole and decapole for spool piece corrections. The dipoles are powered by an electric current of 11.700 A in order to generate a magnetic field with a nominal strenght of 8.33 T. The entire magnetic system is based on the niobium-titaniun (NbTi) Rutherford cables technology and works at a temperature of 2 K, obtained using the superfluid helium. In order to allow two protons beams circulating in opposite directions, every structure of LHC is built with a sofisticated twin-bore design. The particular design also allows to use only one cryogenic structure for the proton rings in the same cryostat, but this ultimately requires the presence of oppositely oriented magnetic fields to allow the coexistence of two proton beams along the same circumference. The two beams are kept on parallel orbits and are brought together in a single beam pipe only near the interaction point (IP). The vacuum is aslo required in the LHC for three mean reasone: the insulation of the cryomagnets, the helium distribution (QRL) and a the beam vacuum. The requirements for the beam vaccum are very stringent to guarantee the beam lifetime and to minimise the background at the experiments. The typical vacua at cryogenic temperatures in the IP requires a pressure around in the range 10^{-10} to 10^{-11} mbar.

The protons beams rotate for many hours in the LHC beam pipes befor they are brought in collision in the four interaction points (the yellow dots in Figure 2.2). In correspondence of the IPs particle detectors are located, in order to analyse the products of the

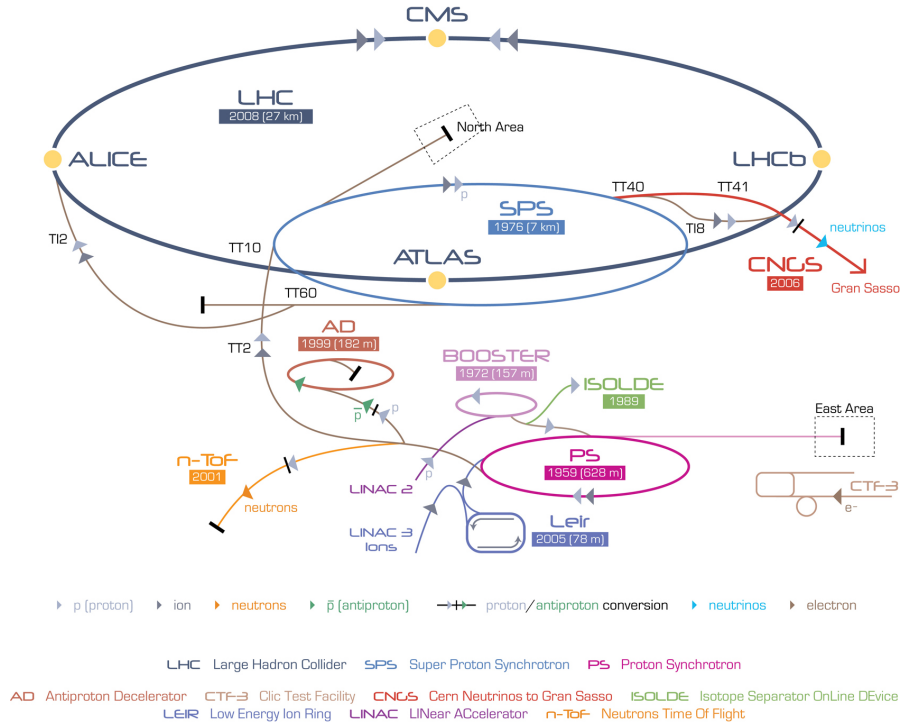

Figure 2.2: The CERN accelerator complex.

collisions. The accelerator complex includes also other facilities like Antiproton Decelerator and the Online Isotope Mass Separator (ISOLDE) and feeds different physics project like the CERN Neutrinos to Gran Sasso (CNGS) and the Compact Linear Collider test area.

2.2.2 Luminosity

For particle colliders is essential to define the *instantaneous luminosity* $\mathcal{L}(t)$, a parameter that links the cross section of a given process with the number of expected events N per unit of time in the collisions.

$$\frac{dN_{event}}{dt} = \mathcal{L} \cdot \sigma_{event} \tag{2.1}$$

where σ_{event} is the cross section for the process under study.
By integrating the 2.1 one can obtain the number of events for a process with given cross section in a known amount of time:

$$N_{process} = L \cdot \sigma_{process} \tag{2.2}$$

where L is called *integrated luminosity*,and it is defined as:

$$L = \int \mathcal{L} dt \tag{2.3}$$

Since the beams which take part to the collisions,at the LHC, have the same energy, the distribution of protons in the transverse directions with respect to the beam could be considered Gaussian. Therefore it is possible to write the instantaneous luminosity as a function of the accelerator parameters in the following way:

$$\mathcal{L} = \frac{N_b^2 n_b f_{rev} \gamma_r}{4\pi \epsilon_n \beta^*} F, \tag{2.4}$$

where:

- N_b is the number of particles per bunch,
- n_b the number of bunches per beam,
- f_{rev} the revolution frequency,
- γ_r the relativistic Lorentz factor $(1 - v^2/c^2)^{-1/2}$,
- ϵ_n the normalized transverse beam emittance,
- β^* the beta function at the collision point, is a measure of how narrow the beam is at the IP,
- F the geometric luminosity reduction factor due to the crossing angle at the interaction point.

The geometric luminosity reduction can be written as follow:

$$F = \left(1 + \left(\frac{\theta_c \sigma_Z}{2\sigma^*}\right)^2\right)^{1/2} \tag{2.5}$$

where θ_c is the full crossing angle of the beams at the interaction point,σ_z is the bunch length and σ^* is the transverse RMS beam size at the interaction point.
For the 2016 operating period, the values of the above parameters are summarized in Table 2.1.

2.2.3 LHC Run 1 and Run 2

In September 2008, the LHC officialy starts to work with its first injections of beams. Unfortunally due to a faulty resistance of an interconnection between two magnets an accident occurred, and the LHC was forced to stop for more two years for repairs and

Parameter	Value
N_b	1.6 $\times 10^{11}$
n_b	1.6 2200
$f_{rev}[MHz]$	40 MHz
γ_r	4260
$\epsilon_n[\mu m]$	2.5
$\beta^*[m]$	0.6
$\theta_c[\mu rad]$	290
$\sigma_z[cm]$	9.4
$\sigma^*[\mu m]$	19

Table 2.1: The LHC machine parameters.

for introducing further safety measures. The operation restarted in 2010 at center of mass energy of $\sqrt{s} = 7$ TeV and continued in the 2011; after another short shoutdown, LHC reaches the 8 TeV center of mass energy in the 2012. The 2010-2013 data taking period is referred to as Run 1. In 2013, the LHC stopped for detector upgrade and maintenance operations, and restarted, after a long shutdown, in 2015, with collisions at a centre-of-mass energy of 13 TeV. The phase that started in 2015 until nowadays is referred to as Run 2. The Table 2.2 shows values of the luminosity delivered by LHC, the luminosity recorded by CMS and the luminosity certified as good for physics analysis. Furthermore, the total luminosity delivered by LHC and collected by CMS during 2017 and a comparison of the luminosity of pp collision data collected in Run 1 and Run 2 are shown In Figure 2.3(a) and in Figure 2.3(b).

Period	$\sqrt{s}$ [TeV]	LHC delivered [fb^{-1}]	CMS Recorded [fb^{-1}]	CMS Validated [fb^{-1}]
Run 1 (2010)	7	40.22×10^{-2}	40.76×10^{-2}	34.68×10^{-2}
Run 1 (2011)	7	6.13	5.55	5.09
Run 1 (2012)	8	23.30	21.79	19.79
Run 2 (2015)	13	4.22	3.81	2.39
Run 2 (2016)	13	40.82	37.76	35.92
Run 2 (2017)	13	49.98	45.14	41.86

Table 2.2: The cumulative luminosity delivered by LHC, recorded by CMS and certified as good for physics analysis, starting from 2010 to 2017.

2.2.4 LHC experiments

As mentioned, the beams interact at four different points along the ring, where the largest experiments are located in order to study the the products of the high-energy collisions. As illustrated in Figure 2.2 in a clockwise order there are

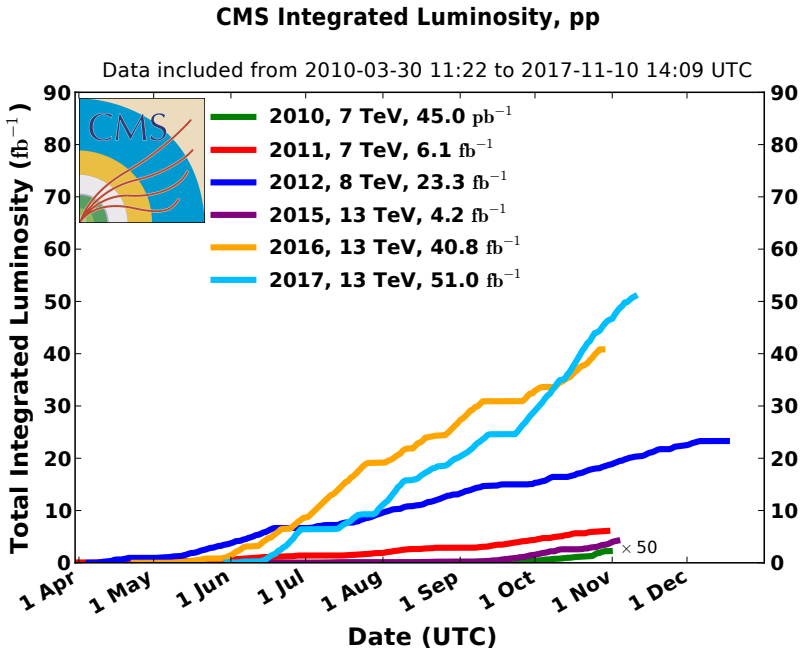

(a) Cumulative luminosity versus day delivered to CMS during stable beams for pp collisions at nominal center-of-mass energy. This is shown for data-taking in 2010 (green), 2011 (red), 2012 (blue), 2015 (purple), 2016 (orange), and 2017 (light blue).

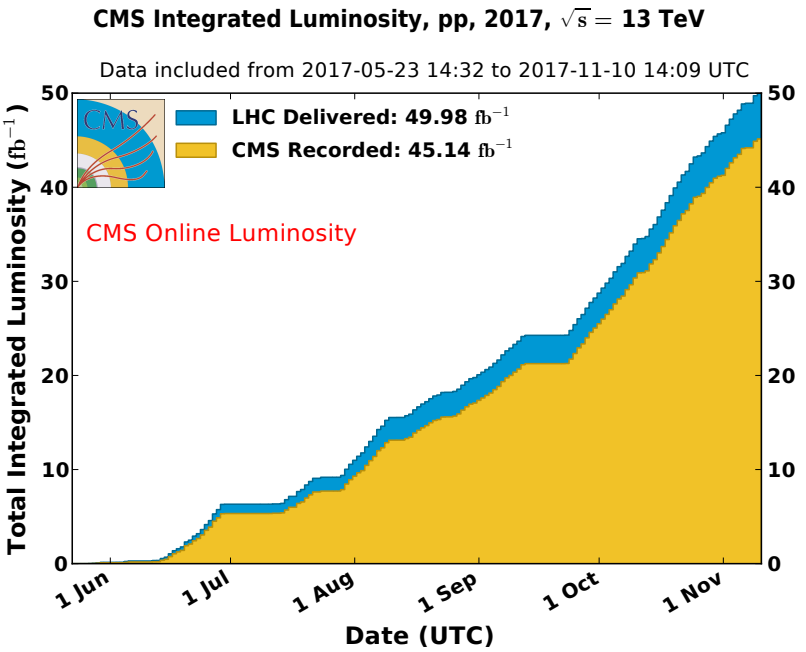

(b) The plot show the measured luminosity delivered by the LHC to CMS (blue) and recorded by CMS (orange) during stable beams and for proton-proton collisions at a 13 TeV center-of-mass energy in 2017.

- ATLAS: *A Toroidal LHC ApparatuS* with a lenght of 44 m, a diameter of 25 m and a weight of 7000 tons, it is the biggest experiment at LHC. ATLAS is a general-purpose detector specialized in provide precision measurements of SM, the search and the study of the Higgs boson, and mechanisms due to new physics.
- ALICE: *A Large Ion Collider Experiment* it studies ion-ion collisions experiment and its main aim is to explore the initial state of matter. High energy densities are required to form the quark-gluon plasma, which are achieved by colliding lead ions with $\sqrt{s} = 2.67$ TeV at a peak luminosity of $L = 10^{27}$ cm^{-2}s^{-1}.
- CMS: *Compact Muon Solenoid* it will be described in section 2.3.
- LHCb: *LHC-beauty* an experiment built for the study of the b quark properties, its production mechanism, and to probe rare decays of B mesons including the CP -violating processes. LHCb requires clean events with low pile-up while it is not necessary a large amount of luminosity, and it works with asymmetric beams: one is at the LHC full energy (up to 7 TeV) and the other is at the injection energy (450 GeV).

2.3 CMS experiment

The Compact Muon Solenoid experiment is one of the four great experiments at the LHC. Its main goals are to provide measurements at the TeV energy scale from the Standard Model, such as high precision tests of QCD, flavour physics electroweak interactions and the Higgs boson properties, and to explore new physics beyond SM trought searches in channels like Supersymmetry or searches for new vector bosons and quarks (the so-called exotic searches).
The huge superconducting solenoid, from which it takes its name, generates an internal magnetic field of 3.8 Tesla, about 10.5 times the magnetic field of the Earth. With his 14.000 tonnes for 15.00 meters of diameter and 28.7 meters of length 2.3, CMS is one of the biggest physics experiment in the world but it could be considered also as a compact design experiment since its relatively small size comperded to its weight. The CMS experiment was designed not only to be compact but also to afford some challenges of high energy studies and also of an high luminosity collider such as LHC; the detector has to be capable of operating in a high radiation environment, to distinguish different process and different particles of interest from the background, to allow analyses where the signal to background production rate is strongly disfavoured even by several orders of magnitude.
In order to cope with these challenges, CMS was designed to have:

- **Geometrical coverage:** full azimuthal coverage is required to make hermetic the detector. In this way it is possible the kinematic closure of the events in the

plane transverse to the beams collision plane and therefore the measurement of the missing transverse energy (MET) is possible.

- **Trigger efficiency:** the huge number of events that happen in a bunch crossing has to face with limitations in the bandwidth at which data can be transferred to the storage facilities; this implies a reduction which has to be performed with an electronic triggering system.
- **High granularity and good time resolution:** the huge amount of particles to be detected requires detectors with high granularity in order to avoid, or at least to limit, the overlap between different particles of the same event or coming from interactions in the same bunch crossing. The effect of this pile-up can be reduced also using fast electronic elements.
- **Radiation endurance:** the high-rate radiation implies consequence on the detectors which have to sustain a severe amount of radiation, and have to maintain good performances over the course of several years of data taking.

These challenges were coped with by making use of a system of several sub-detectors to identify different particles on a wide energy and angular coverage, and influenced the choice of detector layout and geometry that is made up of cylindrical layers coaxial to the beam pipe, called barrel layers, and two endcaps that ensure hermitical closure of the detector.

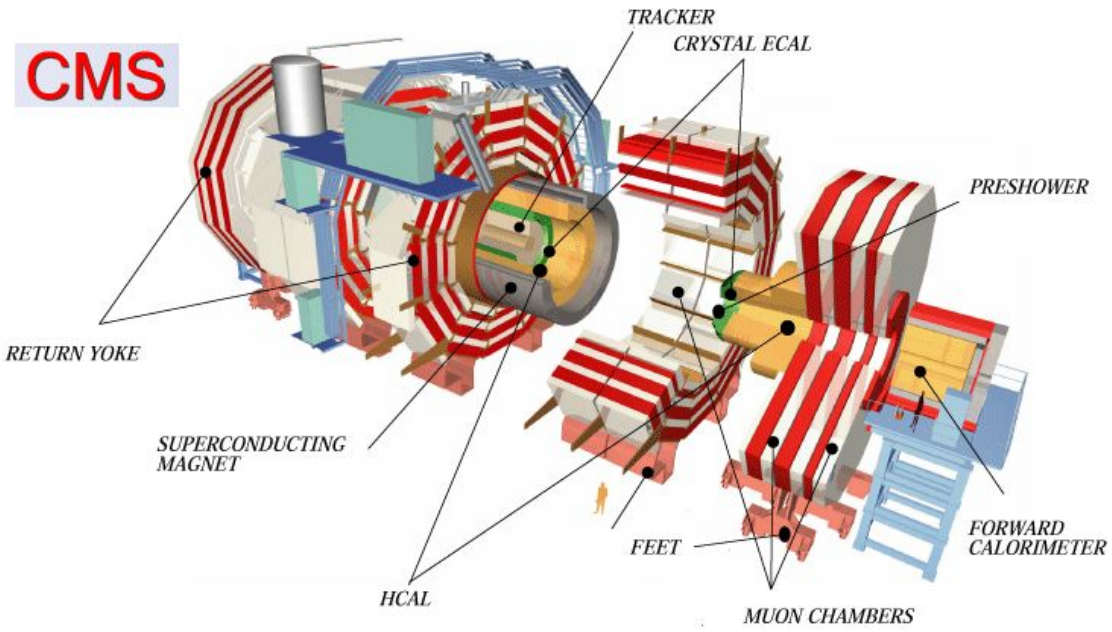

Figure 2.3: CMS 3D view.

2.3.1 The coordinate frame at CMS

The CMS reference frame is defined as follows:

- The coordinate frame is centred at the nominal interaction point;
- $x - axis$ points to the centre of the LHC;
- $y - axis$ points upwards, perpendicular to the LHC plane;
- $z - axis$ along the anticlockwise-beam direction.

By exploiting the cylindrical symmetry of the detector it is possible to introduce a pseudo-angular reference system, as seen in Figure 2.4, defining: the radial distance from the $z - axis$, r; the azimuthal angle taken from the $x - axis$, ϕ; and the rapidity defined as:

$$y = \frac{1}{2} \ln \left(\frac{E + p_z c}{E - p_z c} \right) \tag{2.6}$$

where E is the energy of the particle and p_z is the particle momenta along the $z-$axis. Since for $E \gg m$, the pseudorapidity, η, comes close to the rapidity, it is used for ultra relativistic particles and it is defined as

$$\eta = -ln \left(tan \frac{\theta}{2} \right) \tag{2.7}$$

where θ is the polar angle.

The pseudorapidity and the rapidity are both natural variables for describing angles in a system where the initial momentum along the $z-$axis is unknown, and differences in rapidity Δy (or in pseudorapidity$\Delta \eta$ in the limit of massless particles), are invariant under boosts along the $z-$axis.

Referring to this system, the distance between two particle direction can be written as another Lorentz invariant variable, in the following way:

$$\Delta R = \sqrt{(\Delta \phi)^2 + (\Delta \eta)^2} \tag{2.8}$$

Usually two important variables are p_{T} and E_{T}, referred to the Cartesian system, they are respectively the transverse momentum and the transverse energy, defined as:

$$\vec{p_T} = \sqrt{\vec{p_x}^2 + \vec{p_y}^2} \tag{2.9}$$

$$E_T = E \sin \theta \tag{2.10}$$

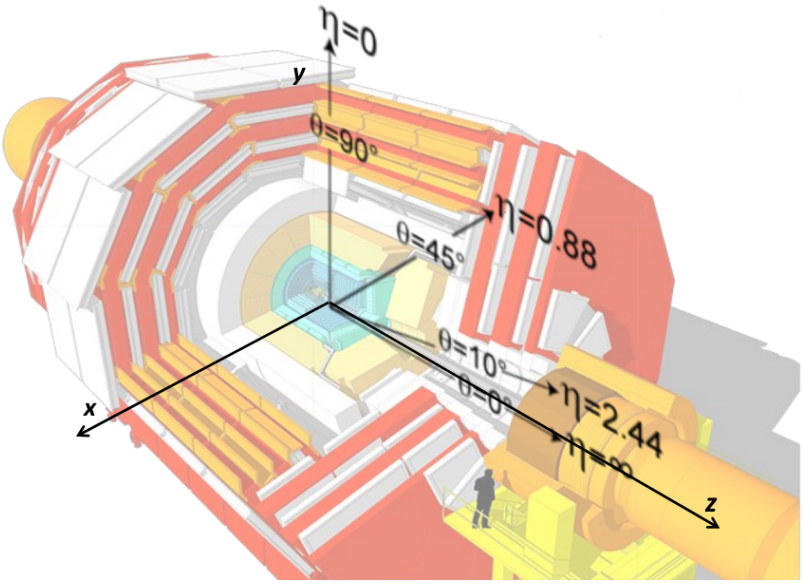

Figure 2.4: The CMS coordinate system: The $x-axis$ points to the centre of the LHC, the $y-axis$ points upwards, perpendicular to the LHC plane, and the $z-axis$ along the anticlockwise-beam direction. In this figure plot of pseudorapidity as a function of the polar angle, θ, is shown: as angle increases from zero, pseudorapidity decreases from infinity.

2.3.2 The CMS subdetectors layout

The CMS detector is made up of several layers of detectors centred on the interaction point as can be seen in Figure 2.5. From the inner to the outer part of the detector we have:

- **The Tracker System**: designed to provide a precise and efficient measurements of the trajectories of charged particles emerging from the LHC collisions. The CMS tracker consist of a silicon pixel detector and a silicon strip detector.
- **The Electromagnetic Calorimeter (ECAL)**: for accurate electron and photon energy measurement.
- **The Hadronic Calorimeter (HCAL)**: crucial for energy measurements of jets and missing energy, provides energy measurements for charged and neutral hadrons. Thanks to the tracker it manages to distinguish between charged and neutral.
- **The Superconducting Solenoid**: the coil generating an internal constant magnetic field of 3.8 Tesla in the direction of the beam axis.
- **The Return Yoke**: interspersed with the Muon system, sustain the structure and it is studied to allow magnetic field lines of the solenoid.

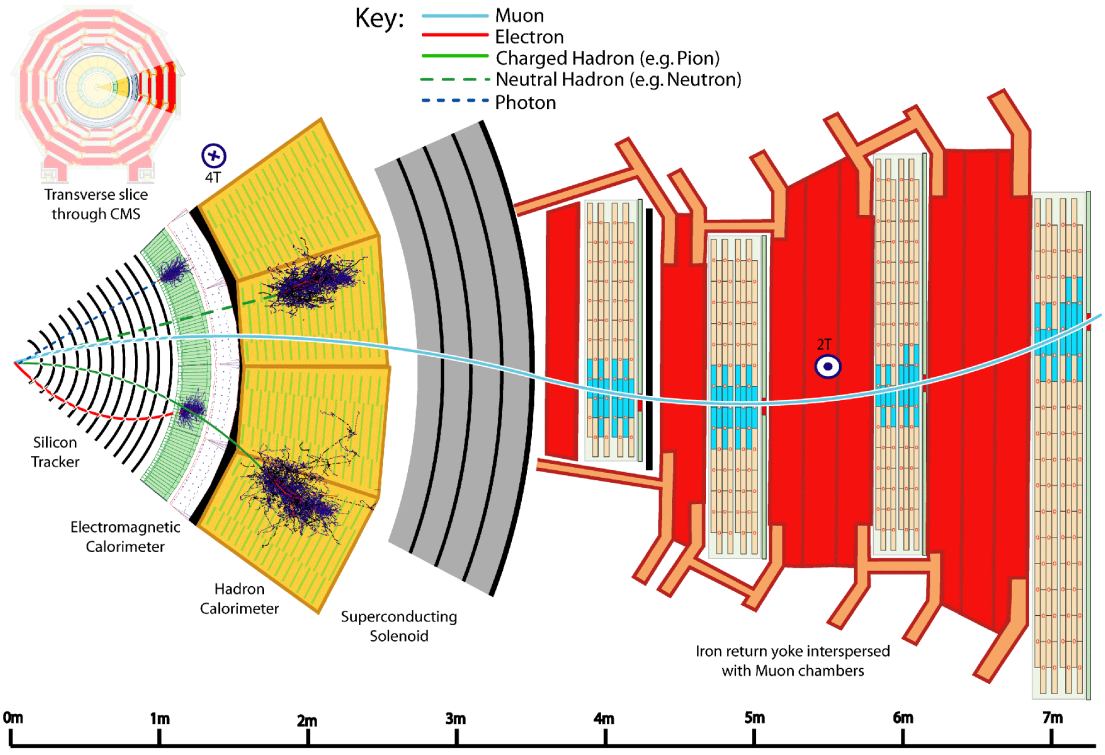

Figure 2.5: The CMS subdetectors system.

- **The Muon System**: designed to have the capability of reconstructing the momentum and charge of muons over the entire kinematic range of the LHC. CMS uses three types of particle detectors for muon identification:
  - Drift Tube detectors;
  - Resistive Plate Chambers;
  - Cathode Strip Chambers.

2.3.3 The Tracking System

At the high energy experiments, the trackers are required to have some general properties in order to satisfy the purpose of the entire apparatus. The Tracker must provide a robust tracking and detailed vertex reconstruction within a strong magnetic field; it must be sufficiently radiation hard in order to guarantee the good functioning of all subdetectors during the full data taking period of the experiment; it has to ensure a fast sub-detectors response to allow an efficient event online trigger. Satysfing these properties the CMS Tracker produces high quality seeds for the track reconstruction algorithm offline, it allows to identify unambiguously tracks coming from multiple vertices and is used to perform fast tracking online in the high level trigger (HLT) for primary vertex reconstruction, electron/photon identification, muon reconstruction, tau identification,

and b-tagging. The CMS Tracker [28, 29] has a radius of 1.25 m and a length of 5.8 m, and its acceptance is of $|\eta|$ <2.5. It is composed by two main sub-detector elements:

- The Pixel vertex detector system, Figure 2.6: it provides a two-dimensional measurements of the hit position in the module planes, ensuring an accurate measurement of the vertex positions.
- The Silicon Strip (SST), Figure 2.7: used for accurate track reconstruction.

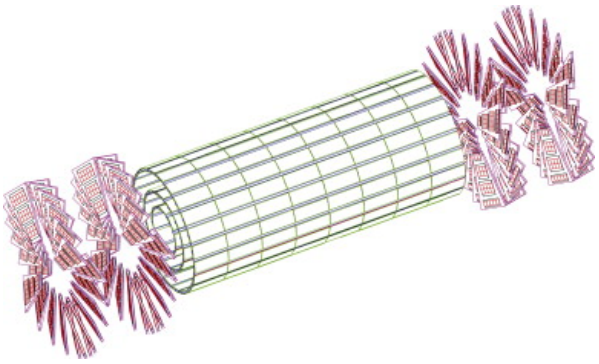

Figure 2.6: Schematics of CMS Silicon pixel system.

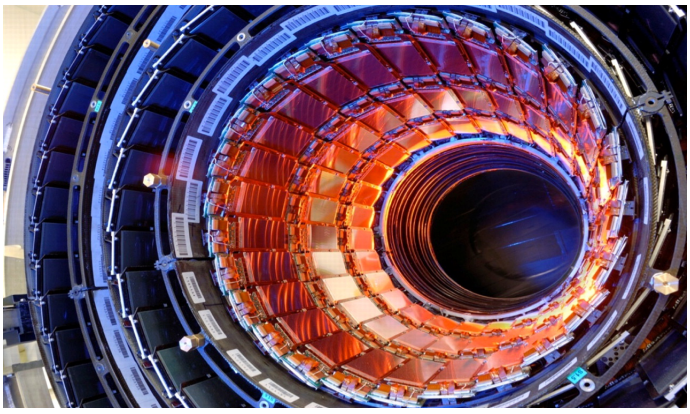

Figure 2.7: Tracker showing silicon strips detectors in the barrel module.

These two detector technologies are arranged in concentric cylindrical volumes, as shown in the Figure 2.8. The region closest to the beams interaction point is surrounded by 150μm $\times$ 150μm silicon Pixel detectors; they are disposed in a barrel geometry, in the central rapidity region, with three barrel layers (BPIX) and with two forward/backward disks (FPIX) at higher values of the rapidity into end-caps. The intermediate region, going outwards with respect to the interaction point, is consist of 4 barrel of Silincon Strip layers parallel to the beam axis, Tracker Inner Barrel (TIB), and 3 disks of Silincon Strip at each end of the TIB, the Tracker Inner Disks, called TID. The outer volume, outside the TIB/TID, is also composed by SST but with different thick and pitches and

is called Tracker Outer Barrel, TOB. At both ends of the TOB are located other Tracker EndCaps named TEC+ and TEC-, whose signs indicate the location along the $z-$axis. The region covered by TEC corresponds to the $|\eta| < 2.5$.

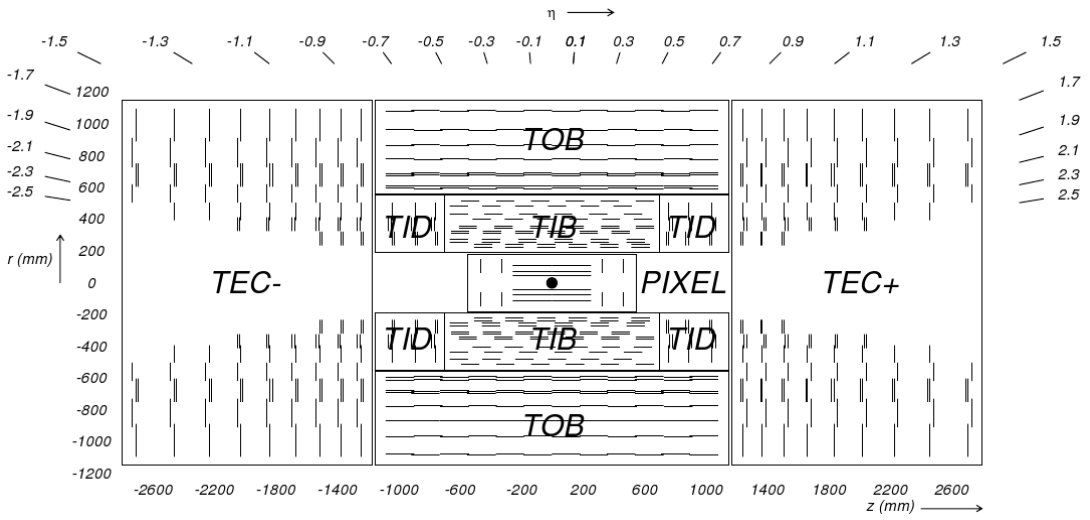

Figure 2.8: Schematic view of the CMS tracker.

2.3.4 The Electromagnetic Calorimeter

The Electromagnetic Calorimeter (ECAL) [31] is an hermetic and homogeneous calorimeter made up of 75848 scintillating crystals of Lead tungstate ($PbWO_4$). The design and the material choosen guarantee some important properties for a calorimeter: high granularity, fast radiation, radiation hardness, a very compact structure thanks to the high density of crystals (8.28 g/cm^3), a small Molière radius (2.2 cm) and a short radiation length (0.89 cm). As shown in Figure 2.9 the crystals are arranged in a barrel section, forming the ECAL barrel (EB), and two endcaps, the ECAL EndCaps EE+ and EE- (the sign indicates the location along the $z-$axis). The barrel covers the pseudorapidity range $|\eta|$ <1.479 and each crystal in this part has a cross-section of ∼22×22 mm^2 and 23 cm corresponding to 25 X_0. The endcap part cover a pseudorapidity range from 1.479 to 3.0, in order to allow high precision energy measurements up to $|\eta|$ =2.6. In this region crystals have a cross-section of ∼30×30 mm^2 and 22 cm corresponding to 24.7 X_0 each; they are grouped in 36 units of 1700 crystals each, called supercrystals. The entire ECAL sturcture is maintained at the temperature of 0.1 ℃ in order to maximize the yield of light. The photons are collected by photodetectors, converted to an electrical signal and then amplified in two different ways: in the barrel region, avalanche photodiodes (APDs) are used, since they are able to provide the higher gain in presence of high transverse magnetic field; in the endcaps the amplification is provide by vacuum phototriodes (VPTs) since the radiation in this region is too high to use

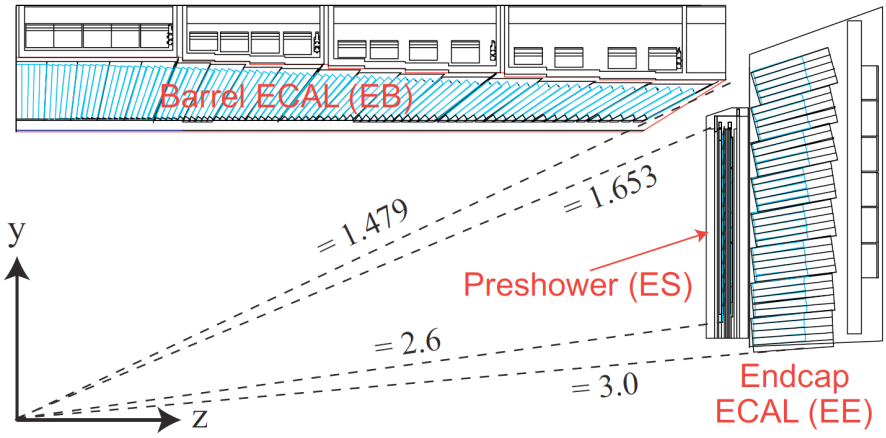

Figure 2.9: Schematic view of the CMS ECAL.

silicon photodiodes.

The ECAL is also equipped with a Preshower detector, installed in front of the endcaps,for three main aim: to increase precision in the position determination, to distinguish between single high-energy photons and close pairs of low-energy photons and therefore to prevent false signals. It is made up of two lead planes followed by silicon sensors strip arranged in a grid in order to cover the crystal endcap.

One of the most important property of an ECAL is the energy resolution that can be parametrized as:

$$\left(\frac{\sigma}{E}\right)^2 = \left(\frac{a}{\sqrt{E}}\right)^2 + \left(\frac{b}{E}\right)^2 + (c)^2 \tag{2.11}$$

where:

- a represents the stochastic term: it takes in account the statistical fluctuations of the signal in the shower containments such as fluctuations in the number of primary particles and/or the number of photons which includes fluctuations in the shower containments collected by a photomultiplier;
- b is the noise term which contains the contributions from electronic noise and PU energy, negligible at low luminosity;
- c is the constant term which takes in account the fluctuations of the longitudinal leakage, of intercalibration errors and of leakage of energy from the back of the crystal.

At the CMS experiment, the energy resolution of the Electromagnetic Calorimeter is:

$$\left(\frac{\sigma}{E}\right)^2 = \left(\frac{2.8\%}{\sqrt{E}}\right)^2 + \left(\frac{0.12}{E}\right)^2 + (0.30\%)^2\,, \tag{2.12}$$

where E is in GeV.

2.3.5 The Hadron Calorimeter

The main aim of the Hadron Calorimeter (HCAL) [32] is to measure the energy of hadrons such as protons, neutrons, pions, and kaons. It is also addicted to look for hints of almost non-interacting particles such as neutrinos. The HCAL is a sampling calorimeter that allows to determine the position, energy and arrival time of particles and it is also an hermetic calorimeter to ensure the capture of every emerging particle from the collisions. The HCAL is composed by alternating layers of active material, fluorescent scintillators, and of absorber, layers of brass. The absorber used is the cartridge brass (C26000), composed by 70% Cu and 30% Zn, with a density of 8.83 g/cm^3, aradiation lenght of X_0=1.49 cm and with a nuclear interaction length of λ_I=16.42 cm. The pseudorapidity range covered by the HCAL is $|\eta|$ <3, while, at higher η values, the coverage is provided by the Forward Calorimeter detectors. The Figure 2.10 shows the different sections that compose the HCAL: the Hadron Calorimeter Barrel (HB and HO), the Endcap (HE) and the Forward (HF) section. The HB and HE regions embrace the ECAL respecting the concentric cylindrical geometry. The Hadron Calorimeter Barrel covers the region η <1.3, and is divided into two half-barrel sections, HB- and HB+ in the verse of the $z-$axis. The HB is segmented into four azimuthal angle sectors, and it is made up of alternating plates of brass absorber, with an interaction length of 16.42 cm, and scintillator tiles embedded with wavelenght shifting (WLS) fibers which are spliced into 16 $|\eta|$ sectors. The HE regions cover the pseudorapidity range 1.3< $|\eta|$ <3, and they are designed to managing high particles rates of the order of the MHz. The Forward sections (HF) are located 11.2 m away from the interaction point, covering the pseudorapidity range 3< $|\eta|$ <5.2. It is made up of quartz fibres embedded within a 165 cm long steel absorber and uses a Cherenkov-based technology in order to optimize the performances in a very high radiation area and in a very high rate environment. The Hadron Calorimeter Outer(HO) is composed by additional scintillators that are placed outside the solenoid to ensure adequate sampling depth and to measure late shower development.

2.3.6 The Superconducting Magnet and the Return Yoke

The entire CMS detector is spanned by an uniform magnetic field of 3.8 T provided by the CMS Magnet. It is a solenoid composed by coils of wire working in superconducting conditions. The main task of the Magnet is to bend the paths of particles emerging from LHC high-energy collisions in order to measure the particle's momentum and its charge. The Tracker and the Calorimeters are installed inside the magnet while the Muon System is located outside the coil. The iron Return Yoke is located outside and surrounding the coil in order to ensure uniform field lines in presence of an intense and constant magnetic field. The Return Yoke is composed of alternating layers, interspersed

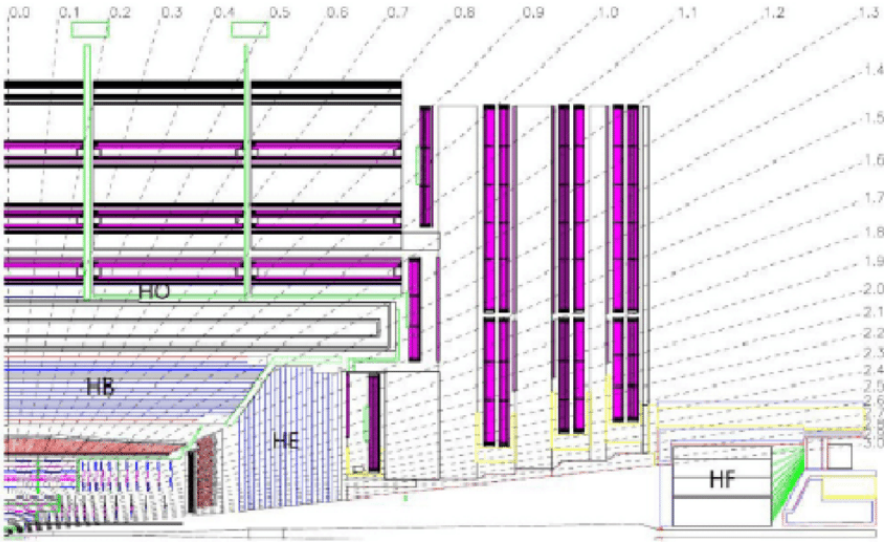

Figure 2.10: View of the CMS detector showing the HCAL subsystems (HB, HE, HO, and HF).

with the muon detectors.

2.3.7 The Muon System

The CMS muon detection system could be considered the flagship of the entire CMS detector. The collection of information of muons caming from protons collision is crucial in particles analyses since they have a clean signature and they appear in final states of many new physics processes. The Muon System provides muon identification, triggering, and momentum reconstruction, and is located in the region outside the magnet. In this outer region, the presence of the return yoke allows the presence of a magnetic field of 1.8 T in the opposite direction with respect to the one inside the magnet. The main reason of the particular position of the Muon System is the fact that muons with energy below the TeV scale lose energy mainly due to ionization, so they can penetrate several meters with few interactions with the matter in the tracker and in the calorimeters. However, muons are charged particles so they leave a trail in the tracking system.
In this way, by combining the hits coming from the muon system and the tracker, it is possible to perform an optimal reconstruction of the muon path and to perform a precise measurment of their momentum. .
The huge volume of the Muon System, compared respect to the innermost detectors, led the choiche of relatively inexpensive materials for the sub-detectors although they have to be reliable and robust to the radiation and they have to provide precise measurment. Following these rules, the Muon System is composed by:

- 250 drift tubes (DTs);

- 549 cathode strip chambers (CSCs)
- 610 resistive plate chambers (RPCs)

The DTs are placed into 4 stations located among the layers of iron yoke plates in the barrel and they cover the pseudorapidity region $|\eta|$ <1.2. The first 3 stations contain 2 layer of 4 chambers each and perform the measure of the muon coordinate in $r-\phi$ bending plane, and one layer of 4 chambers measuring the z coordinate. In order to delete dead spots in the efficiency, every cell of the chambers is separated by a half-cell width with respect to their neighbour. This designed linked with the DTs properties allows to detect passing muon with excellent time resolution, to maximize the efficiency of track reconstruction made by linking together muon hits from different stations and to reject hits coming from the background. Thanks to their good segmentation, their fast response time and their radiation resistance the CSCs have been placed in the endcap regions, where both muon and background rates are higher and the magnetic field is not uniform. The CSCs cover the range 0.9< $|\eta|$ <2.4 and the cathode strips of each chamber provide position measurements in the $r-\phi$ bending plane. The anode wires allow to measure the pseudorapidity and the beam-crossing time of every muons. Since the Muon System covers the $|\eta| < 2.4$ pseudorapidity region, with no acceptance gaps, the muon identification is ensured over the range corresponding to $10^\circ < \theta < 170^\circ$. The offline reconstruction efficiency of simulated single-muon samples is $95-99\%$, while it drops in the transition region between the DT and CSC systems, around $|\eta| = 1.2$. The multiple-scattering caming from the inner detectors influences the offline muon momentum resolution of the standalone muon system. This resolution is about 9% for small values of η and for up to the hundreds of GeV for transverse momenta while at higher energies $\sim$ TeV, it varies between 15% and 40%, depending on $|\eta|$. In this way, a global fit of the muons momentum, performed using also the inner tracker, will improves the momentum resolution by an order of magnitude at low momenta, while at high values (1 TeV) of momentum the resolution is about 5%. The identification and triggering system is completed with the RPCs structure. Those detectors have fast response, excellent time resolution but weaker position resolution than DTs and CSCs. In the barrel region, two RPC layers are located on each of the first two stations of DTs and one layer is on the last 2 stations of DTs: this solution make possible the use of the trigger algorithm even for low-p_{T} tracks that may stop before reaching the outer 2 stations. In the endacap region, one layer of RPCs is installed on each of the 3 DTs stations. The overral design of RPCs, DTs and CSCs station allows the use of trigger coincidences between stations to reduce the background, an improvment of time resolution for bunch crossing identification, and the optimization of p_{T} resolution.

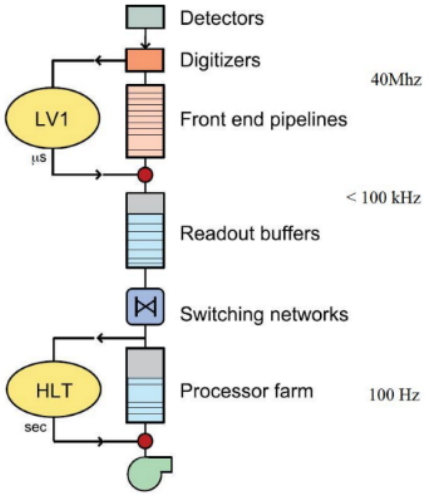

Figure 2.11: Architecture of the CMS trigger system, including the ingoing/rates relative to each step.

2.3.8 The Trigger System

The high interaction rates at the LHC(see also Section 2.2.2) makes impossible to store the entire amount of informations caming from all the LHC collision events. For this reason is required to select only the potentially interesting events and reduce the rate to a few hundred "events" per second, that allows the reading out and storing of the related informations.
The event selection is performed by the Trigger System in two steps called Level-1 (L1) Trigger [34] and High-Level Trigger (HLT) [35]. The L1 Trigger is implemented with a wide use of programmable electronics, while the HLT uses a software filter system working on about one thousand of commercial processors. Together they manage to reduce the rate by a factor of 10^6. The Figure 2.11 shows the scheme of the overall architecture of the CMS Trigger system. The Level-1 Trigger system has the hard task to provide a fast and automatic event selection by looking for simple signs of interesting physics (e.g. particles with a large amount of energy). The trigger is based coarsely segmented data caming from the calorimeters and the muon system; the high-resolution data are holded in pipelined memories in the front-end electronics while the trigger is working. The Level-1 trigger is organized in local, regional and global components. The local components are also called Trigger Primitive Generators (TPG), and they are based on energy deposits in calorimeter trigger towers and track segments or hit patterns in muon chambers. The regional triggers use a pattern logic to sort trigger objects like electron, photon or muon, in limited spatial regions. The global components, Global Calorimeter and Global Muon Triggers, determine the highest-rank calorimeter and the

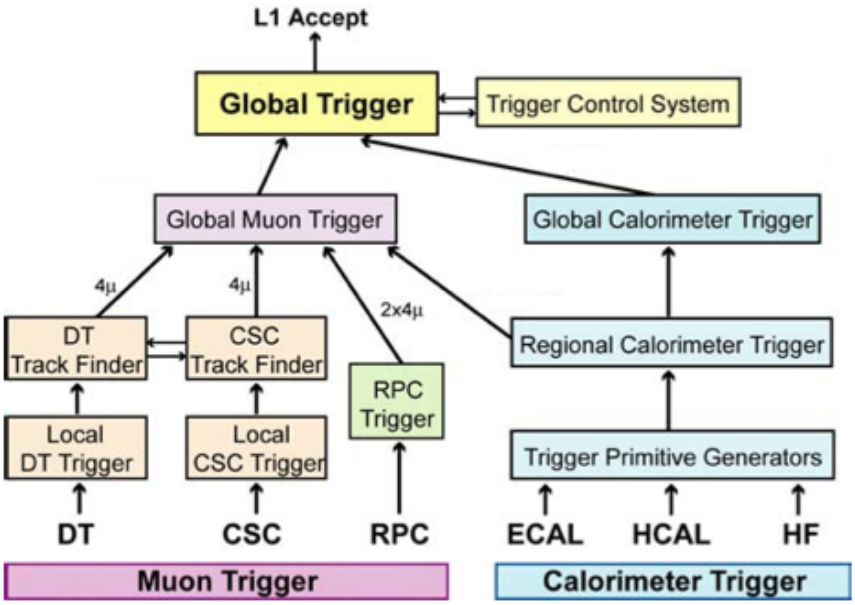

Figure 2.12: Architecture of the Level-1 Trigger.

number of trigger objects across the entire experiment and transfer them to the Trigger Control System (TCS). This last module takes the final decision based on algorithm calculations and on the readiness of the sub-detectors and the DAQ. The Level-1 Accept (L1A) decision is communicated to the sub-detectors through the Timing, Trigger and Control (TTC) system. The architecture of the L1 Trigger can be seen in Figure 2.12. The allowed L1 Trigger latency, between a given bunch crossing and the distribution of the trigger decision to the detector front-end electronics, is 3.2 μs. The processing must therefore be pipelined in order to enable a quasi-deadtime-free operation. The final decision to reject or to accept an event is taken by the HLT. It has the access to the complete read-out data and it perform an analysis based on the physical objects present in the event. For example events with bad vertices reconstruction or events with final objects caracterized by a too low momenta are immediatly refuses by the HLT

Chapter 3

Vector Like Quarks in BSM theories

The Standard Model, as introduced in Chapter 1, is not able to explain all observed phenomena in high energy physics. However, several promising theories have been presented in order to provide predicitions and solve the issues that SM fails to solve. Thanks to the high collisions energy and the high luminosity reached by the LHC during the Run 2, the data taking during this period, could provides some hint to falsify or confirm several of these Beyond the Standard Model (BSM) theories. One of the main issues unsolved by the SM, as mentioned in Chapter 1, is the so-called "hieracy problem" or naturalness. Two broad scenarios will be described that concretely realize naturalness: a Composite Higgs model and theories with extra-dimensions.

The Composite Higgs models propose that the mechanism which protect the Higgs mass is dimensional transmutation: the Higgs is supposed to be a composite state of a new-strongly interacting sector. In this case, the dimensionality of the Higgs mass operator can be $d > 4$, and in this scenarios there are no problems in explaining why the Higgs mass is relatively light.

The Extra Dimension theories predict the existence of extra dimensions beyond the usual space-time $(3 + 1)$ in order to solve, among others, the hieracy problem and the unification of the fundamental interactions. Both theories, Compositness and extra-dimensional, introduce new particles, among which an important role is played by the so called "Vector-Like Quarks" (VLQs). Such particles are coloured fermions, also often referred as "top-partners", that manage to help in solving with the hierarchy problem, as they help to the computation of the radiative corrections to the Higgs mass.

3.1 The Composite theories

The Standard Model introduces elementary particles to explain how the matter is made up and to explain the interactions that occur between them. However, in order to solve some of the open issue of the SM, several theories propose that elementary particles are instead made up of other, yet unknown, constituents which are strongly coupled forming new heavy resonances. For example, in the QCD theory the flavour chiral symmetry of the Lagrangian is broken spontaneously, generating three massless scalar pseudo-Goldstone bosons. A further explicit symmetry breaking is operated by the quark masses, and gives mass also to the pseudo-Goldstone bosons which is, however, much lighter than other mesons in QCD. The three pseudo-Goldstone bosons are the $\pi^{\pm}$ and π^0 particles, which are not elementary but composed of a quark-antiquark pair.

3.1.1 The Composite Higgs boson theory

The Composite Higgs Model was proposed by Georgi and Kaplan [37, 38] in 1984 and it treats the Higgs boson as a composite pseudo Nambu-Goldstone Boson (pNGB), i.e. it is a bound state of a new strongly interacting sector. The model is fully explained in [39] and in [40]. In order to focus the attention on the purpose of this thesis, it will reported a general model shown in [41], in which the Higgs particle is realized as a pNGB associated to the breaking $SO(5) \to SO(4)$ at a scale $f > v$, where v is the vacuum expectation value (VEV) as explained in Chapter 1.
Let start considering a vector Ψ_L of $SO(5)$ which is an enlarged SM left-handed doublet q_L for the third familly of quark (t, b). The $SO(5)$ breaks up as $(2, 2) + 1$ under a $SU(2)_L \times SU(2)_R$ transformation. The SM gauge group $G_{SM} = SU(2)_L \times U(1)$ is here given by $SU(2)_L$ and the σ_3 of $SU(2)_R$ of the new fixed subgroup $SO(4) = SU(2)_L \times SU(2)_R \subset SO(5)$.
The complete fermionic spinor of the third quark generation is:

$$\Psi_L = \left(q = \begin{pmatrix} t \\ b \end{pmatrix}, X = \begin{pmatrix} X^{5/3} \\ X \end{pmatrix}, T\right)_L \Psi_R = \left(t, X = \begin{pmatrix} X^{5/3} \\ X \end{pmatrix}, T\right)_R$$

The right handed states have been introduced in order to give mass to the new fermions. To obtain the correct values of the electric charges, the hypercharges of the new particles have been fixed. The spinor representation is obtained by requiring that the physical left handed b-quark is a true doublet of $SU(2)_L$ and not an admixture of doublet and singlet.
The Yukawa Lagrangian of the fermion sector is made up of an $SO(5)$ symmetric mass term for the top (this guarantees the absence of quadratic divergences in the contribution

to m_H) and the most general gauge invariant mass terms for the VLQ X and T:

$$\mathcal{L}_{top} = \lambda_1 \bar{\psi}_L \phi t_R + \lambda_2 f \bar{T}_L T_R + \lambda_3 f \bar{T}_L t_R + M_X \bar{X}_L X_R + h.c. \tag{3.1}$$

where λ_i with $i = 1, 2, 3$ are the coupling costants, ϕ is the scalar 5-plet containing the Higgs Field and M_X is the mass of the heavy X quark. Using a convenient definition of the various parameter we can rewrite the $\mathcal{L}_{top}$ in the form:

$$\mathcal{L}_{top} = \bar{q}_L H^c(\lambda_t t_R + \lambda_T T_R) + \bar{X}_L H(\lambda_t t_R + \lambda_T T_R) + M_T \bar{T}_L T_R + M_X \bar{X}_L X_R + h.c. \tag{3.2}$$

where$\phi = \binom{H}{H^c}$. Is simple to note that 3.2 is equal to 3.1 up to rotations that preserve all the quantum numbers. Employibg a diagonalization og the mass matrix we obtain the physical fields, that allow to evaluate the fisical quantities. In order to highlight the usefulness of this model and of the introduction of the VLQs, let evaluate the contribution to m_H due to the top loop, and check the absence of the quadratically divergent term. Starting from the potential

$$V = \lambda(\phi^2 - f^2)^2 - A^2 f^2 \vec{\phi}^2 + B f^2 \phi_5, \tag{3.3}$$

where $\vec{\phi}$ are the first four components of ϕ, it can be shown that the Higgs boson mass is controlled by the A parameter, that is by the $SO(5)$-breaking term, $m_H = 2v\sqrt{A}$ for big λ. This relation is fine since if everything were simmetric under $SO(5)$, the Higgs particle would be a massless Goldstone boson. Finally, the divergent part of the one loop correction to A, setting $v = 0$ for simplicity, is evaluated as:

$$\begin{aligned} \delta A &= -\frac{12 f^2}{64\pi^2}\lambda^2 \left(\frac{M_X^2}{f^2} - 4(\lambda_1 + \lambda_3) - 2\lambda_2^2 \right) log\lambda^2 = \\ &= -\frac{3}{16\pi^2 f^2}(\lambda_t^2 + \lambda_T^2)\left(M_X^2 + M_T^2 \left(\frac{2}{1 + \lambda_T^2/\lambda_t^2} \right) \right) log\lambda^2. \end{aligned} \tag{3.4}$$

One can note that there is no quadratic divergence and M_X and M_T take now the role of the cutoff Λ in the original top-loop contribution. In order to avoid that the logarithmic term could produce a δm_H of the same order of the weak-scale expectation value v, and led again to a naturalness problem, the M_X and M_T cannot be too much above 2 TeV.

To obtain the relation $f < v$, some finetuning on the parameter A and B are required. This can be evaluated by the logarithmic derivative:

$$\Delta = \frac{A}{v^2}\frac{\delta v^2}{\delta A} \approx \frac{v^2}{f^2}.$$

Assuming $f = 500GeV$, which means a $\approx 10\%$ of finetune, the "naturalness cutoff" of this model is:

$$\Lambda \approx \frac{4f\pi}{\sqrt{N_g}} \sim 3TeV,$$

with the number of Goldstones $N_g = 4$.

As just shown, the simplified model reported in this Chapter solve the naturalness problem of the SM trought the introduction of the VLQs. However, different problems arise in composite theories like this, such as the fact that usually they hardly pass the electroweak precision tests, or they fail to explain the origin of fermion masses. A full descrption of the properties and of the fenomenology of the VLQs will be given in the Section 3.3.

3.1.2 The Composite Top quark theory

Several models propose that the top quark is not an elementary particle and, similarly to the Composite Higgs, they predict that it is a composite state. In this kind of models, the SM particles get their masses by mixing themselves with composite states thanks to the new strong sector. Thanks to the large mass of the top quark, this models expect that the top quark havs a sizeable admixture of the composite state and therefore it can show the properties of Compositeness. However , the results of the electroweak precision test strongly constrains the possibility of a composite left-handed top, favoring models the focus on right-handed composite top quarks [42].

3.2 Extra Dimension theories

In order to provide an explanation of the gravitational interaction and to describe a subsequent unification between all the fundamental forces, several Extra Dimensions theories have been proposed [43]. The first theory has been developed by the two physicists Theodor Kaluza (1885, 1954) and Oskar Klein (1894, 1977) and it introduces a fifth dimension beyond the usual four of space and time to unify of gravity and electromagnetism.

In particular, Kaluza has worked on a purely classical extension of general relativity to five dimensions [44], while Klein exported Kaluza's classical theory a into a quantum field theory [45]. Klein built his theory around the idea that the fifth dimension is curled and its geometry takes the form of a circle of radius of 10^{-33}.

The introduction of two or more extra dimension is also proposed by the Arkhani-Hamed, Dimopoulos and Dvally (ADD) theory [46]. It is based on the idea that gravity could propagate in these predicted extra dimension, leading to the weakness of the gravity compared to all the other fundamental forces. The extra-dimension proposed should have a size between a millimiter and 10^{-18}m.

In order to solve the hierarchy problem of the Standard Model, in 1999, Lisa Randall

and Raman Sundrum have proposed two models describing the world in term of a 5 dimensional Universe with a warped-geometry. According to the first model (RS1) [47], the extra dimension has a finite size and it is composed by two branes linked each other; the second model (RS2) [48], predict a similar space-time structure, but suggest that one of the two branes is placed infinitely far away to the other, and so there is effectively one brane left in the model. The two branes are called: the Plackbrane, where the gravity is a relatively strong force, and the Tevbrane, that is our home with the SM particles. Since in these models the spacetime is extremely warped, the Plankbrane has positive brane energy while the Tevbrane has negative brane energy.
Several theories based on these fundamental model have been developed: the theories which follow the ADD model are called "*The Large Extra Dimension Theory*"; the ones that let inspiration from the RS models are called "*The Warped Dimensions Theory*".

3.3 Phenomenology of VLQs

The Vector-Like Quarks (VLQ) are spin 1/2 fermions that transform as triplets under the colour gauge group. Their left- and right-handed chiral components have the same transformation properties under the weak-isospin gauge group.
Altough the vector-like quarks are considered amongst the most relevant signatures of physics beyond the Standard Model (BSM), there is still no evidence of their existence. In an Nambu-Goldstone Higgs context, as explained in Section 3.1.1, the VLQs are required to induce electroweak breaking and explain the observed lightness of the Higgs at the TeV scale.
The main effect of the introduction of Vector-Like Quarks is the stabilization of the Higgs boson mass. From a more phenomenological point of view, there are several properties that makes unique the Vector-Like Quarks. First of all, since they have the same colour charges of the analogous SM quarks, they are the simplest example of new coloured fermions that would appear beyond the Standard Model. Moreover since they do not receive their masses from Yukawa couplings to a Higgs doublet, their mass term can be directly inserted into the Lagrangian without breaking the gauge symmetry. This feature makes them unique since their coupling to the Higgs field is unrelated to their mass. Going forward throught their properties, there are no constraints on the existence of vector-like quarks arising from the measured production cross section of the Higgs, because the contribution to loop-induced Higgs boson couplings, i.e. ggH and $\gamma\gamma H$, is suppressed by the heavy quark mass.
Since VLQs can mix with the Standard Model quarks and then modify their coupling to the Z, W, and Higgs bosons, their inclusion into the SM is the simplest way to break the the Glashow-Illiopoulos-Maiani mechanism allowing the flavour-changing neutral currents at the tree-level.

The VLQs come out in four different forms depending on their charge as can be seen in the Table 3.1. The VLQs could be grouped into multiplets of $SU(2)_I$, in particular

VLQ	**Electric charge**
X	+5/3
T	+2/3
B	-1/3
Y	-4/3

Table 3.1: Charge assignment for VLQs.

singlets, doublets or triplets of $SU(2)_I$ as can be seen in the Table 3.2. The VLQs can

Multiplet	**Hypercharge**
Singlets	
(T)	+2/3
(B)	-1/3
Doublets	
(X,T)	+7/6
(T,B)	+1/6
(B,Y)	-5/6
Triplets	
(X,T,B)	+2/3
(T,B,Y)	-1/3

Table 3.2: Hypercharge assignment for Vector-like quarks in different $SU(2)_I$ representations.

be represented as following:

$$\begin{array}{ll} \textit{Singlets} & T^0_{L,R}, B^0_{L,R} \\ \textit{Doublets} & \left(XT^0\right)_{L,R}, \left(T^0B^0\right)_{L,R}, \left(B^0Y\right)_{L,R} \\ \textit{Triplets} & \left(XT^0B^0\right)_{L,R}, \left(T^0B^0Y\right)_{L,R} \end{array}$$

where T_L and T_R are the left- and right- handed components, while T^0 indicates weak eigenstates. For X and Y the weak and the mass eigenstates coincide since they cannot mix via the mass matrix due to their exotic charges. All the VLQs multiplets can be taking into account in the extensions of the Stadard Model, assuming that no other new

physics modifies the electroweak observables. For example when new fields $T^0_{L,R}$ are added to the SM, the resulting up−type mass eigenstates (u, c, t, T) might then contain non-zero components of the $T^0_{L,R}$ fields; this could lead into a changing of the couplings with the Z boson. Since the mixing is proportional to the ratio between the mass of the SM and the VLQ, is not difficult to assume that the VLQs mix only with the third generation of quarks, while m_Q/m_{VLQ} is negligible for the first two generations. These considerations, added to the large Yukawa coupling of the top quark, highlights a link between the top quark and new physics related with electroweak symmetry breaking and the fermion mass hierarchy.
The signatures of VLQ have been analysed both in model independent, signature-based, ways as well as in specific model-dependent scenarios. For the latter case, the possibility of flavour changing neutral currents processes for VLQs interactions lead to a wide range of possible final states, that are still analysed in detail in order to drive the experimental search of these new states.

3.3.1 VLQ production mechanisms

The VLQs production cross section in pp collisions strongly depends on their mixing with SM quarks, particularly on the square of the couplings to the W or Z bosons. The production mechanisms of VLQ can be grouped in the following way:

- Pair Production: it is dominated by QCD production via gluons. Since the cross section of this kind of process only depends on the mass of the new fermion, it is model independent and it decreases for higher masses due to PDF suppression. The process of pair production through QCD interactions is completely analogous to pair production of SM top quarks, and only depends on α_S and the mass of the heavy quark:

  $$gg, q\bar{q} \rightarrow Q\bar{Q}$$

  where $Q = T, B, X, Y$. A small contribution of electroweak gauge bosons, subleading in terms of cross section, is still present. This contribution leads to interesting channels when the production is reached trought charged current process :

  $$\bar{q}q' \rightarrow W^+ \rightarrow \bar{T}X, \bar{B}T, \bar{Y}B$$

  $$\bar{q}q' \rightarrow W^- \rightarrow T\bar{X}, B\bar{T}, Y\bar{B}$$

  However, the electroweak cross sections are strongly suppressed for large masses and their effects on the search strategies can be safely neglected. Rather than the pair production due to QCD interactions, the cross sections of electronweak pair production are model-dependent as they depend on the representation the VLQ belong to. Another relevant electronweak production process is mediated by the

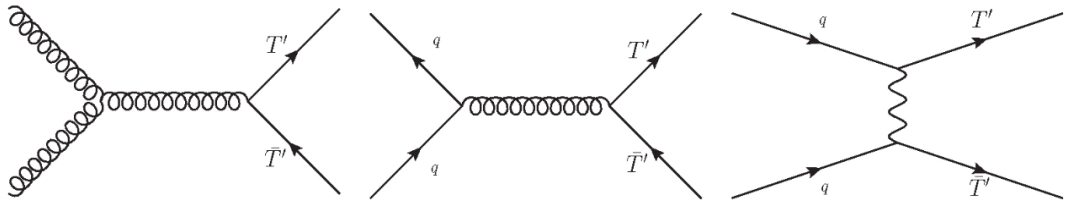

Figure 3.1: Feynman diagrams for pair production of vector-like top quarks via gluon and W,Z or Higgs bosons.

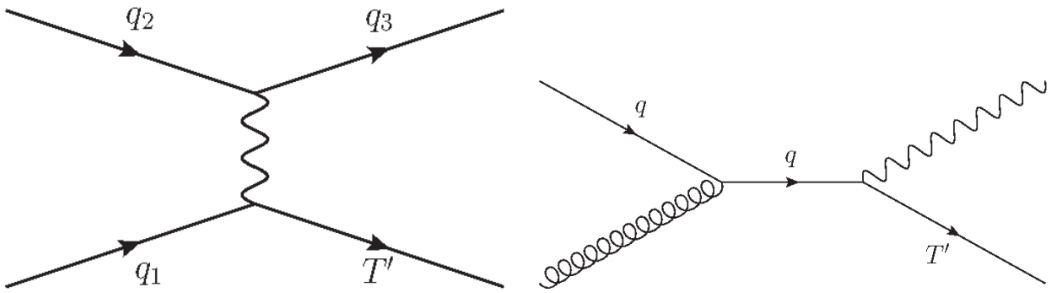

Figure 3.2: Feynman diagrams for single production of Vector-like top quarks.

W or Z or Higgs in the $t-channel$ and is represented by the production of a pair of VLQ, QQ'. This process is completely absent in QCD and, depending on subsequent decays, it can give rise same-sign dileptons or to the following final states: TT, BB, XB, TB, TY with peculiar kinematics. Some Feynman diagrams for pair production of T can be seen in Figure 3.1.

- Single production: it is dominated by electroweak interaction process and it can happen in association with top quarks, jets coming from any light quark or boson (including $W^{\pm}, Z$, and the Higgs H). The single production process depends on the fermion mass, on the mixing parameters with SM particles and on the couplings between the new quarks and the W and Z bosons:

$$qq' \xrightarrow{V^*} qQ \quad V = W, Z$$

The contributions of the Higgs bosons are always suppressed by the small masses of the light quarks. Figure 3.2 shows the single electroweak interaction mediated by a vector boson in t-channel in association with a SM quark and the one mediated by SM quark in association with a vector boson.

The dependece of the pair production and the single production cross sections to the energy is illustrated in Figure 3.3. The plot shows that production process are the dominant process for masses below $m_Q \sim 800 - 1000$ GeV, while they becomes less

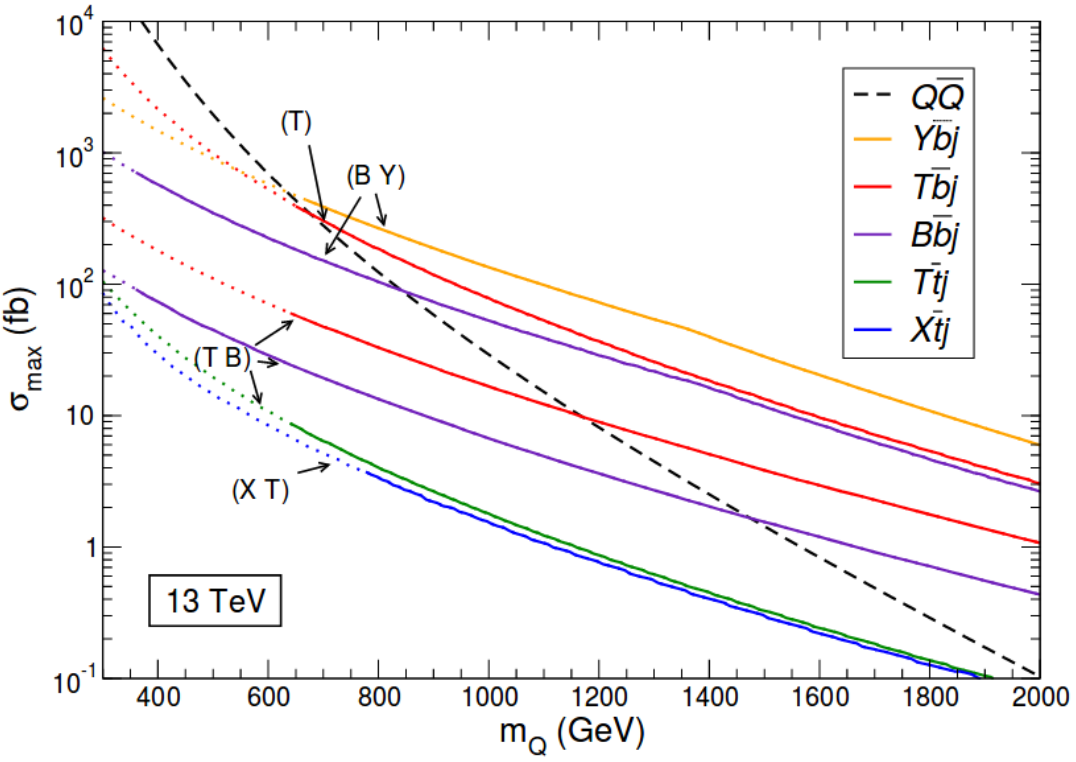

Figure 3.3: Production cross section for Vector-Like Quarks in pp collisions at $\sqrt{s}$ = 13 TeV as a function of their mass, for pair production and for single production in different channels. The black dashed line represents VLQ pair production, while the colored lines represent the singly produced VLQs. The dashed coloured lines correspond to the values of cross section excluded by previous studies.

important for higher masses due to their phase-space suppression.

3.3.2 VLQ decay channels

Vector-like quarks can decay through electroweak interactions into SM particles, also trought flavour-changing neutral currents process since they break the GIM mechanism [36], or into other VLQs. The main allowed decay channels into SM particles generally are:

$$T \to W^+b, Zt, Ht$$

$$B \to W^-t, Zb, Hb$$

$$X \to W^+t$$

$$Y \to W^-b.$$

For the isospin singlets T and B all three decays are possible, the branching ratios for the three channels depend on the mass of VLQ and are not inter-dependent as shown

in the following relation:

$$Br\left(Q \to Wq'\right) + Br\left(Q \to Zq\right) + Br\left(Q \to Hq\right) = 1$$

with $(Q, q, q') = (T, t, b), (B, b, t)$.
The scenario is different for the isospin doublets and triplets. First of all, looking at the small mass difference, the decays to other VLQ are usually suppressed for doublets and triplets, impling that the only allowed decays are into vector bosons and the Higgs boson plus a t or b quark.
In fact, in the case of a (T, B) doublet, the mixing with t and b quarks induces a splitting of VLQ masses and it can be deduced that $m_T \geq m_X$, $m_B \geq m_Y$, and that T quark can be lighter or heavier than B. The depence of the decays channel on the mixing factors of the extended CKM matrix V_{Tb} and V_{tB}. If $V_{Tb} \sim V_{tB}$ implies that the T and B quarks have the same decays as the corresponding singlets but different angular distributions since only the right-handed component of (T, B) couples to the SM quarks. These considerations implies that, due to constraints on the b quark mixing and by mass hierarchy, (i.e. $m_t \gg m_b$, where $V_{Tb} \ll V_{tB}$), the mixing of the heavy quarks with the SM top quark is much stronger and then and the $T \to Wb$ decay is suppressed, as well as $B \to Hb$ and $B \to Zb$.
The possible decays of vector-like quarks are reported in Tables 3.3, 3.4 and 3.5. On the other hand, the branching ratios of the vector-like quarks are model-dependent and they also depend on the heavy quark mass theirselves. In Figure 3.4 are illustrated the branching ratios of the decays of T and B in the case of a VLQ coming from the singlet or doublet of $SU(2)_I$.

Singlets	**Decay modes**
X	W^+t
T	W^+b, Ht, Zt
B	W^-t, Hb, Zb
Y	W^-b

Table 3.3: Allowed decay modes for Vector-like singlets.

3.4 Searches on VLQ at hadronic colliders

Thanks to their rich phenomenology and several decay channels, the VLQs provides a very promising field for searches of physics beyond the Standard Model. Since is

Doublets	**Decay modes**
$\begin{pmatrix} X \\ T \end{pmatrix}$	W^+t Ht, Zt
$\begin{pmatrix} T \\ B \end{pmatrix}$	Ht, Zt W^-t
$\begin{pmatrix} B \\ Y \end{pmatrix}$	Hb, Zb W^-b

Table 3.4: Allowed decay modes for Vector-like doublets.

Triplets	**Decay modes**
$\begin{pmatrix} X \\ T \\ B \end{pmatrix}$	W^+t W^+b, Ht, Zt Hb, Zb
$\begin{pmatrix} T \\ B \\ Y \end{pmatrix}$	Ht, Zt W^-t, Hb, Zb W^-b

Table 3.5: Allowed decay modes for Vector-like triplets.

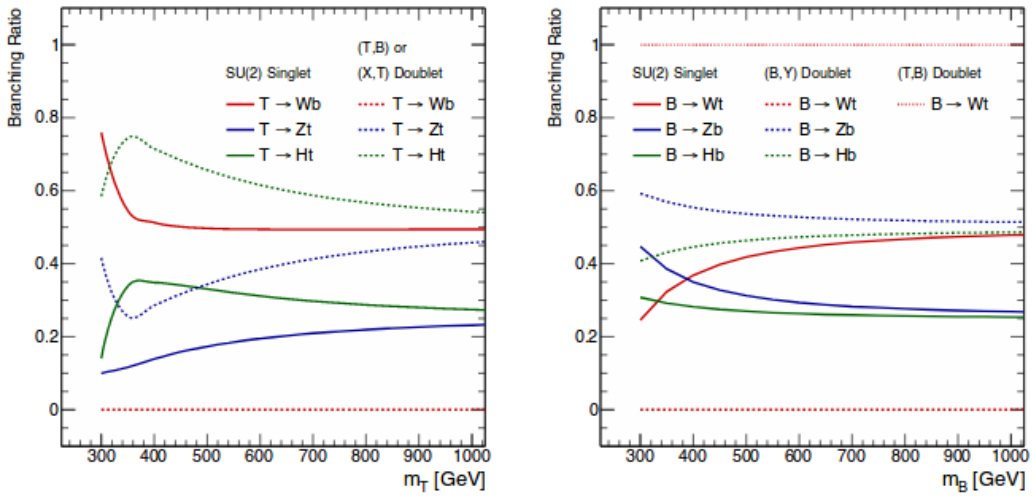

(a) (b)

Figure 3.4: Branching ratio of vector-like top (a) and bottom (b) partners as a function of the heavy quark mass m_T and m_B respectively for isosinglets and isodoublets.

expected that the masses of these particles have to be in proximity of the TeV scale, they are accessible at the powerful particle accelerators and their search is therefore of prime importance. Starting from these assumptions, the Tevatron and the LHC have performed several searches of new heavy states. Although no evidence for the existence of VLQs have been found, limits on the mass and on the branching ratios of the heavy resonance have been provided.

3.4.1 Tevatron searches on VLQ

The two experiments CDF and D0 have made different serches on VLQs with the Tevatron Run II data at $\sqrt{s} = 1.96$ TeV and at a luminosity greater than 5 fb^{-1}.

The D0 Collaboration performed a search for single production of VLQ at 5.4 fb^{-1}. They have searched final states with either W or Z boson and two jets, one coming from the VLQ decay and the other produced in association with VLQ [51]. They also required a leptonic decay of the gauge boson imposing that events must have one lepton from the W or two from Z. A number of jet selected equal or grater than two is also required. Results are given for different values of couplings parameters and branching ratios:

$$\left.\begin{array}{l} m_B > 693 \text{ GeV } at\ 95\% C.L.\ \ BR(B \to Wq) = 100\% \\ m_T > 551 \text{ GeV } at\ 95\% C.L.\ \ BR(B \to Zq) = 100\% \end{array}\right\} \text{no coupling with down quark}$$

$$\left.\begin{array}{l} m_B > 430 \text{ GeV } at\ 95\% C.L.\ \ BR(B \to Zq) = 100\% \\ m_T > 403 \text{ GeV } at\ 95\% C.L.\ \ BR(T \to Wq) = 100\% \end{array}\right\} \text{no coupling with up quark}$$

The CDF Collaboration has performed two analyses on VLQs at integrated luminosity of 5.7 fb^{-1}:

- The search for parily produced heavy particles T decaying to tX where X is an invisible dark matter particle decaying in a full hadronic channel, Ref [49]. The event selection has been made requirinig a number of jet among five and ten and a lot of missing transverse energy. The bounds have been provided for the combination of T and X masses, excluding the presence of T with $m_T \leq 400$ GeV for $m_X \leq 70$ GeV.

- The search for singly produced heavy quarks decaing in Wq, where q is a SM quark of the first generation, Ref [50]. The topology of the decay channel choosen had in the final states a W boson and two jets, where the W is required to decay leptonically. The bounds on the cross section and couplings of VL with SM quarks have been provided for different masses of the heavy quarks, ranging from 300 GeV to 600 GeV.

3.4.2 LHC searches on VLQ

The center of mass energy of $\sqrt{s} = 14TeV$ and the instantaneus luminosity of 10^{34} $\mathrm{cm}^{-2}\mathrm{s}^{-1}$ provided by the LHC Collider allow to study the signatures of single and pair production of VLQs. The ATLAS and the CMS experiment have focused their studies on the searches for 3rd family quark partners. The main serches are based on QCD pair production of charge 5/3, 2/3, and -1/3 partners and their decay into 3rd family quarks and W/Z/H bosons. The analysis strategies have required a lot of different final states: all-hadronic searches, single- or multi-lepton final state, with or without transverse missing energy.

The possible decays that have been studied for the $T\bar{T}$ pair production are:

- The decay of at least one T in Ht and $H \to bb$, or a T in tZ and $Z \to \nu\nu$. The final states required at least one lepton, for the top decay, multi-jets and missing transverse energy [54].
- The search of $T\bar{T}$ both decaying to two Wb pairs with one W decays to leptons and one decays to quarks. Assuming a $Br(T \to Wb) = 100\%$ [55], the analysis was sensitive to the other two decay modes as well as to Vector-like B quarks,.
- The study of the $Zt + X$ final state with exactly one charged lepton and $Z \to \nu\nu$. The analysis has provided an upper limits on the T mass of 0.85 (1.05)TeV, considering the weak-isospin singlet (doublet) model; an upper limit of $m_T \leq 1.16$ TeV for the pure Zt decay mode [56].
- The decay of the T pair to $bWbW \to bl\nu\bar{b}qq'$. Strictly one charged lepton (e or μ), at least 4 jets and a boosted W-tagged are required in the final state. A kinematic fit has been done to fully reconstruct the mass of the T quark, assuming a branching fraction $Br(T \to bW) = 100\%$. The study has provided an upper limit on the T quark mass of 1295 GeV [57].

The searches for $B\bar{B}$ pair production have studied the decays into $tW/bZ/bH$. The analysis strategies follow the same of the $T\bar{T}$ searches. The studies of single production of VLQs have analyzed the following channels:

- production of a T quark decaying to tZ with $Z \to ll$ and $t \to hadrons$ [58];
- production of $B \to bH$ with $H \to bb$ [59].

In the case of the searches for the pair production of charge 5/3 VLQs have been studied the decays into $WtWt$, the analysis covers the single lepton and dilepton same-sign channels [52, 53]. For the single lepton final state have been identified 16 channel using the lepton flavor, the number of b-tagged, W-tagged and top tagged jets while in

the case of the dilepton channel 3 different search regions have been identified based on the lepton flavor.

The most recent results obtained from both the collaborations ATLAS and CMS are reported in the Table 3.6. Moreover in the Figures 3.5 and 3.6 are shown the results of the searches for the single and the pair production of VLQs.

Model	**Observed Exclusion**		**Expected Exclusion**	
	Left Handed	*Right Handed*	*Left Handed*	*Right Handed*
$T \to tZ$	1.2 TeV	-	1.25TeV	-
$B \to Hb$	-	-	-	-
$X_{5/3}X_{5/3} \to tWtW$	1.30TeV	1.28TeV	1.33TeV	1.30 TeV
$T\bar{T} \to bW/tZ/tH$	1.20 TeV	1.28TeV	1.16TeV	1.24TeV
$B\bar{B} \to tW/bZ/bH$	1.17TeV	0.94TeV	1.13TeV	0.92TeV

Table 3.6: VLQ limit summary table.

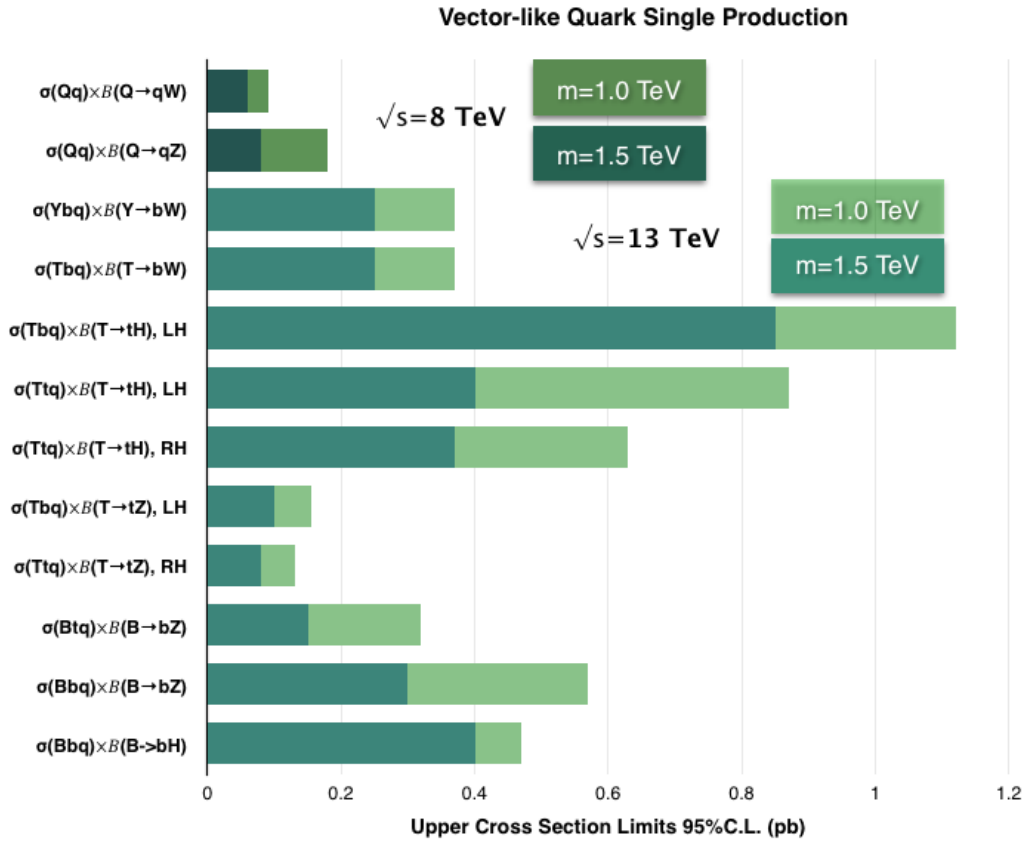

Figure 3.5: Summary of the results of the VLQs single production.

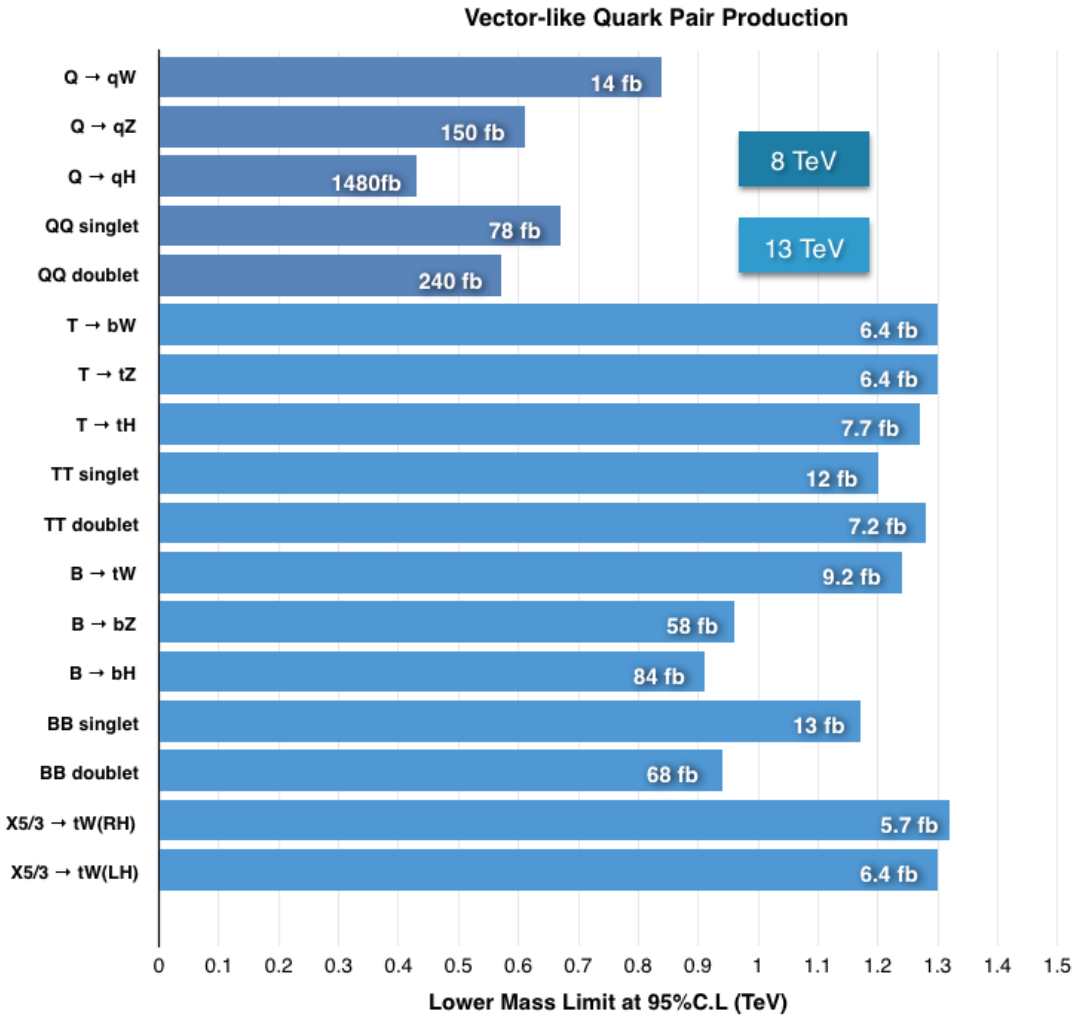

Figure 3.6: Summary of the result of the VLQs pair production.

Chapter 4

Physics objects selection and reconstruction

The main aim of this thesis is the search for the single production of a heavy vector-like quark T of charge + 2e/3. The decay channel under study is the $T \rightarrow$ tZ with a top quark decaying laptonically and the Z boson decaying to a pair of quarks, using 41.5 fb^{-1} of pp collision data delivered by the LHC at a centre-of-mass energy of $\sqrt{s} = 13$ TeV and collected by the CMS experiment in 2017. The Feynman diagram of the analyzed signal process is shown in Figure 4.1. Due to the high centre-of-mass energy, the Z

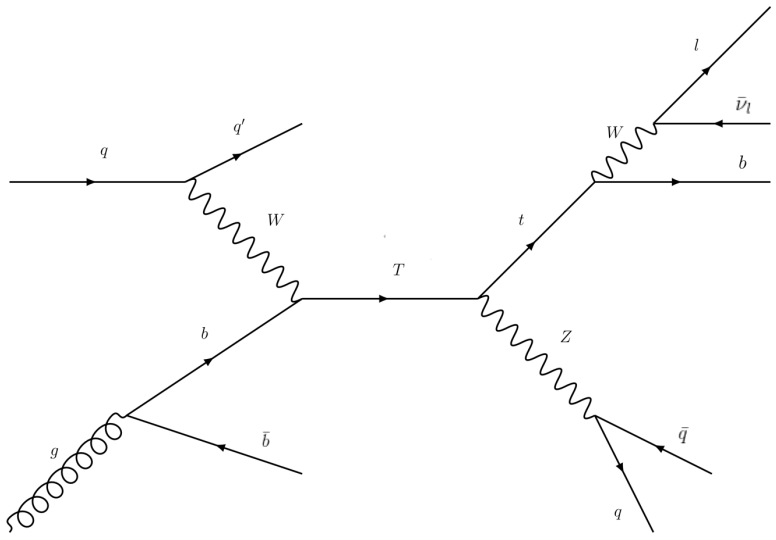

Figure 4.1: Feynman diagram for signal.

boson is produced with an high Lorentz boost, and this implies that its decay products are highly collimates. The choice of this decay channel is justified by several reasons:

- the high branching ration of $Z \rightarrow q\bar{q}$ respect all the other decay channel, that leads to an high statisctics;

- the presence of a low QCD background thanks to the requirement of the leptonic decay of the quark top $t \to Wb \to l\nu b$;
- it is not covered yet. It as high potential for re-interpretation in any signature with a top quark and a Z boson. The hints of the existence of VLQs must be searched in every possible and useful decay channel so this is a good motivation for this analysis;

The search for a vector-like quark T is performed looking for missing transverse energy, jets compatible with the signature of a Z or H boson, as well as b-jets and forward jets.

4.1 Physics objects selection

All stable particles produced through the pp collisions such as electrons, muons, photons, charged hadrons and neutral hadrons, are reconstructed and identifiyed by the Particle Flow (PF) algorithm [61], that uses the informations coming from all CMS sub-detectors to provied an optimal identification and determination of the particles, to determine their direction and their energy and to reconstruct their 4-momenta. In particular the Particle Flow is an interactive tracking algorithm that links togheter blocks of elements that are compatible, e.g. the track of a charged particle is linked with calorimeter deposits if the extrapolated position of the track is within the cluster boundaries. Starting from a PF candidates list, the reconstruction is done in the following order:

- *muons*: a track that is reconstructed from the hits both in the tracker and in the muon system, gives rise to a PF muon. If such particle is identified, the corresponding tracks are removed from the block;
- *electrons*: if the link between a charged-particle track and one or more ECAL clusters are compatible, the PF algorithm reconstructs an electron. The tracks and the cluster are then removed from the list;
- *charged hadrons*: the remaining tracks that are linked to ECAL and HCAL clusters are used to reconstruct charged hadrons. Morover, the momentum is directly evaluated by the tracker and than corrected using the informations coming from the calorimeters;
- *photons and neutral hadrons*: clusters in the ECAL that are not compatible with charged tracks give rise to PF photons; in a similar way, unmatched clusters in HCAL are identified as neutral hadrons ;

These particles are then used to reconstruct high-level objects: to build jets that preserve energies and directions of thethe quarks and gluons they are coming from; to

determine the missing transverse energy which gives an estimate of the direction and energy of the neutrinos and other invisible particles; to estimate the charged lepton isolation with respect to other particles; to identify and to reconstruct taus from they decay products; to understand the flavour of the quarks or the gluons that create jets throught the hadronisation process.

4.2 Primary vertices

A best fit to the intersection of tracks reconstructed in the tracking system is used to reconstruct the vertices; morever, they are defined as good vertices if they satisfy the following requirements:

- more than 4 degrees of freedom in the fit
- less than 2 cm away in the x-y plane from the interaction point
- less than 24 cm away in the z direction from the interaction point

Those positions guarantee that the reconstructed vertices are in the luminous region. In the thesis only events where at least one good primary vertex is found are selected: A vertex is defined as primary vertex if it gets the highest value of the sum of the squared transverse momentum of all the tracks associated with it.

4.3 Leptons

The final state addressed by this analysis is characterised by the presence of an high-energetic lepton in the final state before hadron decays. The major source of background arises from $t\bar{t}$ events and electroweak processes. The contribution from $t\bar{t}$ events arises mostly from decays where a lepton is not identified, therefore a lepton veto is applied. This veto does additionally avoid overlap in the signal dilepton final state. The identification and isolation criteria used are described in the following sections.

4.3.1 Electrons

The reconstruction of electron candidates starts from tracks of electromagnetic clusters with hits both in the Tracker and in the ECAL: they are obteined by using a Gaussian Sum Filter (GSF) fit algorithm [62], taking into account the possible emission of bremsstrahlung photons in the silicon tracker. Moreover, the electrons are selected according to the "veto" selection criteria defined in CMS according to identification criteria with high efficiency but low purity [63]. It is primarly based on the relative isolation

variable, $I^{\mathrm{e}}_{\mathrm{rel}}$, defined as:

$$I^{\mathrm{e}}_{\mathrm{rel}} = \frac{I^{\mathrm{ch.h}} + \max[(I^{\gamma} + I^{\mathrm{n.h}} - \rho \times A), 0]}{p_{\mathrm{T}}}, \tag{4.1}$$

where ρ is the average energy density not clustered in jets, measured event-by-event, by the cone area A, p_T is the transverse momentum of the electron candidate, I^{γ},I^{ch-h} and I^{n-h} are, respectively, the sums of the scalar transverse momentum of the photons, the charged hadrons and neutral ones. The sums are computed in a cone of $\Delta R = \sqrt{(\Delta\phi)^2 + (\Delta\eta)^2} = 0.3$ around the electron direction. The *veto electrons* used requires $I^{e}_{rel} < 0.198 + 0.506/p_T$ for electrons revealed in the ECAL barrel and $I^{e}_{rel} < 0.203 + 0.963/p_T$ in the endcaps, and it hase an average efficiency of -$\sim$ 95%

4.3.2 Muons

The track of the muons are reconstructed in two step: in the tracking system using a technique based on Kalman filter algorithm, and in the muon chamber, combining hits from the drift tubes(DT), cathode strip chambers(CSC), and resistive plate chambers(RPC).
In particular the informations coming from the two the detectors are used in the following ways:

- The *Global Muon reconstruction*: it performs a best-matching search, again based on the Kalman filter technique, between each track reconstructed in the Muon Chamber, called *stand-alone muon*, and the tracks reconstructed in the inner tracking system, referred as *inner tracks*. The track that accomplishes this request is selected as a Globan Muon. This metod is especially useful to reject the background of muons coming from hadronisation and from the particles that interact around the beam pipe and at large transverse momenta because it improves the momentum resolution.

- The *Tracker Muon reconstruction*: it can be considered a complementary approach to the Global Muon reconstruction and it looks for tracker tracks that match at leat one hits deposited in the muon chambers; these particular tracks are identified as Tracker Muons. Since the criteria for tagging a tracker muon are very loose, further requirements are used in the analysis contexts. This method is very efficient for the identification of low momentum ($p < 5$ GeV) muons, that may not leave enough hits in the muon stations for a Global Muon reconstruction.

Two identification criteria defined in CMS [64] are used in this thesis. Muons which pass the "loose" criteria and that have a $p_{\mathrm{T}} > 30$GeV and an $|\eta| < 2.4$ are vetoed. In order to study the trigger efficiency, muons with "tight" selection requirements and with an

$|\eta| < 2.4$ and $p_{\mathrm{T}} > 60$ GeV/c are usedt. Both criteria are based on the I^{μ}_{rel} variable that, in the muon case, is defined as:

$$I^{\mu}_{\mathrm{rel}} = \frac{I^{\mathrm{ch.h}} + \max[(I^{\gamma} + I^{\mathrm{n.h}} - 0.5 \times I^{\mathrm{PU}}), 0]}{p_{\mathrm{T}}}, \tag{4.2}$$

where $I^{\mathrm{ch.h}}$, I^{γ}, $I^{\mathrm{n.h}}$, and I^{PU} are respectively, the scalar p_{T} sums of the charged hadrons, photons, neutral hadrons, and charged hadrons associated with pileup vertices. The sums are computed in a cone of $\Delta R = \sqrt{(\Delta\phi)^2 + (\Delta\eta)^2} = 0.4$ around the muon direction. To pass the loose criteria muons are required to have an $I^{\mu}_{rel} < 0.25$ while for tight criteria $I^{\mu}_{rel} < 0.15$; the corrisponding efficiencies are $\sim 98\%$ and $\sim 95\%$ respectively.

4.4 Jets

The events coming from pp collisions at LHC always contain partons in the final state. However, since quarks and gluons decays trough hadronization process, they can only be undirectly observed trough the showers of particle created by themselves and detected in the tracking chambers and calorimeters. The interaction between constituent partons and the showering into stable particles is well described from perturbative theory and hadronization model. In Figure 4.2 the evolution can be observed of a jet from hard interaction to observable energy deposits.

The jet reconstruction algorithm employed is based on the clustering all the PF candidates reconstructed. First of all, the Charged Hadron Subraction (CHS) correction [65] is applied on the group of hardest particle in order to remove the energetic contribution coming from the pile-up interaction. CMS provides several kind of clustering algorithm:k_{T}, Cambridge Aachen(CA) and anti-k_{T}. In this thesis the last one is used [66]; it is based on two variables: the distance d_{ij} between the particle or PF candidate i and the particle j, and d_{iB}, the distance between the particle i and the beam, ß

$$d_{ij} = min\left(\frac{1}{p^2_{T,i}}, \frac{1}{p^2_{T,j}}\right)\frac{(\Delta R)^2_{ij}}{R^2}$$

$$d_{iB} = \frac{1}{p^2_{T,i}}$$

where:

$$(\Delta R)^2_{ij} = (\eta_i - \eta_j)^2 + (\phi_i\phi_j)^2 \,.$$

R is radius parameter used to define the portion of solid angle covered by the jet, $\eta_{i(j)}$ is the pseudorapidity of the particle $i(j)$, $\phi_{i(j)}$ is the angle in the transverse plane of the particle $i(j)$ and p is a simple parameter. The inclusive clustering process proceeds by evaluating the smallest of the two distances and if it is a d_{ij} recombining entities i and

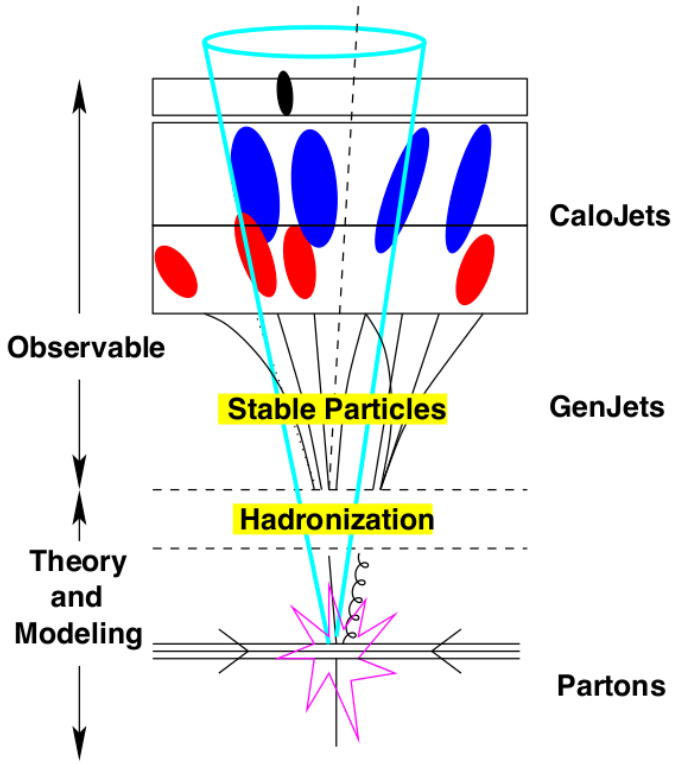

Figure 4.2: Pictorical view of the evolution of a jet.

j, while if it is d_{iB} calling i a jet and removing it from the list of entities. The distances are recalculated and the procedure repeated until no entities are left. Moreover, two different classes of jets are reconstructed: jets with a cone parameter of $R = 0.4$ are named *narrow jets* (AK4), while jets clustered with a cone parameter of $R = 0.8$ are defined as *fat jets* (AK8). The latter are considered for the selection of boosted top quark candidates or Z/H boosted candidates while the former are used to select a forward light-flavour jet produced in association to T quark production. A set of identification criteria ("loose" working point), proviede by the CMS dedicated group that works on Jets and MET, are applied on jets of both collections. It is important to stress that a reconstructed particle can enter both classes of jets, so a disambiguation between jet candidates has to be done a posteriori on the reconstructed categories. AK8 and AK4 jets are selected if they have a p_{T} more than 300 GeV and 30 GeV respectively. Moreover, different corrections are applied while calculating the energy of the jets at various level. Jet Energy Corrections (JEC) scaled the jet energy by a factor that describes the detector response depending on the transverse energy and the pseudorapidity of the jet [69]. The corrections pass trough the following steps:

- removal of the energy due to the contribution of pileup events;
- correction of the response of jets in order to achieve a flat distribution in η;

- correction of the jet response for p_{T}.

The correction factor Jet Energy Scale (JES) is calibrated on the η, p_{T}, energy density, and area of the jet; the Jet Energy Resolution (JER) for the simulated jets is degraded to reproduce the resolution observed in data.

4.4.1 Z and H tagging

Highly boosted Z and H candidates decaying hadronically are reconstructed from AK8 jets and identified according to the jet Z tagging working point based on PUPPI inputs. The mass of the AK8 jet is required to be consistent with the Z and the H masses, so the jet mass computed using the SoftDrop algorithm [70, 71] must satisfy the condition: $65 < M_{SD} < 145$ GeV. For both the boson a a p_{T} grater than 200 GeV is required. Moreover, in order to select only the AK8 that decays hadronically, the angular separation betwwen the Z/H boson and the lepton is required to be $\Delta R(Z/H, lepton) > 1.2$

4.4.2 b-Tagging

Two jet tagged as coming from b quark (called "$bjets$") are expected in the final state under study in this analysis: one coming from the t quark decay and one from the gluon splitting and acting as a spectator. Therfore, an optimal reconstruction of this identities is needed. In this thesis the Deep Combined Secondary Vertex (DeepCSV) algorithm [74], provided by CMS, has been used for identification of jets originating from b quarks. It is uses deep machine learning algorithm and it is based on the reasonable consideration that long living particles, such as B-hadrons, travel a considerable distance from the primary vertex before their decay happens. The Impact Parameter (IP), Figure 4.3, is the variable used to define the distance between the two vertices. It is a Lorentz invariant and so it is also invariant with respect to changes of the long lived particle kinetic energy. The typical value for the B-hadrons corresponds to $c\tau \sim 450\ \mu m$ that, in CMS, can be measured with precision between 30 μm and hundreds μm. Since the uncertainty can be of the same order of magnitude as the IP, so the significance $IP/\sigma(IP)$ is a better observable and takes into account also the resolution. It can be positive or negative, depending on the signs of the scalar product of the IP-vector and the jet direction. It is expected to be symmetric around 0 for decays with short life and mostly positive for particles with longer lifetime. Starting from these considerations, the AK4 jets are considered stemming from a b quark if they have a pseudorapidity located in a central region $|\eta| < 2.4$ and if the discriminant value of the DeepCSV provides a misidentification pobability less than 10% (defined as a “Loose” working point by the CMS Collaboration). Moreover,in order to avoid that one or more b-jets coming from the possible decay channel $Z/H \to b\bar{b}$ were reconstructed as narrow jet, the separation

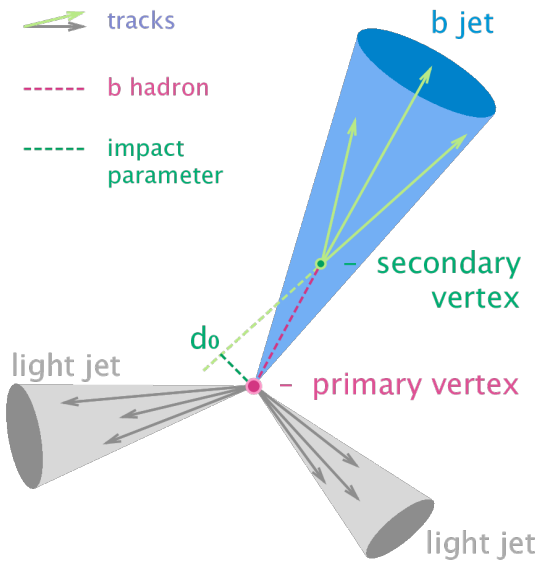

Figure 4.3: Impact Parameter.

distance between b-tagged jet and Z

$$\Delta R(bjet, Z) = \sqrt{(\eta_b - \eta_Z)^2 + (\phi_b - \phi_Z)^2}$$

is required to be larger than 1.2. An interesting feature of the direct production of a single vector-like T quark is the presence of an additional jet that is produced in the forward direction. Forward jets are reconstructed as AK4 jets using the same selections and corrections as defined above, but have 2.4< $|\eta|$ <5.0 and p_{T} >30 GeV.

4.5 Missing transverse energy

The energy imbalance is computed, at the LHC as at any hadron collider, in the transverse view only. Indeed only the longitudinal momentum of the whole proton can be measured, the one of the individual colliding partons is not known, and with large precision can be assumed to be zero their transverse momentum. The missing transverse energy (MET) is reconstructed by the particle flow algorithm using the vectorial sum of the transverse momentum of all PF candidates. However, the MET is also one of the most complex variables to reconstruct, since it is very sensitive to detector malfunctions and particles crossing poorly-instrumented regions of the detector. As done for jets, enenergy corrections due to energy calibration, in particular the JEC, are propagated to the MET, as well as corrections to the scale of the particles that are not clustered into jets. Filters to the MET are applied that remove pathological events from data, referred in this thesis as MET *filters* . The MET is one of the most important variables for discriminating leptonic decays of W bosons and top quarks from background events

which do not contain neutrinos, and for this purpose it will be used in this analysis. It is also a crucial variable to search for Beyond Standard Model physics, since many models predicts particles that would not leave any trace in the detector. The presence of particles that do not interact in the detector can be measured with MET since they create an energy imbalance.

4.6 Background description

The main backgrounds for the final state under study, illustrated in Figure 4.4, are:

- $t\bar{t}$: processes where a $t\bar{t}$ quark pair is produced are the dominant background. In particular events where one t quark decays semi-leptonically, namely through the chain $t \to Wb \to l^{+}\nu b$, and the other top quark decays hadronically, namely through the chain $t \to Wb \to b\mathrm{q}\bar{\mathrm{q}}$, have several features in common with signal events. Indeed the top quark signal behaviour can be mimicked by the top that decays leptonically while the top quark that decays hadronically can fake the Z boson topology. A Z boson decaying to a $b\bar{b}$ pair can be faked by the b-originated hadrons from the top quark decay, while a Z decaying to light quarks can be faked by a W boson-originated fat jet from the top quark decay.

- Single top : similarly, single top quark processes can reproduce in some cases the signal topology if the two quarks in the final states are reconstructed as a Z boson.

- W + jets: in this decay if the gluon is emitted close enough to the couple of b-jets it might be misidentified as a Z boson.

- Z+jets: if one lepton is not recontructed and the couple of quarks and a gluon emitted in the next-to-leading order in Z+Jets processes can be mistaken for a T quark decay.

- QCD: produces a high number of jets that can also simulate the signature of the process where large MET arises from mis-reconstructed jets. However they can be reduced through event selection and appear as a negligible fraction in the final region.

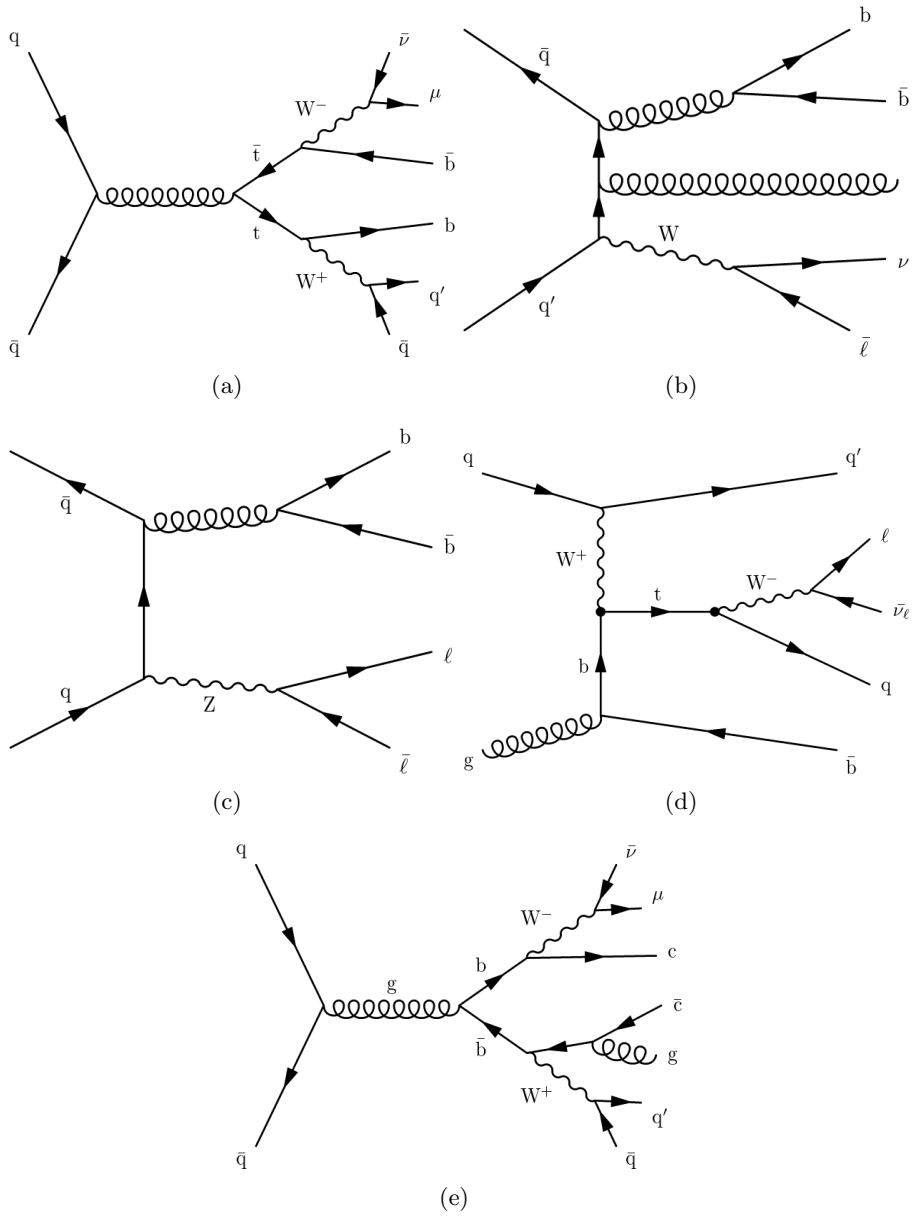

Figure 4.4: Feyman diagrams of background processes: $t\bar{t}$ (a),W + jets (b), Z+jets(c), Single top(d) and QCD(e).

Chapter 5

Analysis strategy

In this Chapter, the strategy used to extract the single T signal is described. The analysis aims at constraining the backgrounds directly from data in a region enriched with signal events. The strategy starts from an event selection in order to study only the events with a topology close to the one of the signal. The decay products of the candidate T include a lepton, a b-jet, a neutrino, manifesting as missing energy, forming the top quark, and a single jet forming the Z or Higgs candidate. The reconstruction of the top quark is performed, and in case more than one b-jet is present, the correct jet is selected by defining a χ^2 metrics to identify the best combination of lepton, missing energy and b-jet based on simulation studies. Moreover, six event categories have been defined by varing two variables related to the substructure of the AK8 jet considered as a Z/H boson: the number of b-subjets and the N-subjettines described below. In these regions, a maximum likelihood fit on the reconstructed invariant mass M_T of the T candidate is performed, allowing to set limits at the production cross section of the T.

5.1 Data and simulated samples

The analysis is performed on pp collision data recorded by CMS in 2017, with a centre-of-mass energy of $\sqrt{s} = 13$ TeV. The Table 5.1 shows the list of data sets used; the labels SingleMu and SingleEl refer to the triggers used to select the data set, the label Run2017B through F refers to the data taking period, 31Mar2017 refers to the date in which the data sets have been processed and the MINIAOD label refers to the file format and content according to CMS standard definitions. The data set used corresponds to an integrated luminosity of 41.5 fb^{-1}. The signal and the main background events are taken from Monte-Carlo simulations, performed by CMS Generator Group, using different software frameworks in order to:

- generate matrix elements either at leading order corrections (LO) or at next-to-

Data set	Integrated luminosity $[fb^{-1}]$
/SingleMu/Run2017B-31Mar2018-v1/MINIAOD	4.792
/SingleMu/Run2017C-31Mar2018-v1/MINIAOD	9.755
/SingleMu/Run2017D-31Mar2018-v1/MINIAOD	4.319
/SingleMu/Run2017E-31Mar2018-v1/MINIAOD	9.424
/SingleMu/Run2017F-31Mar2018-v1/MINIAOD	13.57
/SingleEl/Run2017B-31Mar2018-v1/MINIAOD	4.792
/SingleEl/Run2017C-31Mar2018-v1/MINIAOD	9.755
/SingleEl/Run2017D-31Mar2018-v1/MINIAOD	4.319
/SingleEl/Run2017E-31Mar2018-v1/MINIAOD	9.424
/SingleEl/Run2017F-31Mar2018-v1/MINIAOD	13.57

Table 5.1: List of data sets of pp collision data produced at $\sqrt{s} = 13$ TeV and collected by CMS in 2017, employed in the thesis. Data collected correspond to an integrated luminosity of 41.5 fb^{-1}.

leading order corrections (NLO), with programs like Madgraph5_aMC@NLO [76] or*POWHEG 2.0* [79];

- generate and simulate the hadronization of outgoing particles produced in proton-proton collisions, in order to reproduce accurately the event properties of a wide range of processes, such as Pythia [77] or Herwig [78];
- simulate particle interaction with CMS sub-detectors, such as GEANT 4 [80].

The event generator Madgraph, matched to the Pythia generator for the parton-shower simulation, is used to generate the signal event samples. They are simulated with different model-dependent benchmarks based on the possible T quark mass, ranging from 700 up to 1800 GeV in steps of 100 GeV. The generated signal samples for the T process and the corresponding leading-order (LO) cross sections are reported in Table 5.2. Instead, for the generation of the different backgrounds events several MC generators are used. The $t\bar{t}$ pair production process is generated with *POWHEG 2.0* [79, 81, 82], evaluating its cross section at the next-to-next-to leading order (NNLO) in perturbative QCD. Two additional simulated samples are generated to increase the $t\bar{t}$ process statistics in the signal region, by generating events where the mass of the $t\bar{t}$ pair is greater 700 GeV, and the corresponding cross sections are evaluated at NLO. The Single Top events are simuleted using a match of *POWHEG 2.0* and Pythia as well. Multijet QCD production, W + jets, and Z+Jets samples are generated with the MADGRAPH 5 [76] tree-level matrix-element generator matched to PYTHIA 8 [83] for the parton-shower simulation, their cross section are instead calculated at leading order (LO). Simulated Monte Carlo samples for background processes used in this thesis are listed in Table 5.3 with the corresponding theory cross sections [87]. The possible presence of additional pp

collision that overlap on top of the primary interaction, known as *Pile-Up* (PU) events, are taking into account by CMS by computing the number of primary vertices from the instantaneous luminosity. However, since the PU distribution in simulation does not reproduce the one observed in data, a *reweighting* is needed, wigh is accomplished by applying multiplicative factors to MC sample events to correct for the discrepancy with the distribution of primary vertices in the data.

Mass [GeV]	Cross section [fb]
700	78.04
900	23.34
1000	13.62
1100	8.23
1300	3.25
1400	2.12
1500	1.41
1600	0.94
1700	0.64
1800	0.44

Table 5.2: Simulated $Tb \rightarrow$ tZ samples employed in the analysis with their corresponding production cross sections.

5.2 Event selection

5.2.1 Trigger

The presence of strictly one highly energetic lepton the final state, as described in Section 4.3, characterized the signal events. Therefore, the events that satisfy trigger conditions based on the presence of only one muon with p_{T} more than 50 GeV, SingleMu, or only one electron with p_{T} more than 110 GeV, SingleEl, are selected. The trigger conditions provided by CMS and used in this anlysis are:

- HLT_ Ele115_ CaloIdVT_ GsfTrkIdT && HLT_ Ele27_ eta2p1_ WP75_ Gsf for the electrons;
- HLT_ TkMu50 && HLT_ Mu50, for the muons.

where the statement && indicates that both the conditions are simultaneously required.

5.2.2 Kinematic requirements

In order to reduce the possible selection of background events, a set of requirements based on different kinematic variables are applied on the physics objects present in the

Sample	Cross section [pb]
$t\bar{t}$ (0-700)	831.76 *
$t\bar{t}$ (700-1000)	80.5
$t\bar{t}$ (1000-Inf)	21.3
QCD (HT100-200)	27990000
QCD (HT200-300)	1712000
QCD (HT300-500)	347700
QCD (HT500-700)	32100
QCD (HT700-1000)	6831
QCD (HT1000-1500)	1207
QCD (HT1500-2000)	119.9
QCD (HT2000-Inf)	25.24
W+Jets (lν,HT 100-200)	1345
W+Jets (lν,HT 200-400)	359.7×1.21**
W+Jets (lν,HT 400-600)	48.91×1.21**
W+Jets (lν,HT 600-800)	12.05×1.21**
W+Jets (lν,HT 800-1200)	5.501×1.21**
W+Jets (lν,HT 1200-2500)	1.329×1.21**
W+Jets (lν, HT 2500-Inf)	0.03216×1.21**
Z+Jets ($\nu\nu$, HT 100-200)	280.35×1.23**
Z+Jets ($\nu\nu$, HT 200-400)	77.67×1.23**
Z+Jets ($\nu\nu$, HT 400-600)	10.73×1.23**
Z+Jets ($\nu\nu$, HT 600-800)	2.559×1.23**
Z+Jets ($\nu\nu$, HT 800-1200)	1.1796×1.23**
Z+Jets ($\nu\nu$, HT 1200-2500)	0.28833×1.23**
Z+Jets ($\nu\nu$, HT 2500-Inf)	0.006945×1.23**
Single top ($\bar{t}$, t-channel)	80.95
Single top (t, t-channel)	136.02
Single top (tW)	71.17
Single top (s-channel)	10.32

Table 5.3: Standard-model background samples and their corresponding production cross sections. Many of the samples listed are split in order to increase the available statistics by generating more events in more extreme regions of the phase space. $t\bar{t}$ samples are divided considering different ranges of $t\bar{t}$ per mass: $0-700$ GeV, $700-1000$ GeV and $1000-Inf$ GeV, instead other samples such as QCD or $W+$jets and $Z+$jets are split taking in account different values of the total transverse momenta.

* This is an inclusive cross section, then it is correct to remove the 80.5 pb e 21.3 pb of the other two $t\bar{t}$ samples.

** The cross section is multiplied by the scale factor obtained from the ratio NLO / LO.

final state. First of all, the presence of one neutrino coming from the top quark decay allows to require MET with p_{T} greater than 100 GeV. Moreover, if the lepton is a muon, it is required to have a $p_{\mathrm{T}} \geq 60$ GeV. The final state is also caracterized by the presence of narrow jets from b-jets reconstruction as well as fat jets coming from the Z/H deacy. For this reason, the events are required to have at least one b-tagged jet with p_{T} >30 GeV and an $|\eta|$ <4.0, and at least one fat jet with p_{T} >200 GeV and $|\eta|$ ≤2.5. As described in Section 4.4.1, the AK8 jets are required to have a SoftDrop mass $65 < M_{SD} < 145$ GeV, in order to select only the jets coming from the Z/H boson decay. In particular an AK8 jet with $65 < M_{SD} < 105$ is considered a Z boson while an an AK8 jet with $105 < M_{SD} < 145$ is considered an Higgs boson Moreover, in order to not select the leptons that could came from the Z decay or that overlap the bjet, two different angular separation constraint are required: ΔR the AK8 jets and the lepton must be more than 1.2 while angular separation between the b-jet and the lepton is required to be more than 0.15. In a similar way, in order to not take in account twice the b-jets that can be reconstructed as AK4 or as a part of an AK8 jet, the angular separation ΔR between the b-jet and the AK8 jets is required to be more than 1.2. The multiplicity of leptons, b-jets, and AK8 jets associated to a Z and Higgs boson, evaluared after this selection, are shown in Figure 5.1.

The set of requirements is summarized here:

- MET p_{T} >100 GeV;
- exactly one muon with p_{T} more than 60 GeV or exactly one electron with p_{T} more than 110 GeV;
- at least one b-tagged jet with p_{T} >30 GeV, $|\eta|$ <4.0 and $\Delta R(bjet, AK8) > 1.2$;
- at least one fat jet with p_{T} >200 GeV, $65 < M_{SD} < 145$ GeV and $\Delta R(lepton, AK8) > 1.2$.

5.2.3 Top quark reconstruction

In this analysis, the top quark is reconstructed as composed by three objects: the lepton, the b-jet, and MET. The kinematic variable choosen to study the good reconstruction of the top quark is the invariant mass, evaluated as:

$$M_{top} = \sqrt{\left(\sum_{i}^{3} E_i\right)^2 - \|\sum_{i} \vec{p_i}^2\|} \tag{5.1}$$

where E_i and $\vec{p_i}$, are the measured energy and three-momenta of the lepton, b-jet and neutrino. The momentum of neutrino is evaluated as in [84]. First of all, his transverse component $p_{\nu T}$ is equal to the negative of the vectorial sum of the transverse momentum

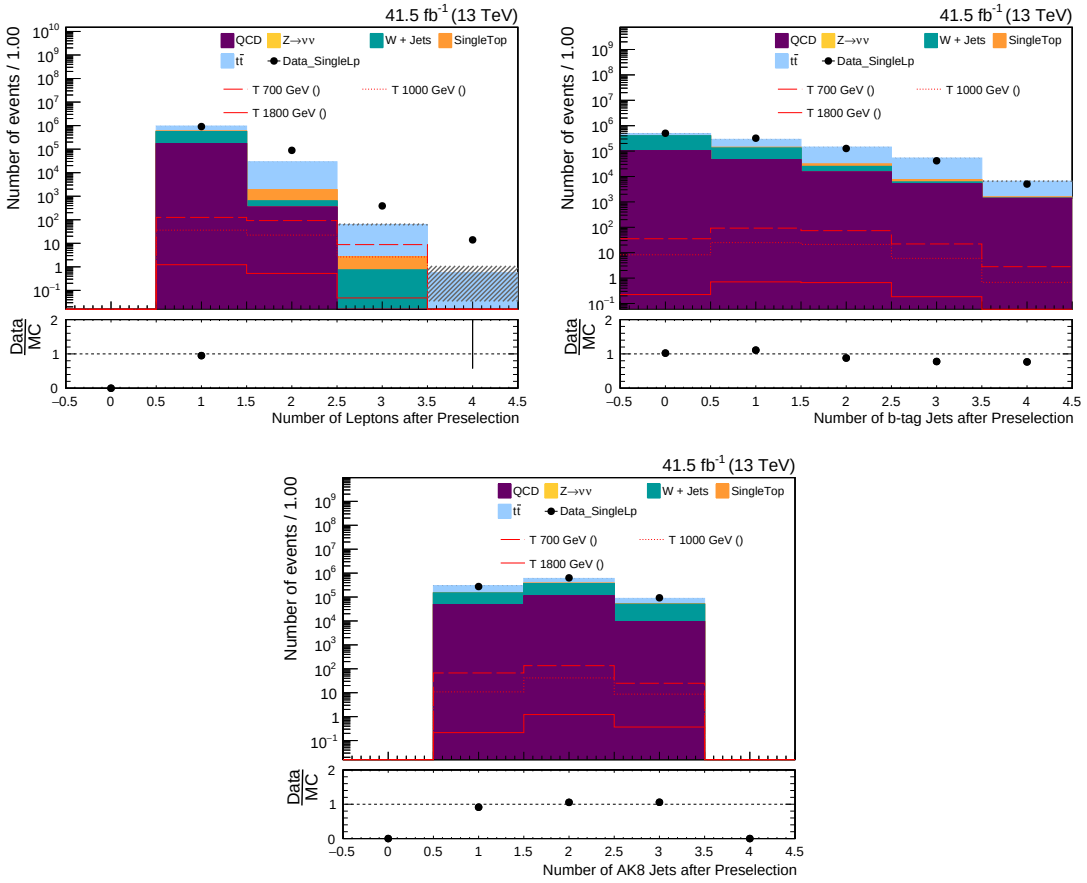

Figure 5.1: Multiplicity of leptons (a), bjets (b), and fatjets (c), after kinematic requirements.

of all the PF particles $\not{p}_T$. Moreover, the longitudinal momentum of the neutrino $p_{z,\nu}$ can be evaluated constraining the mass of W boson at 80.4 GeV [85] and assuming the energy-momentum consevation at the $W \to l\nu$ vertex:

$$p_{z,\nu} = \frac{\Lambda p_{z,l}}{p_{T,l}^2} \pm \frac{1}{p_{T,l}^2}\sqrt{\Lambda^2 p_{T,l}^2 - p_{T,l}^2(E_l^2 \not{E}_T^2 - \Lambda^2)}, \tag{5.2}$$

where:

$$\Lambda = \frac{m_W^2}{2} + p_{T,l}\vec{\cdot}\,\vec{\not{p}_T}. \tag{5.3}$$

m_W is the mass of the W boson, E_l and $p_{T,l}$ are the energy and the transverse momentum of the lepton and $\not{E}_T$ is the MET. The discriminant in Equation 5.2 is usually positive and the solution with the smallest absolute value is chones. In the other cases, the imaginary component is eliminated by imposing that the discriminant, as the square-root term, is null behaving a quadratic relation between $p_{x,\nu}$ and $p_{y,\nu}$, with two possible solution and one remaining degree of freedom. The solution that leads to a minimum

vectorial distance between $p_{\nu T}$ and $\not{p}_T$ is chosen.

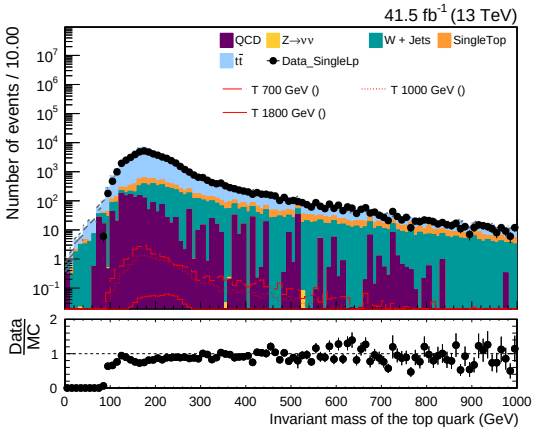

Figure 5.2: Distribution of the minimum of the invariant mass of the top quark filled with every bjet selected by the kinematic requirements.

The reconstructed top quark candidate invariant mass, shown in Figure 5.2, highlights that there are some discrepancies between data and MC events as well as a very large tail in the distribution. The main reason is that, without further requirements, for some MC events, the invariant mass is reconstructed by using the "wrong" b-jet, namely the b-jet that does not come from the top quark decay. Simulation is used to construct a χ^2 metrics to select the bjet associated to the quark top. First of all, a gaussian fit, is performed on the invariant mass reconstructed with the b-jets and leptons that are associated to the top quark according to the MC truth. The plot in Figure 5.3 shows the fit performed for an hypotesis of the T mass equals to 1 TeV; the mean and the standard deviation extracted from this fit are:

$$\bar{M} = 174.729 \quad \sigma = 28.8723$$

The fit has been repeated for different hypothesis of the T mass and no significant differences have been detected. The $\bar{M}$ and σ values has been used to determine the Chi Squared distribution, as reported in Figure 5.4. The Chi Square has been evaluated as

$$\chi^2 = \frac{M_{top} - \bar{M}}{\sigma^2} \tag{5.4}$$

In this way, the b-jet that minimizes the χ^2 is selected as associated to the top quark. The distribution of the top quark invariant mass, re-evaluated after this process, is shown in Figure 5.5. One can notice that the discrepancy is significantly reduced.

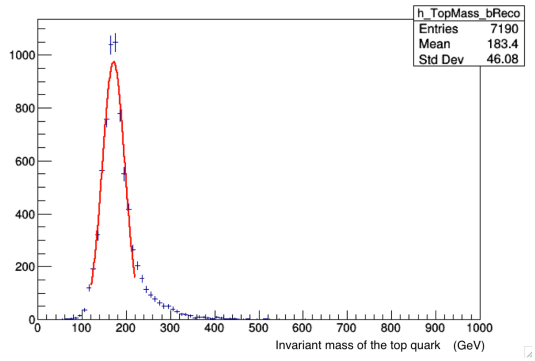

Figure 5.3: Fit on the top quark invariant mass performed for an hypotesis of the T mass equal to 1 TeV.

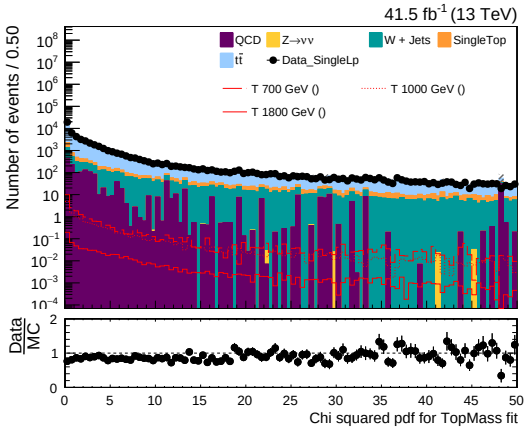

Figure 5.4: Distribution of the Chi Squared variable defined as in Equation 5.4.

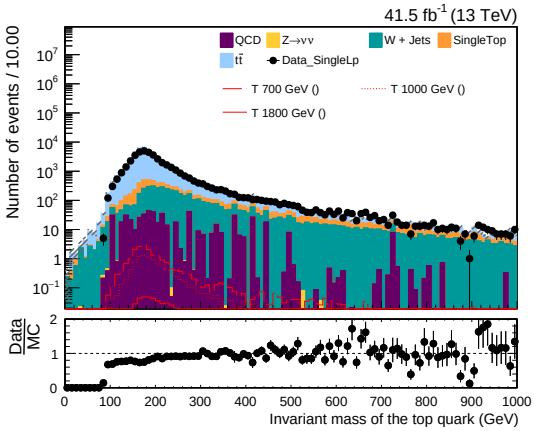

Figure 5.5: Distribution of the minimum of the invariant mass of the top quark filled only with the b-jets that maximize the χ^2.

5.2.4 Angular cuts optimization

The suppression of the backgrounds and the choice of phase space regions that are enriched with signal events is crucial for the search of rare signal as it is the case in this analysis. To reach this goal, the distributions of different kinematic variables of the physics objects in the final state have been studied. Three variables have been choosen since they allow to account for the angular separation to be expected in the case of a T signal event, allowing to potentially discriminate against background events with a different structure: the $\Delta\phi$ which is the difference between the lepton and the MET measured ϕ angles, referred as $\Delta\phi_{LMET}$, the ΔR between the Z boson and the lepton, referred as ΔR_{ZL}, and the $\Delta\phi_{ZMET}$. The distributions of those kinematic variables are shown in Figure 5.6.

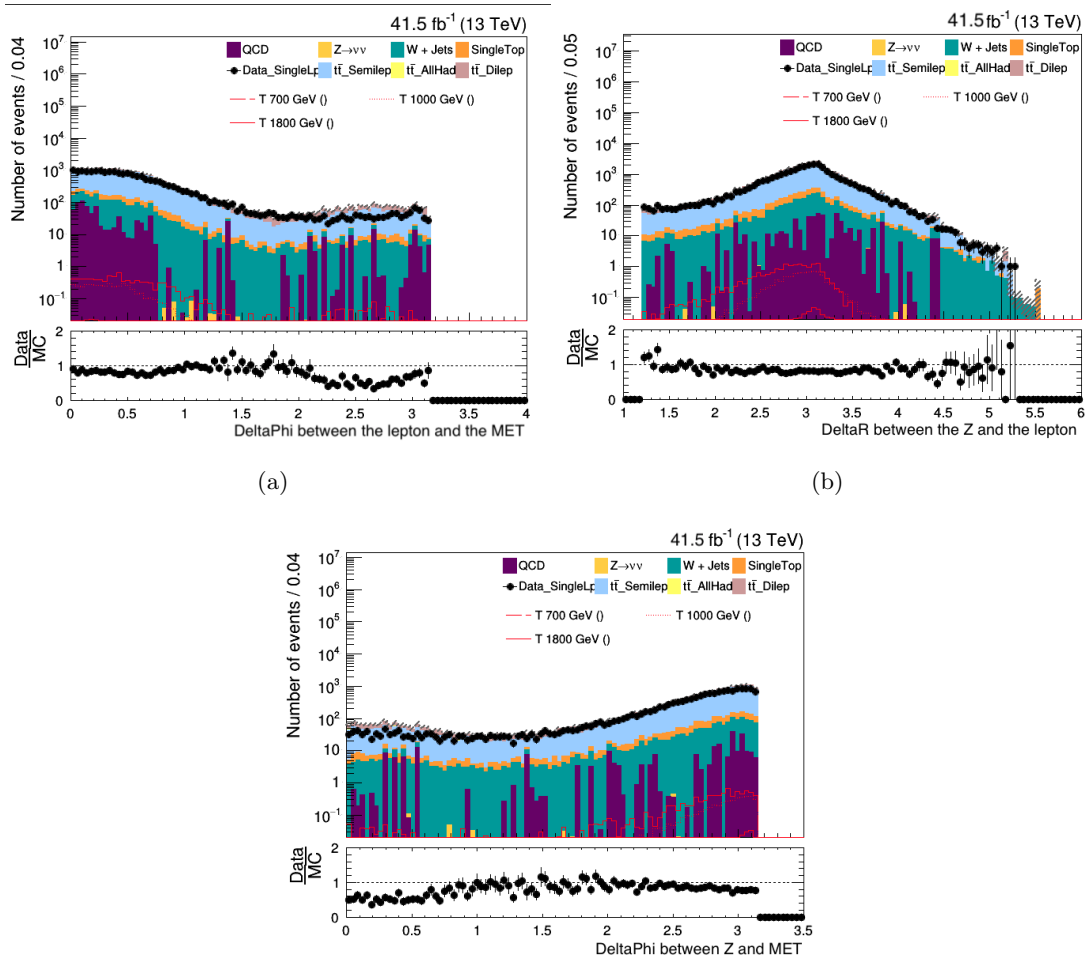

(a) (b)

(c)

Figure 5.6: Distribution of the three variables choosen to perform the optimization cuts. From top to bottom: $\Delta\phi_{LMET}$, ΔR_{ZL}, $\Delta\phi_{ZMET}$.

$S/\sqrt{B}$ is evaluated as a figure of merit (FoM) for identifying the best upper and

lower requirement, or cut, to apply on each variable. The study is done by fixing the cut on one end, and evaluating the corresponding FoM. The fixed requirements are: for $\Delta\phi_{LMET}$ the end is fixed at $\Delta\phi_{LMET} = 0$; for $\Delta\phi_{ZMET}$ is at 4.0; for ΔR_{ZL} is at 3.2. First the lower cut of the ΔR_{ZL} distribution is let floating, not applying any cut to the upper value. Then, the lower cut is fixed at the otimal value, and the same procedure is applied for the upper cut. The distributions of the $S/\sqrt{B}$ variables in function of the cuts are reported in Figure 5.7. Since the variable $\Delta\phi_{ZL}$ results higly correlated to the ΔR_{ZL}, the cuts are performed only on the other two variables, defining the following regions:

$$1.55 \leq \Delta R_{ZL} < 4.00 \quad 0 < \Delta\phi_{LMET} \leq 0.72$$

The distribution of kinematic variables after the cuts required are shown in Figure 5.8 and 5.9

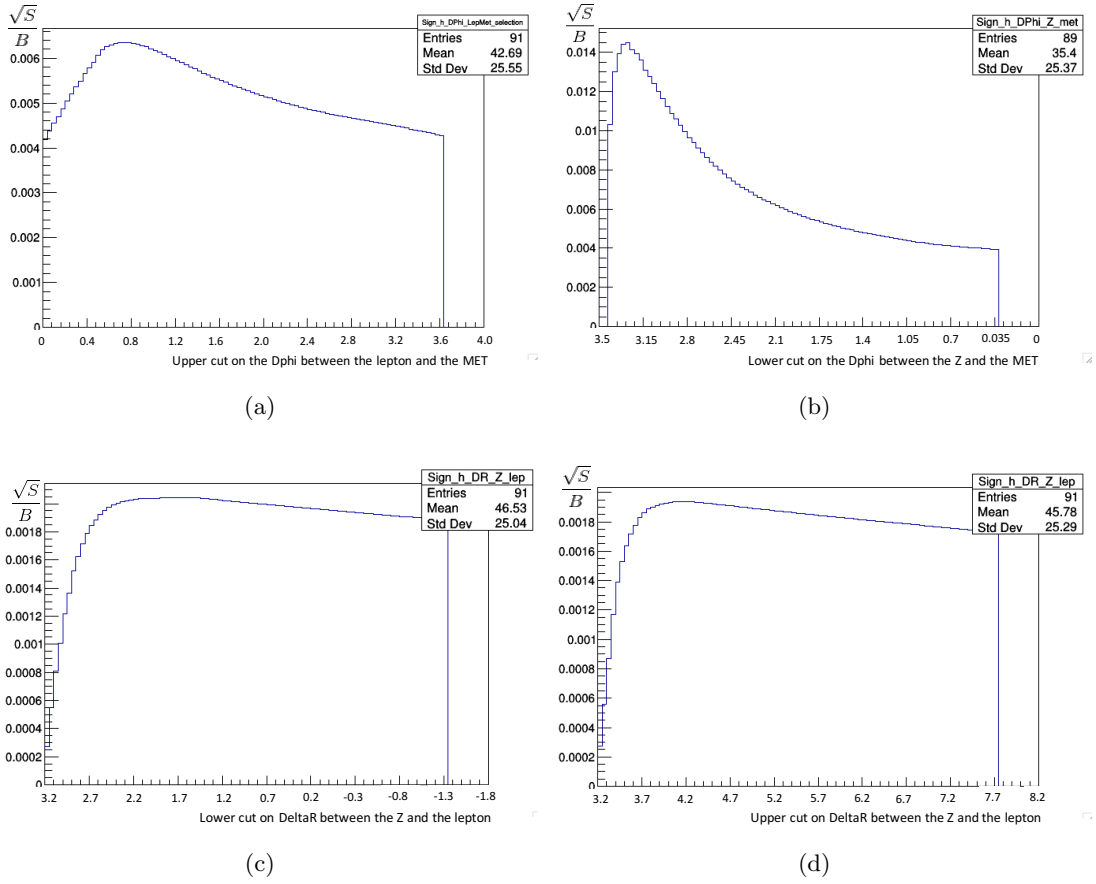

Figure 5.7: Distribution of the ratio $S/\sqrt{B}$ for the three different variables: $\Delta\phi_{LMET}$ (a), $\Delta\phi_{ZMET}$ (b), ΔR_{ZL} for value less (c) and more (d) than 3.2.

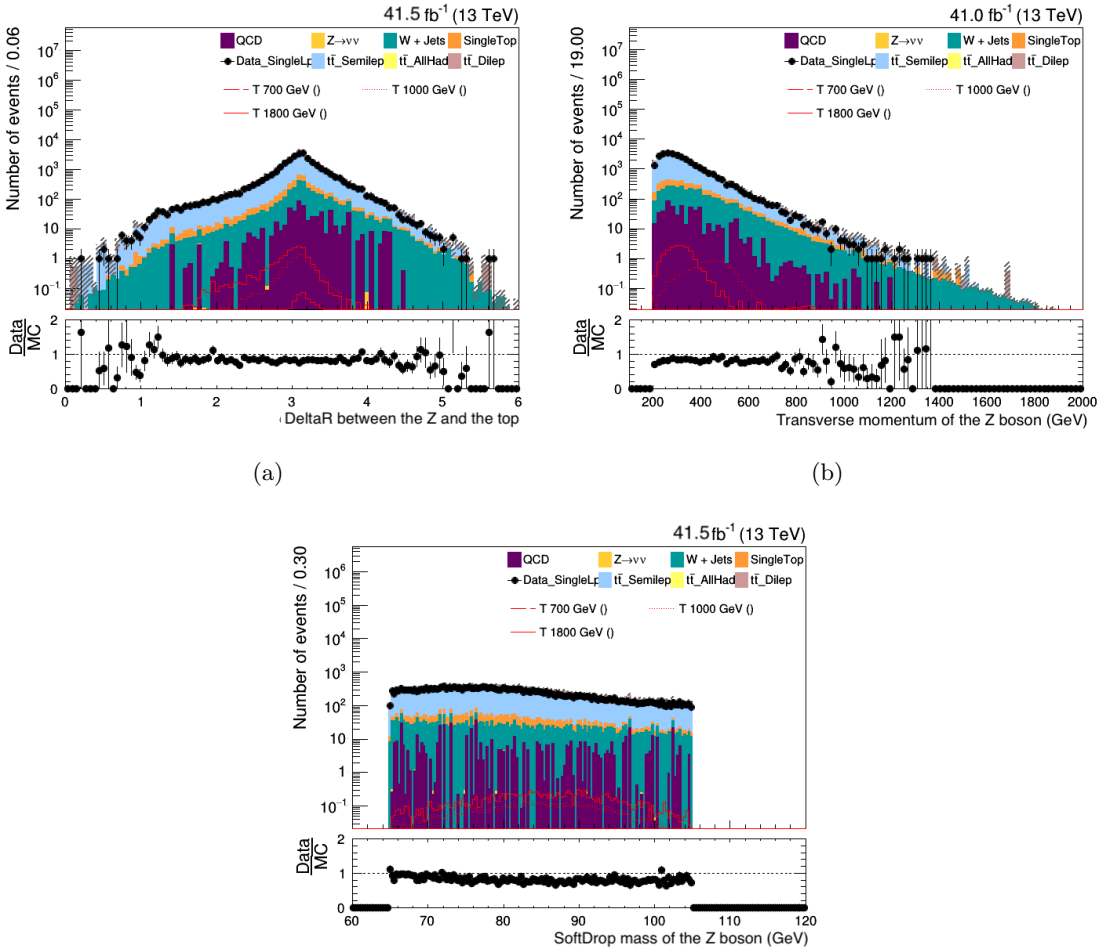

(a) (b)

(c)

Figure 5.8: Plots of kinematic variables distributions of different final state objects: the ΔR between the Z boson and the to quark (a), the transverse momentum of the Z boson (b), the SoftDrop mass of the Z boson (c).

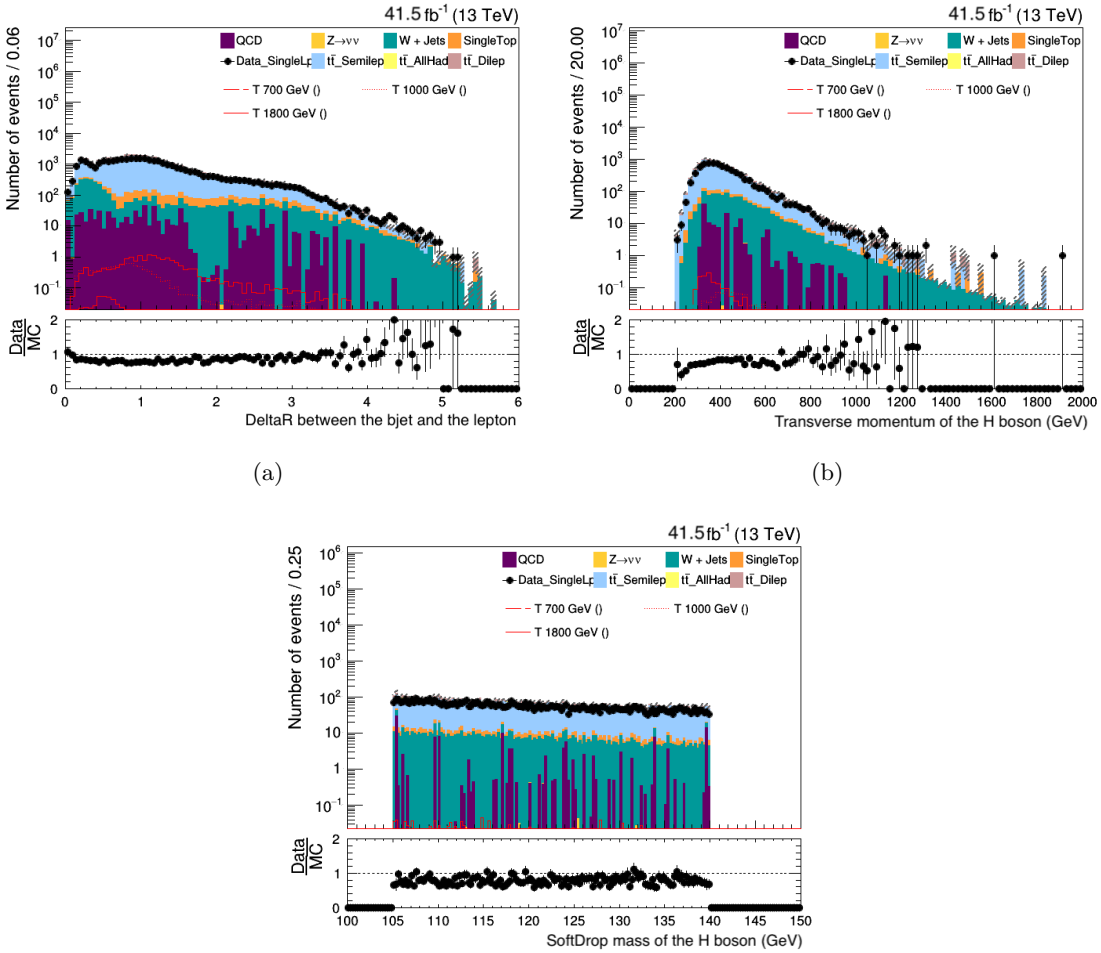

(a) (b)

(c)

Figure 5.9: Plots of kinematic variables distributions of different final state objects: the ΔR between the Z boson and the lepton (a), the transverse momentum of the H boson (b), the SoftDrop mass of the H boson (c).

5.2.5 Signal and control regions

The previous optimization is preparatory to the definition of signal enriched regions, called *signal regions*, and background enriched regions, referred as *control regions*. Those regions, are characterized by different values of two substructure variables of the AK8 jet representing the Higgs or the Z boson:

- the number of b-tagged subjets N_{bsub} coming from the AK8 jet. The discriminating power of this variable could be simply evaluated when, for example, the branching ratio of the Higgs boson are considered. The high probability for an Higgs boson to decay in a $b\bar{b}$ pair, ensures to regard the region with 0 b-subjet as a possible control region. Starting from this reason, three region with number of b-subjets equal to 1, 2 and 3 have been created.

- the ratio τ_2/τ_1. The variable τ_N is the so called *N-subjettiness* [86] and evaluates the consistency of a jet with the hypotesis that it is composed of N sub-jets. It is defined as:
$$\tau_N = \frac{\sum_k p_{T,k} min\left(\Delta R_{1,k}, \Delta R_{2,k}, ..., \Delta R_{N,k}\right)}{\sum_k p_{T,k} R_0} \tag{5.5}$$
where k indicates all the constituents of the jet, $\Delta R_{j,k}$ is the distance of the candidate subjet j and the particle k and R_0 is the jet radius. The value of τ_N goes to zero if the jet is compatible to have N components or fewer. Istead, a τ_N values that goes to one, shows that the part of the jet energy is spread at a larger angle, and it is more likely that the jet has at least $N+1$ subjets. The discriminating power of the ratio τ_2/τ_1 relies on the evidence that a Z/H jet is more consistent with two subjets than only one, while the high energy spread of an AK8 jets coming from higly bosteed gluon or light quark makes itself consistent both with the hypotesysis of being composed by two and one jet. Therefore, the ratio Z/H bosons is smaller than the one for multijets background, expecially for QCD. In this analysis, values of $0 < \tau_2/\tau_1 \leq 0.45$ define the so called "Tight" region, while values of $0.45 < \tau_2/\tau_1 \leq 0.60$ define the "Loose" region.

The combination of the N_{bsub} and τ_2/τ_1 values define six regions for each AK8 jet mass range, as mentioned before.

5.2.6 Forward jet selection and categories identification

Another feature that can be used to further separate the background events from signal events is the presence of a forward jet, i.e. a narrow jet with $|\eta| > 2.4$, coming from the light flavour quark produced in association with the T. This topology allows to define two categories, one requiring strictly one forward jet and problably enriched in signal and one requiring 0 forward jets in final state, that helps to improve the final

sensitivity since it has higher statistics but a lower purity respect to the former category. The number of the events in the two categories is shown in Figure 5.10.

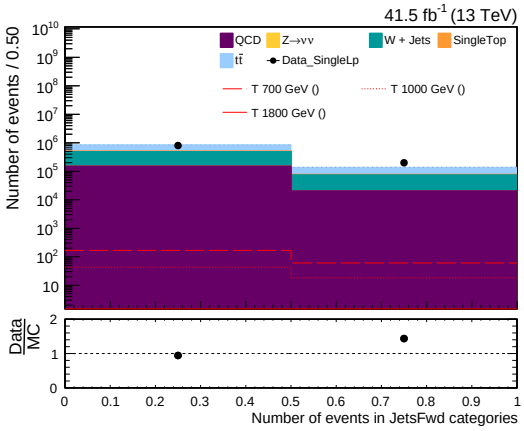

Figure 5.10: Distribution, for both data and simulation, of the number of events in the different catefories after the kinematic requirements.

5.2.7 Discriminating variable

The variable that has been chosen to discriminate signal from background is the invariant mass of the VLQ T, defined as:

$$M_T = \sqrt{\left(\sum_i E_i\right)^2 - \|\sum_i \vec{p_i}\|^2} \tag{5.6}$$

where E_i and $\vec{p_i}$, are the measured energy and three-momenta of the top quark and of the Z boson. The distributions of the invariant mass for all regions are shown in Figure 5.11 and 5.12, while the ones considering 1 and 0 forward jets are shown in Figure 5.13. Moreover, the distributions of M_T in 0 b-subjets regions, for events in which an Higgs-tagged jet is present, are used as cross-check for the invariant mass reconstruction since those regions are, almost surely, depleted of signal events. The distribution are reported in Figure 5.14

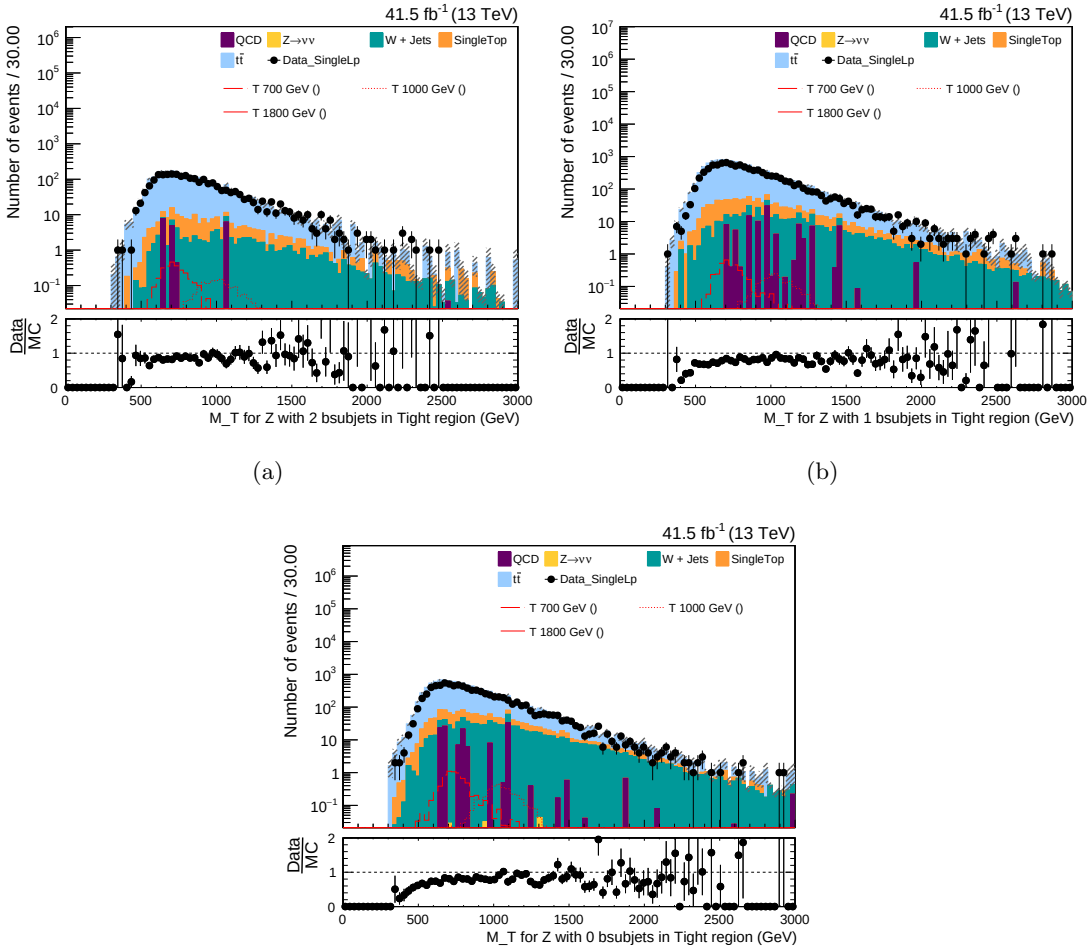

(a) (b)

(c)

Figure 5.11: Invariant mass distribution for data and MC samples after the full selection for the regions Tight with: 2 b subjets (a), 1 b subjet (b) and 0 b subjet(c).

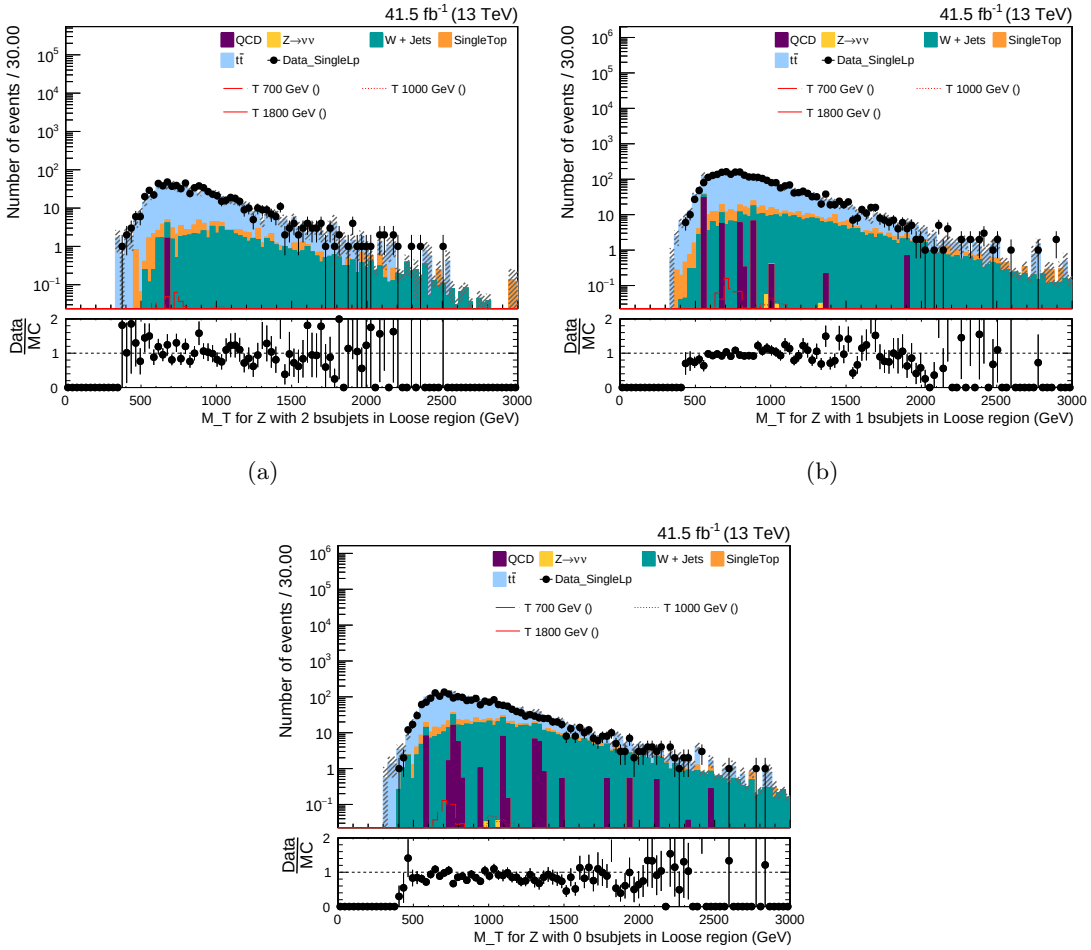

(a) (b)

(c)

Figure 5.12: Invariant mass distribution for data and MC samples after the full selection for the regions Looose with: 2 b subjets (a), 1 b subjet (b) and 0 b subjet(c).

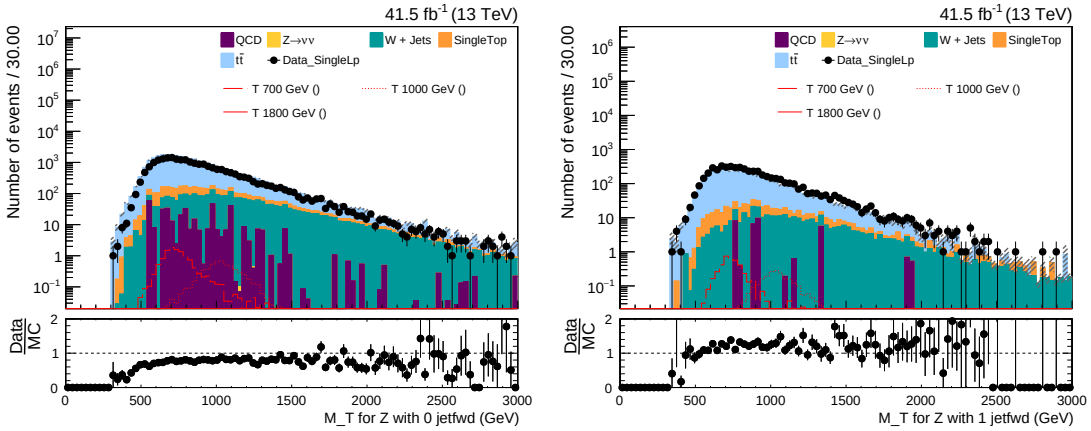

(a) (b)

Figure 5.13: Invariant mass distribution for data and MC samples after the full selection and the requirement of 0 forward jets (a) and strictly 1 forward jet (b).

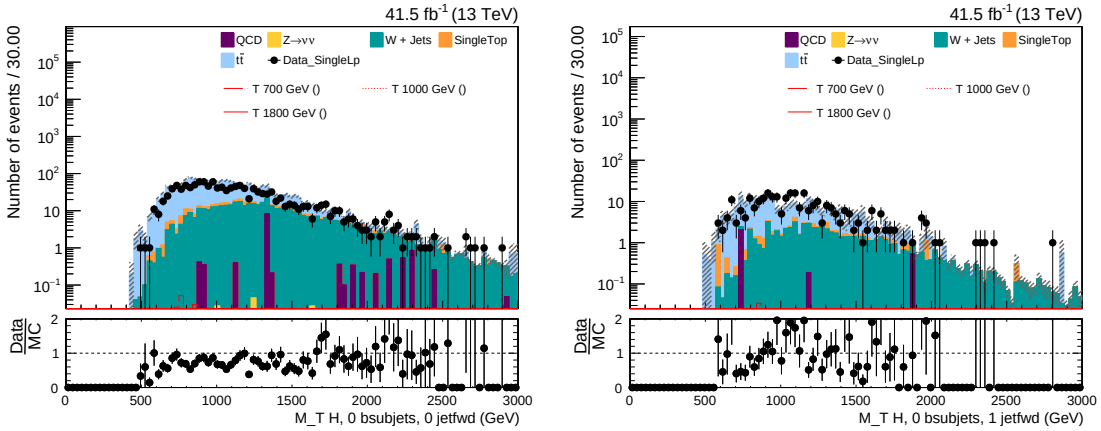

(a) (b)

Figure 5.14: Distribution of the T invariant mass distribution for events with an Higgs boson and the request of 0 b-subjets for the region with 0 forward jets (a), and with 1 forward jets (b).

5.2.8 Signal and background extimation

In this analysis the data, signal and background expected event after the kinematic requirements have been evaluated from the MC samples and the data. The results have been reported in Table 5.4

Samples	Number of events
$t\bar{t}$	29315 ± 123
W + Jets	2639 ± 22
QCD	414 ± 81
Single Top	1913 ± 20
Z$\rightarrow \nu\nu$	0.48 ± 0.12
m_T 700 GeV	15.82 ± 0.4
m_T 1000 GeV	8.22 ± 0.11
m_T 1400 GeV	2.04 ± 0.02
m_T 1800 GeV	0.43 ± 0.01
Data	28265

Table 5.4: Number of expected data, signal and background events after the kinematic requirements and normalized to the luminosity $41.5 fb^{-1}$.

5.3 Systematics uncertainties

This section includes a list of the relevant systematic uncertainties for this analysis and a description on how they are estimated. Systematic uncertainties do affect the background and signal prediction, and have to be taken into account when extracting the signal value from the fit. The effect of the systematics can be of two types:

- **Yield effect only**, modify just the integral of the distribution of the variable used in the fit, changing in a flat way the distribution.
- **Yield and shape effect**, modify the integral and the shape of the distribution of the variable used in the fit, changing not only in a flat way the distribution but also re-shaping it.

In the following Table 5.5 are summarized the uncertainties used and is specified their effect on the variables considered in the fit.

Uncertainty	Yield effect only	Yield and shape effect
Luminosity	✓	
b-tagging and mis-tag	✓	
Pileup modeling	✓	
PDF	✓	
q^2		✓
W and Z tagging	✓	
Simulation statistics		✓

Table 5.5: Summary table of the uncertainties considered in this thesis. The uncertainties are classified to take in account their effect on the distribution of the variables used in the fit.

Luminosity

The CMS collaboration provides the standard uncertainty of 2.6% on the amount of integrated luminosity of the data sample at 13 TeV, 35.89 $cm^{-2}s^{-1}$,that has been applied in this work [88].

Pileup modeling

The number of primary vertices in the simulated MC samples is corrected by a scale factor (SF) in order to reproduce the one present in the data. The systematic uncertainties related to pileup modelling are taken into account by varying by $\pm 4.6\%$ the minimum bias cross section of 69.2 mb, used to calculate the data pileup distributions.

Parton Distribution Function (PDF)

The parton distribution function choosen for MC samples also introduce a systematic uncertainty. It is evaluated by reweighting all the backgrounds distributions with the different NNPDF3.0 [89] replicas. For signal events only the effect of this uncertainty on acceptance is considered.

Factorization and renormalisation scales (q^2)

The theoretical uncertainty introduced by the choice of the factorisation and renormalisation scales is estimated by using distributions obtained by halving or doubling the scales. The uncertainties for the different backgrounds are considered uncorrelated. Only the effect on acceptance is considered for signals MC samples, while also the cross section is considered for the minor backgrounds.

b-tagging and mis-tag efficiency scale factors

The efficiencies of b tagging and jet misidentification algorithms are evaluated from control samples in 13 TeV data [75]. In order to reproduce efficiencies observed in data, some scale factors are applied to MC samples. However, this procedure leads to the introduction of a new systematic effect, due the scale factors. For this reason, the nominal values are varied "up"$(+1\sigma)$and "down"(-1σ) both for the b tagging and mistag efficiency and the uncertainty of the b-tagging efficiency SF is estimated in different p_{T} bins. The uncertainty due to jets originated by a c quark, is considered as twice the error for b-jets, while the one related to SF for light jets is estimated as a flat scale factor. The uncertainty of the b tagging SF is assumed to be fully correlated for b and c jets, while it is assumed to be uncorrelated with light jets.

Z tagging scale factors

Scale factors are also applied on MC events in order to correct the efficiency in tagging a boosted fat jet as a W, Z or Higgs boson. The errors introduced by these scales factors are evaluated by summing or subtracting the associated uncertainty to the nominal value. The variations from the central value obtained in this way represent the systematic uncertainties for the different tagging.

Simulation statistics

The limited number of events in the simulated samples also introdueced a systematic uncertainty; it is included by allowing each bin of the M_T distribution to fluctuate up and down, around the nominal value. The value of these uncertainty stems from the

poisson uncertainty of the bin. A minimum of 10 events for each bin is constrained to ensure the proper funcioning of this procedure.

5.4 Fit procedure

In this thesis,two hypothesis of existence of the singly produced VLQ T have been tested:

- $\mathbf{H}_0$ assumes the absence of new physics, that means the signal is absent or is too little to be detected;
- $\mathbf{H}_1$ that assumes the presence of the VLQ T.

A binned Maximum Likelihood fit [91], is performed on the T invariant mass M_T for 12 regions cominig from the combination of the 6 regions defined in Section 5.2.5 and the requirement of 0 forward jets and strictly 1 forward jet. Since the signal distributions depend on the T mass, the models considered include 12 mass points ranging from 700 GeV up to 1800 GeV in steps of 100 GeV. The likelihood $\mathcal{L}\left(obs \mid \mu, \theta\right)$, is the product of a Poissonian distribution multiplied a second term that represents the signal and background models,

$$\mathcal{L}\left(obs \mid \mu, \theta\right) = Poisson\left(n, \mu \cdot s\left(\theta\right) + b\left(\theta\right)\right) \prod_{k=1}^{Nevent} f\left(x_k \mid \mu, \theta\right) \tag{5.7}$$

where μ, namely the *signal strength*, is defined as the ratio of the values of the fitted parameter before and after the fit, θ is the set of systematics uncertainties, named nuisance parameters, n is the number of events, $s(\theta)$ and $b(\theta)$ are the expected yields of signal and background depending from the unknown parameters, respectively, while the probability distribution function $f\left(x_k \mid \mu, \theta\right)$ is defined as a combination of two PDFs one for signal f_s and one for background:

$$f\left(x_k \mid \mu, \theta\right) = \frac{\mu \cdot s\left(\theta\right)}{\mu \cdot s\left(\theta\right) + b\left(\theta\right)} f_s\left(x, \theta\right) + \frac{b\left(\theta\right)}{\mu \cdot s\left(\theta\right) + b\left(\theta\right)} f_b\left(x, \theta\right).$$

A shape analysis is performed considering a a nuisance parameter for each independent source of systematic uncertainty. The background normalization uncertainties are modeled with a coefficient for the background templates with a log-normal prior. The shape uncertainties, instead, are modeled by choosing a Gaussian prior for the nuisance parameters, and are used to interpolate between the nominal template and other two, obtained shifting up and down the nuisance parameters by 1σ.

The fit results are returned in term of *signal strength* μ and shown in Figure 5.15. Since no signlificative excess that could be ascribed to the production of a new particle

is observed, and data are compatible with the only background hypothesis, H_0, upper limits are set on the product of the production cross section and branching fraction of a VLQ T decaying to tZ.
The limits are evaluated with the *Combine tool* [95] dedicated software, which is able to provide a measure of the level of incompatibility of data with a signal hypothesis. The modified frequentist method [92–94] has been used to measure the expected and observed upper limits while the systematic uncertainties described in Section 5.3, are taken into account as nuisance parameters, affecting both the signal and the background. The introduction of such limits allows to take in account the possibility of variations, not yet considered, introduced by new physics that could influence the production cross section rates in the final state investigated.

The test statistics used for the evaluation of the limits is the ratio:

$$\lambda(x) = \frac{\mathcal{L}\left(x \mid H_1\right)}{\mathcal{L}\left(x \mid H_0\right)} \tag{5.8}$$

between the likelihood of the hypothesis H_0 and H_1. According to the Neyman-Pearson lemma $\lambda(x)$ is the most powerful discriminator since minimises at a significance level α the so called error of type-II, i.e. the probability of not rejecting H_1 if H_0 is true. If H_0 is verified as true, H_1 is rejected if the ratio is smaller than a chosen constant value depending on α. Considering the nuisance parameters of the two hypotheses, another profile likelihood ratio has been used as test statistic, and, as described by the Neyman-Pearson lemma, it is defined as:

$$q_\mu = -2\ ln\frac{\mathcal{L}\left(obs \mid \mu, \theta_\mu\right)}{\mathcal{L}\left(obs \mid \mu' + b,\ \theta\right)} \tag{5.9}$$

where θ_μ is the set of nuisance parameters, that maximises the numerator for a given value of μ, while θ give a constraint on the estimation of the likelihood maximum since it is the set of nuisance parameters that maximises the denominator, and μ' the value of μ that maximises the denominator. The equation 5.9 highlights that events with $q_\mu \geq 0$ appear to be under the H_0 hypothesis, while events with $q_\mu < 0$ for the background plus-signal hypothesis.
The bound for the production of VLQ T is placed by using a Confidence Level method. The confidence level for the signal can be defined as the ratio between the confidence level observed for the signal+background hypothesis, CL_{s+b}, and the confidence level observed for the background-only hypothesis, CL_b:

$$CL_s = \frac{CL_{s+b}}{CL_b} \tag{5.10}$$

where CL_{s+b} is defined as the probability to have, for a given value of μ, a value of the test statistics equal or larger than the value observed in the experiment, under the

hypothesis of signal+background H_1:

$$CL_{s+b} = P_{s+b}\left(q_\mu \geq q_\mu^{obs}\right) \tag{5.11}$$

while CL_b is the probability to have for a given value of μ a value of the test statistics equal or larger than the value observed in the experiment, under the hypothesis of background only, H_0:

$$CL_b = P_b\left(q_\mu \leq q_\mu^{obs}\right).$$

5.5 Results

The total cross section for the singly produced VLQ T decaying in a generic final state X can be written as:

$$\sigma\left(C_1, C_2, m_T, \Gamma_T, X\right) = C_1^2\ C_2^2\ \hat{\sigma}_{AW}\left(m_T, \Gamma_T\right) \tag{5.12}$$

where C_1 and C_2 are the production and the decay couplings corresponding to the interactions through which a T quark is produced and decays, and $\hat{\sigma}_{AW}$ is the reduced cross section for a resonance of arbitrary width (AW). The width can be written as $\Gamma_T = \Gamma\left(C_i, m_T, m_{decays}\right)$, as it depends on the T quark mass, on the masses of all its decay products, and on its couplings to all decay channels, C_i. The values of C_1 and C_2 are obteined by making use of the theoretical framework taken in consideration [96, 97] while the cross sections are reported in Table 5.2. The results are reported in Figures 5.15 and 5.16.

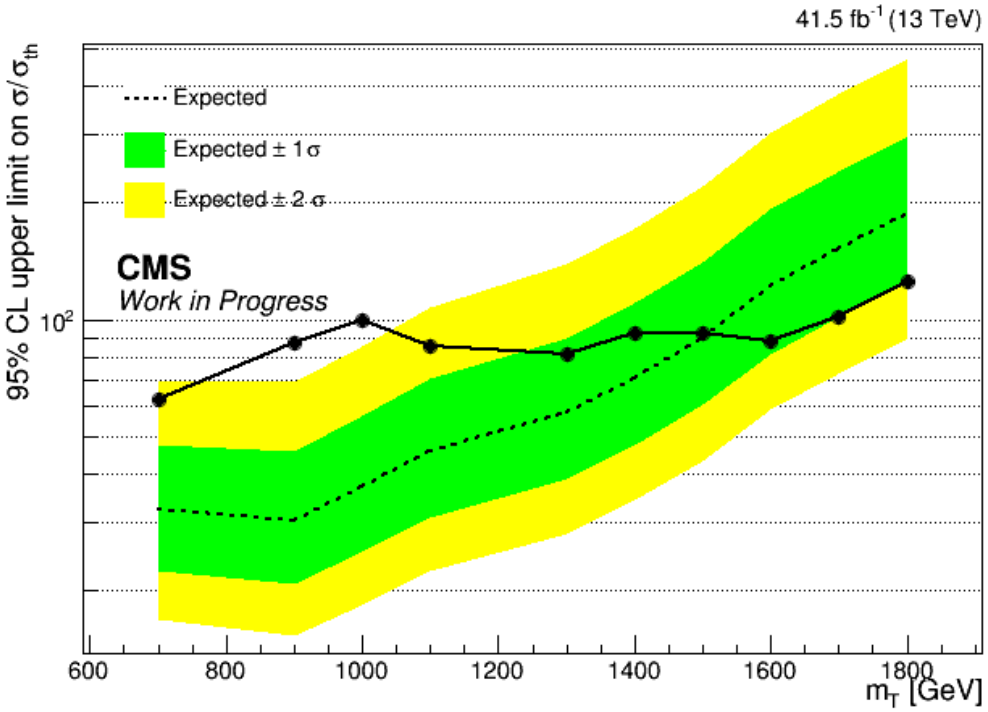

Figure 5.15: The observed and expected 95% CL upper limits of the VLQ T quark ratio of the observed over expected production cross section as a function of the signal mass, resulting from the fit.

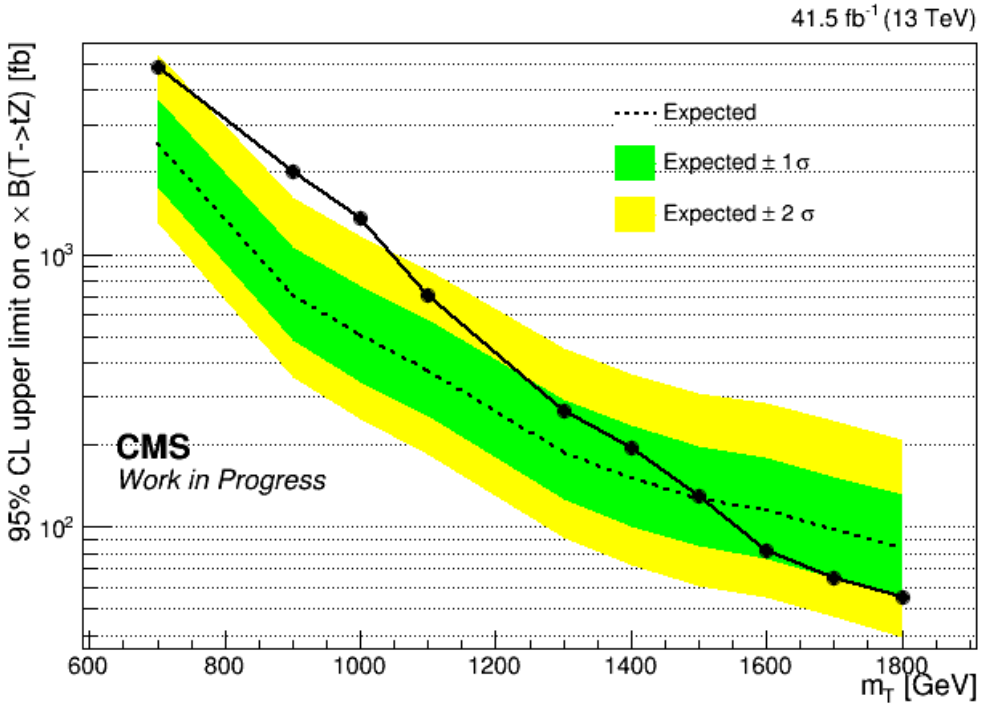

Figure 5.16: The observed and expected 95% CL upper limits of the VLQ T quark production cross section, with T decaying to tZ, as a function of the signal mass, resulting from the fit.

Conclusions

The search for a singly singly produced Vector-Like Quark T decaying to a top quark and a Z boson is presented in this thesis; it is performed using a data set collected in 2017 by the CMS experiment at the LHC, at a centre-of-mass energy of 13 TeV, and corresponding to an integrated luminosity of 41.5 fb^{-1}.
The final state investigated is characterized by the presence of a leptonic decay of the top quark and a Z boson decaying hadronically. The final state is therefore characterized by missing transverse energy, exactly one lepton, and jets.
The presence of a forward jets in the final state, coming from the spectator quark, is exploited by identifying two categories, the first with zero forward jets and the second with exactly one forward jet.
The top quark is reconstructed in the final state from the lepton, b-jet, and missing energy. The kinematic reconstruction is performed by fixing the invariant mass of the W to its measured value, and cases where more than one b-jet is present are dealt with by choosing the best permutation by making use of a χ^2 variable identifying the top quark whose reconstructed mass is the closest to the one expected from simulation, accounting for detector effects. Substructure variables of the fatjet present in the final state have been chosen to define multiple signal enriched regions. Kinematic cuts have been performed in order to optimize the signal enriched regions. A binned maximum likelihood fit is performed on the T reconstructed invariant mass distribution, M_T, taking into account systematic uncertainties.
Different benchmark models are tested based on the hypothesis made on the T quark mass, ranging from 700 up to 1800 GeV.
A deviation of roughly 3σ from the SM expectations is observed for the hypothesis of m_T =900 GeV, which would deserve further investigation. However, the results obtained with the presented analysis allow to set limits upper limits on the cross sections at 95% C.L..
Quite the same analysis strategy could be applied to the search of T decaying in to a top quark and an Higgs boson, and this is the main improvement to tha analysis itself. Other remarkable improvments are: the optimization of the lepton selection requirements for hypotesis of an high mass T, and the extension of the selection at not collimated jets

for low mass hypotesis. The analysis developed could be also applied to the data set collected by CMS at 13 TeV over the years 2016-2018, which would provide an important legacy measurement for the LHC Run-II.

Acknowledgements

The first thanks iI would to like to do goes to my supervisor and friend Dr. Alberto Orso Maria Iorio for his extraordinary willingness and patience to help me in the growth of this thesis. He is an example to follow not only for his professionality but also for his positive behaviour and his tireless availability.
I would to like also to thank my other two supervisors Prof. Luca Lista and Prof. Francesco Tramonanto for their proficient advice given to me during this thesis.
I would like to thank all the member of the CMS Naples group for the support, and for the laughs, they gave to me for the whole duration of the thesis .
I would like to thank my family for supporting during this period and helping me in the hard times. They have been teach to me the values of the culture, of the study, of the work and of the perseverance and i will never stop to thank them.
I would like to thank Flavia for taking care of me in the last year, for restoring confidence to me above all my errors and for being by my side on every day of this wonderful year.
I would like also to thank my historical friends to grant me a laugh in the hard times and to provide an advice for the difficult choices I have made. I will never forget what you have done for me and everything we have done togheter.
I would like to thank all the people who played a role in my life since they have shaped the person that i am today.
Last but not least, i would like to thank those who are no longer here for being by my side in my hearth and in my mind and for having addressed my thoughts every day of my life.

Bibliography

[1] G. Arnison et al., Phys.Lett. 122B (1983) 103; 126B 398, (1983).

[2] M. Banner et al., Phys. Lett. 122B 476, (1983).

[3] P. Bagnaia et al., Phys. Lett. B129 130, (1983).

[4] Abe F. et al, CDF Collaboration, Phys Rev. D50 2966 and Phys. Rev. Lett. 73 225, (1994).

[5] ATLAS Collaboration, "Observation of a new particle in the search for the Standard Model Higgs boson with the ATLAS detector at the LHC". Phys.Lett.B, (2012).

[6] CMS Collaboration, "Observation of a new boson at a mass of 125 GeV with the CMS experiment at the LHC". Phys.Lett.B, (2012).

[7] F. Englert and R. Brout, "Broken Symmetry and the Mass of Gauge Vector Mesons", Phys. Rev. Lett., 13:321-323, (1964).

[8] P.W. Higgs, "Broken Symmetries and the Masses of Gauge Bosons", Phys. Rev. Lett., 13:508-509, (1964).

[9] G.S. Guralnik, C.R. Hagen and T.W.B. Kibble, "Global Conservation Laws and Massless Particles", Phys. Rev. Lett., 13: 585–587, (1964).

[10] S. Glashow, "Partial-symmetries of weak interactions", Nuclear Physics, 22:579-588, (1961).

[11] S. Weinberg, "A model of leptons", Phys. Rev. Lett., 19:1264-1266, (1967).

[12] A. Salam, N. Svalthrom ed., "Elementary particle theory: relativistic groups and analyticity", Nobel symposium. (1968)

[13] H.D. Politzer, "Reliable perturbative results for strong interactions", Phys. Rev. Lett., 30:1346–1349, (1973).

[14] D.J. Gross and F. Wilczek, "Ultraviolet behavior of non-abelian gauge theories", Phys. Rev. Lett., 30:1343–1346, (1973).

[15] G. Zweig, "An SU(3) model for strong interaction symmetry and its breaking", Technical Report CERN-TH-401, CERN, Geneva, (1964).

[16] A. Ceccucci, Z. Ligeti, Y. Sakai, "CKM Quark-Mixing Matrix", PDG review, (2018), http://pdg.lbl.gov/2019/reviews/rpp2018-rev-ckm-matrix.pdf

[17] E.Fermi, "Tentativo di una teoria dell'emissione dei raggi beta", Ricerca Scientifica. 4 (1933) 491-495

[18] The CMS Collaboration, "Measurment of the ratio $B(t \to Wb)/B(t \to Wq)$ in pp collisions at $\sqrt{s} = 8TeV$, Phys. Lett. B 736 (2014) 33, https://arxiv.org/pdf/1404.2292.pdf

[19] S.Bethke, G.Dissettori, G.P. Salam" Quantum Chromodynamics" , (2017), PDG review, http://pdg.lbl.gov/2018/reviews/rpp2018-rev-qcd.pdf

[20] M.Y. Han and Y. Nambu, "Three-triplet model with double SU(3) symmetry", Phys. Rev., 139:B1006-B1010, (1965).

[21] O.W. Greenberg, "Spin and Unitary Spin Independence in a Paraquark Model of Baryons and Mesons", Phys. Rev. Lett., 13:598-602, (1964).

[22] P. Langacker, "Introduction to the Standard Model and Electroweak Physics", Phys.Lett. High Energy Physics-Phenomenology, (2009), http://arxiv.org/abs/0901.0241.

[23] J.Donoghue, " The fine-tuning problems of particle physics and anthropic mechanisms", (2007), Physics Department Faculty Publication Series, https://pdfs.semanticscholar.org/bb86/fb412d581478bfe946e4481216bd55cfc803.pdf

[24] B. Odom et al., "New Measurement of the Electron Magnetic Moment Using a One-Electron Quantum Cyclotron", Phys. Rev. Lett. 97 (3 2006) 030801, http://link.aps.org/doi/10.1103/PhysRevLett.97.030801

[25] ALEPH Collaboration, DELPHI Collaboration, L3 Collaboration, OPAL Collaboration, LEP Working Group for Higgs Boson Searches, Phys. Lett. B, 565 (2003), http://arXiv:hep-ex/0306033

[26] Tevatron, " New Phenomena and Higgs Working Group for the CDF and DØ Collaborations", FERMILAB-PUB-09-060-E,http://arXiv:0903.4001

[27] "LHC machine", Journal of Instrumentation 3 no.8, (2008) S08001. http://iopscience.iop.org/1748-0221/3/08/S08001.

[28] CMS collaboration, "The CMS tracker system project: technical design report", CERN-LHCC-98-006, http://cdsweb.cern.ch/record/368412.

[29] CMS collaboration, "The CMS tracker: addendum to the technical design report", CERN-LHCC-2000-016, http://cdsweb.cern.ch/record/490194.

[30] CMS collaboration, "CMS Technical Design Report for the Pixel Detector Upgrade", CERN-LHCC-2012-016, https://cds.cern.ch/record/1481838.

[31] CMS collaboration, "The CMS electromagnetic calorimeter project : Technical Design Report", CERN-LHCC-97-033, https://cds.cern.ch/record/349375.

[32] CMS collaboration, "The CMS hadron calorimeter project : Technical Design Report", CERN-LHCC-97-031, https://cds.cern.ch/record/357153.

[33] F. Kircher et al., "Final design of the CMS solenoid cold mass", IEEE Trans. Appl. Supercond., 10 (2000) 407.

[34] CMS collaboration, "The TriDAS project, technical design report. Volume 1: The level-1 trigger", CERN-LHCC-2000-038, http://cdsweb.cern.ch/record/706847.

[35] CMS collaboration, "The TriDAS project, technical design report. Volume 2: Data acquisition and high-level trigger technical design report", CERN-LHCC-2002-026, http://cdsweb.cern.ch/record/578006.

[36] Luciano Maiani, "The GIM Mechanism: origin, predictions and recent uses", https://arxiv.org/abs/1303.6154.

[37] D.B. Kaplan and H. Georgi, Phys. Lett. B136 (1984).

[38] D.B. Kaplan, Nucl. Phys B365 (1991).

[39] G. Panico, A. Wulzer "The Composite Nambu-Goldstone Higgs", Book, Springer (2016)

[40] K. Agashe, R. Contino, A.Pomarlo "The Minimal Composite Higgs Model", Nucl.Phys.B719:165-187,2005 arXiv:hep-ph/0412089

[41] P. Lodone, "Vector-like quarks in a composite Higgs model", JHEP 0812:029 (2008), arXiv:0806.1472

[42] H. Georgi, L. Kaplan, D. Morin, and A. Schenk,"Effects of top compositeness",Phys. Rev. D51(1995) 3888,https://arxiv.org/abs/hep-ph/9410307.

[43] A. Pomarol, "Extra Dimensions" http://pdg.lbl.gov/2014/reviews/rpp2014-rev-extra-dimensions.pdf

[44] Th. Kaluza, "On the Unification Problem in Physics" Int. J. Mod. Phys. D, Vol. 27, No. 14 (2018) 187001 (translation); Sitzungsber. Preuss. Akad. Wiss. Berlin (Math. Phys.) 1921, 966-972 (original), arXiv:1803.08616

[45] O. Klein, "Quantentheorie und fünfdimensionale Relativitätstheorie" , Physik (1926) 37: 895. https://doi.org/10.1007/BF01397481

[46] N. Arkani-Hamed, S. Dimopoulos, G. Dvali, "The Hierarchy problem and new dimensions at a millimeter", (1998), Physics Letters. B429 (3–4): 263–272. arXiv:hep-ph/9803315

[47] L. Randall, R.Sundrum, "Large Mass Hierarchy from a Small Extra Dimension", (1999), Physical Review Letters. 83 (17): 3370–3373. arXiv:hep-ph/9905221

[48] L. Randall, R.Sundrum, "An Alternative to Compactification", (1999), Physical Review Letters. 83 (23): 4690–4693. arXiv:hep-th/9906064

[49] T. Aaltonen et al.[CDF Collaboration],"Search for a Heavy Top-Like Quark in pp Collisions at $\sqrt{s} = 1.96$ TeV", Phys. Rev. Lett. 107 (2011) 261801 https://arxiv.org/pdf/1107.3875.pdf

[50] CDF public note:https://arxiv.org/pdf/www-cdf.fnal.gov/physics/new/top/2010/tprop/HQ_public/HQpub.pdf

[51] V. M. Abazov et al. [D0 Collaboration],"Search for single vector-like quarks in pp collisions at $\sqrt{s} = 1.96$ TeV", Phys. Rev. Lett. 106 (2011) 081801 https://arxiv.org/pdf/1010.1466.pdf.

[52] CMS Collaboration, "Search for heavy vector-like quarks decaying to same-sign dileptons", http://cds.cern.ch/record/2256747?ln=en

[53] CMS Collaboration, "Search for top quark partners with charge 5/3 in the single-lepton final state at $\sqrt{s} = 13$ TeV",http://cds.cern.ch/record/2264686?ln=en.

[54] ATLAS Collaboration, "Search for pair production of up-type vector-like quarks and for four-top-quark events in final states with multiple b-jets with the ATLAS detector",https://arxiv.org/abs/1803.09678

[55] "Search for pair production of heavy vector-like quarks decaying to high-p_T W bosons and b quarks in the lepton-plus-jets final state in pp collisions at $\sqrt{s} =$ 13 TeV with the ATLAS detector", https://arxiv.org/abs/1707.03347.

[56] ATLAS Collaboration,"Search for pair production of vector-like top quarks in events with one lepton, jets, and missing transverse momentum in $\sqrt{s} = 13$ TeV pp collisions with the ATLAS detector",https://arxiv.org/abs/1705.10751.

[57] CMS Collaboration, "Search for pair production of vector-like quarks in the $bW\bar{b}W$ channel from proton-proton collisions at $\sqrt{s} = 13$ TeV",https://arxiv.org/abs/1710.01539.

[58] CMS Collaboration, " Search for single production of a vector-like T quark decaying to a Z boson and a top quark in proton-proton collisions at $\sqrt{s} = 13$ TeV", https://arxiv.org/abs/1708.01062.

[59] CMS Collaboration, "Search for a singly produced vector-like quark B decaying to a b quark and a Higgs boson in a fully hadronic final state using boosted topologies ",https://cds.cern.ch/record/2273909.

[60] Mihailo Backovi et al.,"Discovering heavy new physics in boosted Z channels:$Z \to l^+l^-$ vs $Z \to \nu\bar{\nu}$",https://arxiv.org/abs/1501.07456

[61] CMS Collaboration, "Particle–Flow Event Reconstruction in CMS and Performance for Jets, Taus, and $\not{E}_{\mathrm{T}}$", CMS Physics Analysis Summary CMS-PAS-PFT-09-001, (2009).

[62] CMS Collaboration, "Reconstruction of electron tracks with the Gaussian-Sum Filter in the CMS tracker at LHC", CMS Analysis Note RN-2003-001 (2003)

[63] CMS Collaboration, "Electron cut-based Identification",https://twiki.cern.ch/twiki/bin/view/CMSCutBasedElectronIdentificationRun2#Electron_.

[64] CMS Collaboration, "Baseline Muon Selection", https://twiki.cern.ch/twiki/bin/viewauth/CMS/SWGuideMuonIdRun2#Tight_Muon.

[65] CMS Collaboration, "Pileup Removal Algothitms", CMS-PAS-JME-14-001, https://cds.cern.ch/record/1751454/files/JME-14-001-pas.pdf

[66] M. Cacciari, G. P. Salam, and G. Soyez, "The anti-k_{T} jet clustering algorithm", JHEP 04 063, https://arxiv.org/abs/0802.1189, (2008)

[67] CMS Collaboration, "Jet Performance in pp Collisions at $\sqrt{s} = 7$ TeV", CMS Physics Analysis Summary CMS-PAS-JME-10-003, CERN, 2010.

[68] "Particle Flow Jet ID",https://twiki.cern.ch/twiki/bin/viewauth/CMS/JetID.

[69] T. C. collaboration, "Determination of jet energy calibration and transverse momentum resolution in CMS", Journal of Instrumentation 6, no. 11, P11002, (2011).

[70] M. Dasgupta, A. Fregoso, S. Marzani, and G. P. Salam, "Towards an understanding of jet substructure", JHEP 09 (2013) 029, https://arxiv.org/abs/1307.0007.

[71] A. J. Larkoski, S. Marzani, G. Soyez, and J. Thaler, "Soft Drop", JHEP 05 (2014) 146, https://arxiv.org/abs/1402.2657.

[72] S. D. Ellis, C. K. Vermilion, and J. R. Walsh, "Techniques for improved heavy particle searches with jet substructure", Phys. Rev. D 80 (2009) 051501, https://arxiv.org/abs/0903.5081.

[73] CMS Collaboration, "Identification techniques for highly boosted W bosons that decay into hadrons", JHEP 12 (2014) 017, https://arxiv.org/abs/1410.4227.

[74] CMS Collaboration, "Identification of heavy-flavour jets with the CMS experiment in pp collisions at 13 TeV",2018, JINST 13 P05011 ,https://arxiv.org/pdf/1712.07158.pdf.

[75] CMS Collaboration, "Identification of b quark jets at the CMS Experiment in the LHC Run 2", CMS Physics Analysis Summary CMS-PAS-BTV-15-001, CERN, http://cds.cern.ch/record/2138504, (2015).

[76] J. Alwall et al., "The automated computation of tree-level and next-to-leading order differential cross sections, and their matching to parton shower simulations", JHEP 1407 (2014) 079, https://arxiv.org/abs/1405.0301.

[77] T. Sjostrand, "PYTHIA 6.4 Physics and Manual", 2006, https://arxiv.org/pdf/hep-ph/0603175.pdf.

[78] M. Bähr et al., "Herwig++ physics and manual", Eur. Phys. J. C 58 (2008) 639,https://arxiv.org/abs/0803.0883.

[79] S. Frixione et al., "Matching NLO QCD computations with Parton Shower simulations: the POWHEG method", (2007),https://arxiv.org/abs/0709.2092v1.

[80] S. Agostinelli et al., "Geant4. A simulation toolkit", Nuclear Instruments and Methods in Physics Research Section A: Ac- celerators, Spectrometers, Detectors and Associated Equipment, no. 3, volume 506 (pag. 250−303), 2003, https://www.sciencedirect.com/science/article/pii/S0168900203013688.

[81] P. Nason, "A New method for combining NLO QCD with shower Monte Carlo algorithms", JHEP 0411 (2004) 040,https://arxiv.org/abs/hep-ph/0409146.

[82] S. Alioli, P. Nason, C. Oleari, and E. Re, "A general framework for implementing NLO calculations in shower Monte Carlo programs: the POWHEG BOX", JHEP 1006 (2010) 043,https://arxiv.org/abs/1002.2581.

[83] T. Sjostrand, S. Mrenna, and P. Z. Skands, "A Brief Introduction to PYTHIA 8.1", Comput.Phys. Commun. 178 (2008) 852–867, https://arxiv.org/abs/0710.3820.

[84] CMS Collaboration, "Cross section measurement of t-channel single top quark production in pp collision at $\sqrt{s}$ = 13 TeV", Phys.Lett. B772 (2017) 752-776, arXiv:1610.00678

[85] J. Beringer et al. (Particle Data Group), PR D86, 010001 (2012), http://pdg.lbl.gov/

[86] J. Thaler, K. Van Tilburg , "Identifying Boosted Objects with N-subjettiness", JHEP 1103:015,2011, arXiv:1011.2268

[87] CMS Collaboration, "Summary table of samples produced for the 1 Billion campaign, with 25 ns bunch-crossing", https://twiki.cern.ch/twiki/bin/viewauth/CMS/SummaryTable1G25ns.

[88] CMS Collaboration, "Cms luminosity based on pixel cluster counting – summer 2013 update", CMS Physics Analysis Summary CMS-PAS-LUM-13-001, https://arxiv.org/abs/1012.2466., (2013).

[89] M. Botje et al., "The PDF4LHC Working Group interim recommendations", https://arxiv.org/abs/1101.0538, (2011).

[90] CMS Collaboration, "Determination of jet energy calibration and transverse momentum resolution in CMS", JINST 6 P11002, https://arxiv.org/abs/1107.4277.

[91] L. Lista, "Practical Statistics for Particle Physicists", https://arxiv.org/pdf/1609.04150.pdf

[92] A. L. Read., "Modified Frequentist Analysis of Search Results (The CLs Method)", CERN OPEN, 2000-205, https://cds.cern.ch/record/451614/files/open-2000-205.pdf.

[93] T. Junk, "Confidence level computation for combining searches with small statistics", Nucl. Instrum. Meth. A 434 (1999) 435, https://arxiv.org/abs/hep-ex/9902006.

[94] G. Cowan, K. Cranmer, E. Gross, and O. Vitells, "Asymptotic formulae for likelihood-based tests of new physics", Eur. Phys. J. C 71 (2011) 1554, https://arxiv.org/abs/1007.1727.

[95] CMS Collaboration, "Documentation of the RooStats-based statistics tools for Higgs PAG (rev. 106)", CMS twiki page, (2013), https://twiki.cern.ch/twiki/bin/viewauth/CMS/SWGuideHiggsAnalysisCombinedLimit?rev=106.

[96] A. Carvalho, S. Moretti, et al., "Single production of vector-like quarks with large width at the Large Hadron Collider", https://arxiv.org/abs/1805.06402v1.

[97] CMS Collaboration, "Search for single production of vector-like quarks decaying to a b quark and a Higgs boson", https://arxiv.org/abs/1802.01486.